# Understanding the Mechanics of Golf Ball Impact

*The Characterisation of the Materials used in Golf Ball Construction for Use in Finite Element Analysis*

Alistair W. Pugh

A thesis presented in fulfilment of the requirements for the degree of Doctor of Philosophy.

Department of Mechanical Engineering
The University of Strathclyde,
Glasgow.

November 2011

# Copyright statement

The copyright of this thesis belongs to the author under the terms of the United Kingdom Copyright Acts as qualified by University of Strathclyde Regulation 3.49. Due acknowledgement must always be made of the use of any material contained in, or derived from, this thesis.

*We will never know our own full potential unless we push ourselves to find it.*

(Travis Rice – The Art of Flight)

*Enjoy the ride…*

## Acknowledgments

The journey that is a PhD is an interesting one. There are hard times, frustrating times, moments of shear elation and some truly brilliant experiences. If these experiences were singled purely to elation and brilliance this acknowledgments section would be rather dull, however it is the hard and frustrating times that highlight the importance of the support received throughout the process.

I would like to extend thanks to The University of Strathclyde. Specifically, Dr David Nash and Dr Bobby Hamilton for their technical knowledge, experience and continued guidance and support throughout the PhD. Considerable thanks are extended to Dr Steve Otto and Dr Andrew Johnson at R&A Rules Ltd. for surpassing all expectations with providing knowledge, constructive criticism, advice and countless exceptional lunches. Without their expertise and direction, the study wouldn't have been nearly as enjoyable or demanding. Thanks to Dr Jorgen Bergström for providing the PolyUMod and MCalibration software, which was used so heavily throughout the study. His knowledge of the materials examined is inspiring and helped determine the route the work would follow.

Without friends and colleagues the experience would have been extremely lonely. I would like to thank everyone in the postgraduate suite at Strathclyde, specifically Andrew Beveridge, Mark Symington, Wael Elmayyah and James Ure who provided a lot of laughter, academic support and general good times.

Without the support of my family there is probably no way I would've started the PhD never mind finish it. Love to my mum, my dad, Richard, Christopher and my dog, Otto, for helping me through the process, whether they know it or not. Additional thanks are extended to my dad for providing both technical and personal guidance from his first hand experience of PhD's. Final thanks are saved for Aileen Thom who has, without doubt, helped me more than anyone else...don't worry Aileen, you don't have to read the whole thing.

Thank you all.

## Abstract

As golf equipment evolves, science and engineering become more important in the understanding of relationship between the technology and materials involved. The complex nature of the interaction between the golf ball and club, and in particular how material characteristics affect the mechanisms of the impact are not yet fully understood. The overall aim of the present work is to develop suitable material tests and use the acquired data to produce a fully validated finite element (FE) model that is capable of predicting hysteresis during cyclic loading as well as coefficient of restitution (COR) on high speed impacts.

A detailed experimental study has been carried out in order to establish accurate and reliable material properties. The golf ball used in this study consists of two layers with varying material properties and can be regarded as multi-material system. Test samples were produced from the golf ball cover and core. Due to geometric constraints the core samples have only been tested in compression and the cover samples in tension. The core was sectioned into samples of various geometries, each tested in compression. It has been reported in previous studies that the golf ball is highly heterogeneous and the material tests have addressed this to create an FE model that represents the material heterogeneity. Linear viscoelastic models have been presented in the literature to describe the materials used in golf ball construction with varying success; however the presented work shows the material to be non-linear viscoelastic

and therefore requires different models to describe its behaviour. The non-linear, viscoelastic Bergstrom-Boyce (BB) model was initially selected as it is capable of predicting the large strain, loading-unloading behavior, including hysteresis, present in polymeric materials. Various mathematical models, which are used to describe the behaviour of the spring and dashpot elements within the material models have been investigated.  The material parameters used to describe each optimized model have been used in the finite element package ABAQUS, as a user defined material, to predict the stress-strain response upon cyclic loading.

The present experimental work points the way towards new methods of obtaining accurate, reliable material data at higher strain rates. This approach will allow a more physically representative model of the impact between the club and ball using finite element analysis techniques.

# Contents

# 1  Introduction

The R&A (R&A Rules Ltd.) are responsible for ensuring that the skill of the golfer and not the technical merit of the golfer's equipment is the deciding factor in the outcome of a competitive game. For this to be achieved, understanding the mechanics of golf ball impact is an area of paramount importance. This thesis describes the work of a funded study, by R&A Rules Ltd., in this area of research.

## 1.1  The Game of Golf

Golf was once famously described by Mark Twain [1] as "a good walk spoiled". It is an incredibly difficult and addictive sport, which tens of millions of people around the world enjoy regularly. The origins of golf are somewhat unclear. Some say that it is a descendant of the Roman game "paganica"; others trace the game to the French and Belgian game "chole", the Dutch game "het kloven", the French game "jeu de mail" and the English game "cambuca". However the most accepted theory is that golf originated from Scotland in the 1100s when Scottish shepherds knocked stones into rabbit holes in the area where the world famous St Andrews Golf Club lies [2].

The object of golf is very simple, to complete the round in as few strokes as possible. Golf courses generally consist of 9 or 18 holes, with each hole having a par, which is determined by the length and difficulty of the hole. A popular

legend explaining why golf courses have 18 holes dates back to the links at St Andrews, which originally had 22 holes, 11 holes each played twice. It is said the players noticed that it took precisely 18 holes to finish a fifth of scotch, a shot per hole.

## 1.2   The Golf Ball

The earliest golf balls were reported as being manufactured from hardwoods such as beech and boxroot and crudely rounded using basic tools. As there are no known surviving artefacts from this period, the 14th Century to the 17th Century, the facts are based on written information [1].



**Figure 1.2-1 – "The Featherie" golf ball.**

The earliest known example of a golf ball is "The Featherie" (Figure 1.2-1) which experienced the longest period of stability in the history of the golf ball, ranging from as early as the 14th Century through to the 18th Century. As the name suggests, the Featherie was a leather pouch filled with feathers. The manufacturing process was very time consuming and required considerable

expertise, [3][4]. The leather was from untanned bull's hide and consisted of two round pieces for the ends and a middle piece cut to suit the desired weight. The pieces were then softened and sewn together leaving a hole in which the manufacturer would stuff the feathers. This small hole also allowed the pouch to be turned inside out resulting in only smooth seams being shown on the outside of the ball, [3][4]. As a result of the intricate and time consuming process the Featherie was extremely expensive, each costing as much as 4 shillings. The ball was not very durable and on a wet day the player would use up to 6-8 balls. Despite the crude techniques the Featherie was reported to roll quite well and could travel in excess on 250 yards [4], which is not far off the standards of professional golfers today. [5]

The modern era of golf ball construction can be traced back to the 1850's (circa), with the introduction of the "gutta-percha" ball (Figure 1.2-2).



**Figure 1.2-2 – The Gutta-percha golf ball.**

Due to the industrial revolution gathering pace in the UK, companies began to produce more and more products from rubber and it was only a matter of time

before this was applied to golf technology. Surprisingly it was a golf mad reverend that sparked the change in golf ball manufacture [3][4]. Rev. James Patterson of Dundee discovered a rubber-like material on a trip to Malaysia known as Gutta-percha that comes from the dried sap of the sapodilla trees in East Asia. Rev. James Patterson sent a statue back to Scotland using the rubber he had found as a protective packaging. On his return he began experimenting with the material and decided he would attempt to produce a golf ball out of it. Shortly after this there were many companies producing Gutta-percha balls and using metal moulds to get a perfectly round sphere. Initially the balls were perfectly smooth but golfers soon realised that the balls flight became more controlled and predictable as surface imperfections appeared. In comparison to the featherie, Gutta-percha balls could be produced in a matter of minutes by a skilled worker and were soon being produced at quarter of the cost of the Featherie. This opened up the game to the masses as it suddenly became more affordable.



**Figure 1.2-3 - The Bramble golf ball.**

The next stage in the evolution of the golf ball was "the Bramble" (Figure 1.2-3). The bramble was essentially a Gutta-percha ball covered with a bramble type pattern, hence the name. Between 1880 and 1890 various cover patterns were investigated and the bramble pattern became the preferred option.

1898 marked the introduction of the Haskell ball (Figure 1.2-4), which was the first ball more recognisable by today's standards [5]. The Haskell ball consisted of a solid rubber core surrounded by threads of tensioned rubber, encased by a Gutta-percha cover. In comparison to the Gutta-percha ball, the Haskell ball was reported to travel further on iron shots but was more difficult to control as the player got nearer to the hole. Throughout the 20th Century many variants of the Haskell ball were developed. These included those with liquid cores, a pouch containing silicone oil, and various different cover materials.



**Figure 1.2-4 - The Haskell golf ball.**

Nowadays, the vast majority of golf balls are solid construction meaning that they consist of layers of different rubbers each having their own unique material properties. Spalding introduced the first two-piece solid construction ball, in 1968 [8], whilst the first multi-piece solid construction ball was patented

in 1984 [9]. By 1989, the solid two-piece ball had a 75% share of the golf ball market with three-piece, liquid core, wound balls taking the remaining 25% [10]. The solid construction ball accounted for 85% of the golf ball market by 1998, although 81% of balls used on the PGA Tour were still wound construction. At this stage the solid construction ball did not offer the same "control" as a wound construction ball therefore professional golfers still chose to play wound ball [11]. The solid construction ball now dominates the market as manufacturers can produce high performance solid balls, which are extremely durable and have very little, if any detrimental affect on distance and control.

## 1.3   Golf Ball Selection

When selecting the type of golf ball they wish to use, the golfer takes various factors into consideration. The performance characteristics of the ball change with the materials and number of layers used, generally two-piece balls are marketed towards beginner and intermediate golfers and are categorised as distance balls. The aforementioned group of golfers tend to be less accurate in their impact position and often create too much backspin on long shots, resulting in a loss of distance. Due to poor technique they also often produce undesirable tilting of the spin axis, which results in wayward golf shots.

The, higher end, multi-piece balls have the addition of a soft polyurethane cover, which increases the control the golfer has over the ball. This is due to the amount of spin that can be generated for higher lofted clubs. Typically, more

accomplished golfers are in better control over the position of their golf club upon impact with the ball. In comparison to the beginner/intermediate group the accomplished golfer can use backspin and sidespin to their advantage and it becomes beneficial to use a higher-end golf ball.

## 1.4   Golf Ball Construction

The golf balls used in this study can be categorised as solid construction meaning that there is no liquid core or tensioned rubber. Solid construction golf balls are further categorized by the number of different rubbers involved. A one-piece ball is simply one type of rubber compression moulded into a sphere. A two-piece ball has a separate core and cover (Figure 1.4-1). The core is generally produced from a filled polybutadiene rubber and the cover from an ionomer rubber [12]. Three-piece balls tend to have similar cores to two-piece balls and a similar ionomer layer encasing the core but they have the addition of a soft polyurethane cover [12].



The Core
Typically a filled polybutadiene rubber displaying *hyperelastic* and *viscoelastic* behavior.

The Cover
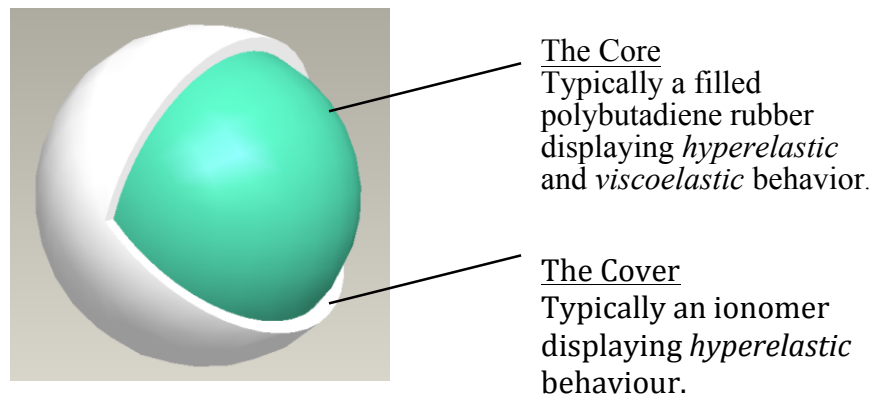Typically an ionomer displaying *hyperelastic* behaviour.

Figure 1.4-1 - Graphical representation of a two-piece golf ball.

Each manufacturer uses specific filler contents for the core, resulting in a blend of which the consumer does not know the exact material properties. After the

core formulation has been chosen the rubber is ready for the manufacturing process. To create the core material the selected chemicals are mixed at high temperature (90-100 $^o$C). This elevated temperature makes mixing easier and the mixing process ensures that the resulting material is homogeneous. The material is then cooled and prepared into a cylindrical shape. This cylindrical slug is placed in a mould consisting two hemispherical halves. The halves are pressed together and seal around the material creating a spherical mould containing the ball core material.

The mould is preheated and the core material is held in the mould prior to curing. The temperature is then increased and maintained for the duration of the curing process. After the curing process is complete the core is removed from the mould.

The outer layers of the ball can either be manufactured using injection or compression moulding. For injection moulding the core is held centrally by retracting pins in a spherical cast, which has the same dimensions and dimple pattern as the finished ball. The outer material is then injected into the free space, surrounding the core.

## 1.5  Aims and Objectives

As with any popular sport the technology involved has become increasingly advanced. These technological advances are monitored by R&A Rules Ltd., who govern the sport across the world, excluding North America and Mexico. R&A

Rules Ltd. seek to ensure that skill remains the dominant aspect in determining success.

An overall aim of this thesis is to produce a fully validated finite element (FE) model of a commercially available golf ball. For the model to be deemed "fully validated" it is required to be able to predict material hysteresis upon cyclic loading along with coefficient of restitution (CoR) on normal impacts. Previous studies for example [13], have used a technique known as "tuning" where the results of a FE analysis are compared to the experimental results and the parameters describing the model are then altered or tuned, the finite element analysis is then re-run hopefully to match the experimental results. The present work, described in this thesis aims to characterise the material accurately and reliably through experimentation prior to the FE analysis stage so that the model can fully predict the behaviour without the need to tune the model. This has the advantage of not requiring experimental data, in this case impact data, to tune the parameters. The simulation can predict the behaviour of a ball before it has been manufactured thus reducing the costs involved with product development and also providing the facility to extrapolate beyond currently available material combinations.

Although research has been carried out in this field in the past, which will be discussed in Chapter 2, a documented methodology that fully describes the procedure of experimentally establishing material data and modelling a golf ball using finite element (FE) analysis in a clear, concise and logical manner would

further benefit the field. This study addresses the above and give details on experimental material characterisation, FE modelling, computational material models and FE simulation may be used to pave the way for future work in understanding golf ball impact mechanics.

# 2 Background and Theory

## 2.1 Overview of Previous Research

The overall aim of this work was defined by R&A Rules Ltd. and was the development of a fully validated FE model of a golf ball. The requirements of such a model would be the ability to satisfactorily predict ball behaviour at a range of strain rates. Such a model should be able to capture deformation, impact force variation, material non-linearity, static and dynamic behaviour (e.g. strain rate dependent response). However the difficulty involved in developing such a comprehensive model should not be underestimated. There are many papers in the literature describing golf ball finite element studies and finite element studies of polymer materials, however there are certain papers that can be highlighted as significant to the present study as a consequence of their modelling techniques and results. Tanaka *et al.* [13] discussed experimental testing and FE modelling of golf balls. This paper states that in order to make previous models more accurate, finer meshing and more accurate material properties are required. The authors determined various dynamic properties of the golf ball through experimentation. Impact load histories, ball outer diameter deformation histories and rebound velocity were measured for normal impacts. Rebound velocity, rebound angle and spin rate were obtained for oblique impacts. The above data was used for comparison to the FE model that was also created. Iwastsubo *et al.* [14] used linear elastic properties to define their ball model and Lucas [15] introduced hyperelasticity to the core of

the ball whilst keeping the cover linear elastic. The FE model that Tanaka *et al.* constructed differed from previous models in that it included both viscoelastic and hyperelastic material models. The cover material model consisted of purely hyperelastic material properties whereas the mid layer and core consisted of both hyperelastic and viscoelastic models. One point to highlight is that the paper used tuning. Although time consuming, tuning works well when the experimental target data from a golf ball is known but is not as useful or even possible when trying to predict the behaviour of a ball that is in the design phase or is yet to be manufactured.

Mase et al [16] carried out an experimental investigation to obtain material properties that could be used to describe material model in FE analysis. The ball cover was removed and remoulded using the DuPont moulding recommendations [17] into standard test sample geometry. Dynamic Mechanical Thermal Analysis (DMTA) was utilised to establish the material properties. The obvious disadvantage of this method is the need to re-mould the golf ball rubbers, which will inevitably alter the material properties. The constructed model represents coefficient of restitution for impact speeds of 35-55m/s but under estimated CoR values for speeds below 30m/s. The impact times predicted by the model were also less than measured experimentally.

Johnson [12] investigated the properties of the materials used in golf ball construction and how they are affected as a result of the manufacturing process. It was found that the golf ball core experiences significant changes in properties

across the radius. It is possible that this is a result of the curing involved in the manufacturing process. The work also introduced various experimental methods for producing test samples from commercially available golf balls and was used as a template for the experimental investigation carried out as part of the present work.

Together, the overall objective of the work and the conclusions from the above documents gave an indication of the route the present work would take. Tanaka et al [13] produced good results but their computational material model required tuning. Mase et al [16] had the uncertainty of reprocessing and remoulding the components of the ball into a standard geometry for material characterisation and Johnson [12] identified the material heterogeneity of the golf ball core. As a result it was decided to try and model the material heterogeneity using finite element analysis and create a model that did not require tuning and a sample preparation technique that didn't involve remoulding. Although there are other papers that provide good background knowledge, they do not directly relate to this study therefore will not discussed in detail. Relevant literature shall be discussed through the thesis in relation to specific points.

It is worth noting at this point, that a fuller overview of research literature in the field of golf ball research can be found in the work of Johnson [12] and Quintavalla [20] who between them cover the fundamentals of golf terminology, the manufacture of golf balls, modelling the impact behaviour of golf balls,

materials testing and modelling techniques. This is not repeated or expanded on in the present work for the purposes of brevity.

## 2.2 Material Model Terminology

### 2.2.1 Hyperelasticity

Under loading, a simple linear elastic material would produce a stress-strain curve akin to the image on the left in Figure 2.2-1. The loading path would be linear and the unloading path would follow the gradient of the loading path. A hyperelastic material [18] is a non-linear material that can experience very high strains and fully recover. It is recommended by Jorgen Bergström [19] that a hyperelastic model be used when the strain is greater than just 1%. For smaller strain simulations, hyperelastic models will successfully predict the behaviour but might take more time computationally due the increased complexity of the material models. More importantly, the loading/unloading path of a hyperelastic material is not necessarily linear. Hyperelastic material models accurately describe such material behaviour and are capable of predicting non-linear curves but cannot predict material hysteresis and show no strain-rate dependence. Figure 2.2-1 displays the characteristic response of linear elastic and hyperelastic materials.
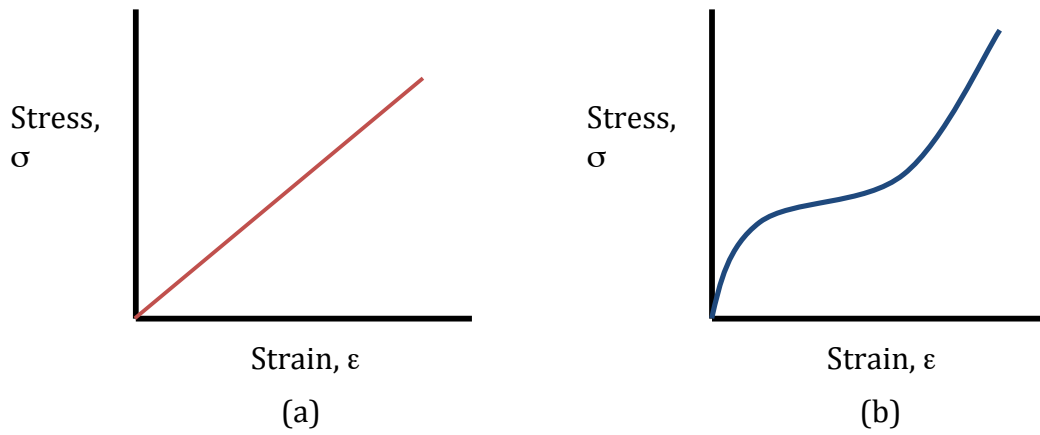
**Figure 2.2-1 - Examples of linear elastic (a) and hyperelastic (b) material response.**

Most hyperelastic elastomers (solid, rubber-like materials) have very little compressibility compared to their shear flexibility. In applications where the material is not highly confined, the degree of incompressibility is typically not crucial [18]. The materials are therefore often assumed to be incompressible. The relative compressibility of a material can be assessed relative to its initial bulk modulus, $K_0$ and initial shear modulus, $\mu_0$. This can be presented in terms of Poisson's ratio, $v$, since:

$$v = \frac{3K_0/\mu_0 - 2}{6K_0/\mu_0 + 2}$$

.....Equation 2.2-1

Due to the properties of the materials used in golf ball construction it can be assumed that the representative Poisson's ratio is approximately equal to 0.49 throughout the study. A fully incompressible material would have a Poisson's ratio of 0.5, if the equation above were manipulated to be presented in terms of $K_0$; a Poisson's ratio of 0.5 would result in an infinite bulk modulus. Using a value of 0.49 has been used previously by Tanaka et al [13] and provides a good representation of incompressibility. Quintavalla [20] justified the assumption of

15

incompressibility through examination of the apparent dilation of the samples under compressive strain. He reported that a material with a Poisson's ratio of 0.45 would show a volumetric contraction of 5% and the materials used in golf ball construction were showing a maximum apparent dilation of approximately 1%. Given this it was felt that incompressibility, broadly assumed for elastomers, may be used in this case.

### 2.2.2 Viscoelasticity

Rubber-like materials typically exhibit energy loss upon cyclic loading. The stress strain curves, characteristically, look like the graph shown in Figure 2.2-2. This material hysteresis or the "loop" in the stress strain curve is a product of the material energy dissipation. This behaviour, under cyclic loading, and where the material returns to its original stress-strain value after unloading is called viscoelasticity. Viscoelasticity [21] is a term used to describe a material with behaviour that is intermediate between the idealised behaviour of elastic solids and viscous liquids. Viscoelastic materials generally also display rate dependence upon loading. This naturally means that the stress strain response is different at one strain rate to another. Typically the faster strain rate results in a stiffer material response. Another typical attribute to viscoelastic materials is that unloading curve follows a different path to the loading curve. The area between the loading and unloading curves (as shown in Figure 2.2-2) is known as material hysteresis and represents the energy dissipated.
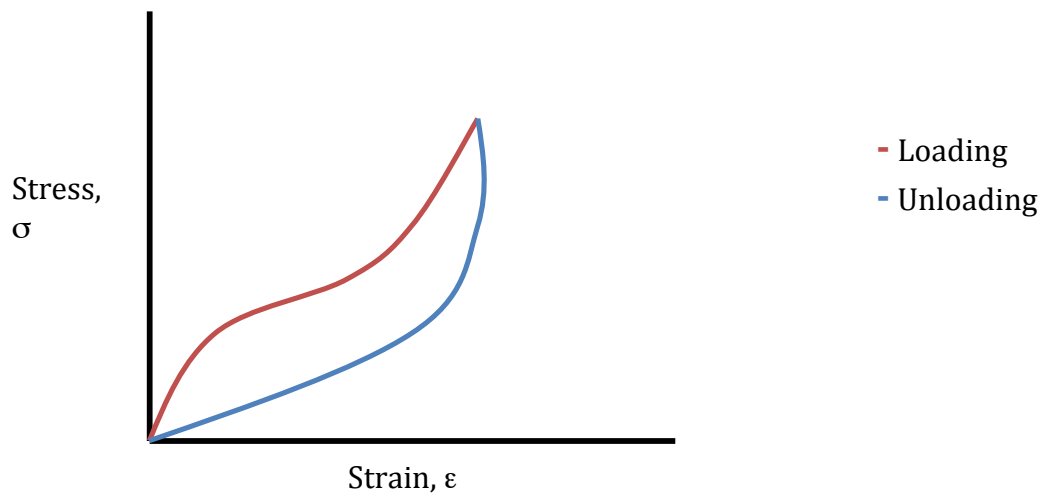
**Figure 2.2-2 – Example of viscoelastic material under cyclic loading.**

### 2.2.3 Linear and Non-Linear Viscoelasticity

Previous research in the field [13] has focussed on using the ABAQUS Prony series modelling technique it is not fully suited to the application of modelling golf ball impact, since the golf ball core is, to some extent, non-linear viscoelastic. The non-linear viscoelastic nature of the golf ball core material was an outcome of the experimental investigation carried out as part of this thesis and will be discussed in depth in the following relevant section.

ABAQUS assumes viscoelastic materials are defined by a Prony series expansion of the dimensionless relaxation modulus [18]. The Prony series can be defined by letting $G_r(t)$ be the shear stress relaxation modulus. Define $G_\infty$ and $G_0$ by the following limits:

$$G_\infty = \lim_{t \to \infty} G_R(t)$$

$$\text{and } G_0 = G_R(0).$$

.....**Equation 2.2-2**

17

From the shear relaxation modulus a dimensionless relaxation modulus can be defined from:

$$g_R(t) = \frac{G_R(t)}{G_0} \quad .$$

The normalised shear stress relaxation modulus is often represented by a series expansion in exponential terms:

$$g_R(t) = 1 - \sum_{i=1}^{N} g_i \left[ 1 - e^{\frac{-t}{\tau_i}} \right],$$

where $N$, $g_i$ and $\tau_i$, $i=1,2,...,N$, are material parameters. This series expansion is called the Prony series [22]. Figure 2.2-3 shows a schematic representation of a three-element model. In a linear viscoelastic model, Network A would be described with a hyperelastic material model giving the instantaneous elastic response of the material. Network B gives the material rate dependence and would be described using a viscoelastic material model. If the Prony series were used, Network B would contain a linear spring and linear dashpot. Conversely, if a non-linear viscoelastic material model was used (e.g. the Bergström Boyce model [23]) the spring and dashpot in Network B would be non-linear. Network A would still use a hyperelastic material model to characterise the instantaneous elastic response.
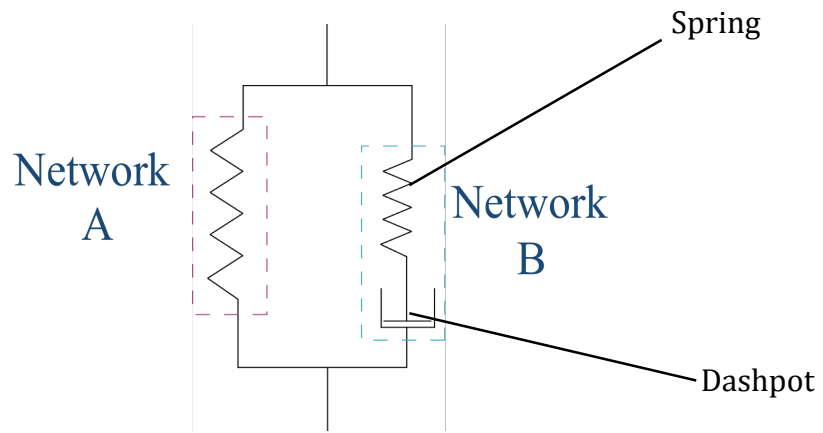
**Figure 2.2-3 - Schematic representation of a three-element model.**

Although the Prony series model can be used to model the response of a non-linear elastic material it is still a linear viscoelastic model meaning that it should be used for materials that agree with the following rules. If the applied strain is doubled the resultant stress should double [21] and the relaxation curves should follow the same path regardless of what the applied strain is [19]. It is documented [19] that linear viscoelastic models do not handle loading well for polymer rubbers (also known as elastomers) and are mainly used for small strain simulations. Additionally the strain rates experienced should be in a relatively narrow range. As the long term aim of this study is to produce a FE model that can predict hysteresis upon cyclic loading along with CoR on high-speed impact it would suggest that linear viscoelastic models are not sufficient.

Non-linear viscoelastic material models are reported [19] to be useful for large strain simulations (greater than approximately 5%) and simulations that cover a wide range of strain rates. Non-linear viscoelastic material models consist of various springs and dashpots, similar to Figure 2.2-3. There are various spring

(elastic response) and dashpot (flow response) mathematical models that can be used to describe the overall response of the model. It is the user's responsibility to select correct spring and dashpot models that suit the application and also suit the experimental data used to calibrate them, this will be discussed in the relevant section later in this thesis.

## 2.3   Complications Associated with Polymetric Materials

There are various complications associated with modelling polymers using finite element analysis. The testing standards for polymers are not as clear as that of steels [24]. The material non-linearity and behaviour under different loading conditions mean that, often, test programmes have to be designed around the experimental data that can be collected and eventual application of the model [19][24]. Deciding on specimen geometry, strain rates, strain magnitudes is therefore a little more time consuming than conventional metallic materials. In the case of testing and modelling the materials associated with golf ball construction there are further geometric complications. The test standards available [25] describe cylindrical test samples, which are difficult to obtain due to the spherical geometry of commercially available golf balls. Polymeric materials also exhibit a behaviour known as the "Mullins" effect. This has been documented in past literature and therefore will not be exhaustively discussed as part of this study [20][26]. In the Mullins effect, the behaviour of the material changes over the first few cyclic loads. The initial response is a one-time event that is never repeated. It is documented [27] that the sample will steadily soften through the first few loading cycles and converge towards a response until the

sample experiences a strain greater than the previous maximum [28]. This behaviour was addressed in the experimental phase of this study by running the samples through a few conditioning cycles before actual loading was applied.

## 2.4  Testing Standards for Polymers

When designing a test program to establish mechanical properties it is important to consider the overall aim. This means that the geometry of the sample has to be considered when designing the test procedure. The cover of the golf ball, for example, cannot easily be tested in bi-axial tension due to the curvature of the component. It is important to understand that it is not always necessary to follow the available testing standards when characterising polymers [19]. The appropriate experiments are not yet clearly defined by national or international standards organisations [24]. This difficulty derives from the complex mathematical models that are required to define the non-linear and the nearly incompressible attributes of elastomers [24]. When deciding on  an appropriate loading sequence it is important to employ realistic strain levels that capture the elastomer behaviour that applies to the analysis. FE analysis was performed on specimen geometry by Miller [24] to determine the specimen geometry to achieve a state of simple tensile strain. The results of the analysis showed that a specimen has to be at least ten times longer in the stretch direction than the width and thickness of the sample. Additionally since the characterisation tests are not intended to fail the specimen there is no need to use a traditional "dogbone" shape.

Compression tests are popular for polymers due to their simple sample geometry and the relatively simple equipment required to perform them. When testing for analysis pure states of compressive strain are desired but this is especially difficult to achieve due to the presence of friction between the compression platens and sample. This friction restricts the lateral expansion of the sample resulting in material shearing. Figure 2.2-4 shows a representation of the effect friction has on the sample.



**Figure 2.4-1 – Original cylindrical sample between compression platens. Result of friction on sample geometry during compression testing.**

This shear straining, which can often exceed the compressive strain, alters the stress-strain response and if the data is used to calibrate a computational material model it could result in the material being artificially stiff. Addressing this problem requires the use of a lubricant. There are various products that can be used to lubricate the sample, a popular choice being PTFE (polytetrafluoroethylene) tape. PTFE is a thermoplastic polymer and has the third lowest friction coefficient of any known solid at 0.05 to 0.1 [29]. Inserting PTFE tape between the sample and the compression platens therefore reduces

the coefficient of friction sufficiently to assume that the sample is free to expand in the lateral direction due to Poisson's effect.

In a filled elastomer (simply represented in Figure 2.4-2), polymer chains are attached to the filler particles (A and B) [12]. In the unstressed state, some chains are relaxed (red chain) and others are near their extension limit (blue chain).
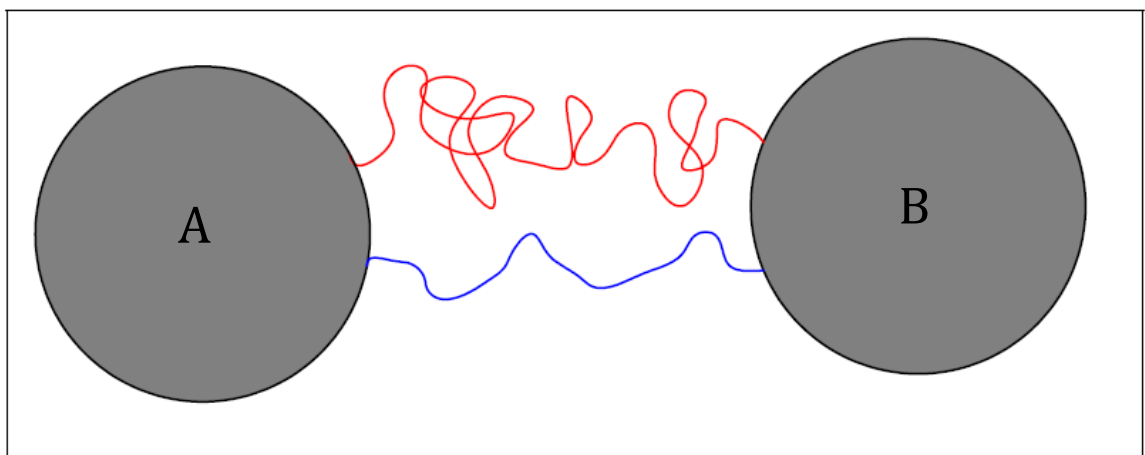


**Figure 2.4-2 – Representation of polymer chains [12].**

When the filled elastomer is strained the relaxed chains have the extra length to accommodate the extension whereas the chains already near their extension limit do not and become detached from the filler particle or break. On subsequent deformation cycles the broken chains cannot support the stress generated through deformation therefore cannot contribute to the resistance of deformation. The result of this is that the material becomes softer; therefore the presence of the Mullins effect has to be considered when testing elastomers for analysis. As stated previously, in this study, conditioning cycles of loading were

applied to the sample to reduce the presence of Mullins effect to a level where it could be assumed to be negligible. It should be noted that if the data of interest were the initial response, this program of conditioning cycles would not be required.

There are various complications associated with modelling polymers using finite element analysis. Unlike steels, there are not the same testing standards so deciding on specimen geometry, strain rates, strain magnitudes is a little more time consuming than conventional metallic materials. In the case of testing and modelling the materials associated with golf ball construction there are further geometric complications. Trying to produce samples of standard geometry from commercially available, spherical golf balls is difficult due to the fact that most standard test geometries are cylindrical. Machining samples from the spherical core that adhered to the test standards involved clamping and milling to the correct size, this process is discussed in depth during the following chapter.

# 3   Experimental Investigation – Phase 1

The aim of the experimental investigation was to establish a robust and repeatable experimental procedure from which accurate and reliable material properties that could subsequently be used in a computational material model of the golf ball construction using FE analysis. There were distinct stages to the experimental investigation. The first part explored the testing of small cylindrical samples that represented the material properties at various points throughout the golf ball core with the aim of capturing enough material data to facilitate a heterogeneous FE model of the golf ball core. This model would have the advantage over previously published homogenous models [13][16] of containing multiple materials that would represent the material heterogeneity that Johnson [12] observed in his thesis. A two-piece ball with a polybutadiene core and an Ionomer resin cover [12] was chosen as the primary focus for the study. This ball was chosen as it is a standard configuration, readily available two-piece golf ball that many beginner to intermediate golfers choose to use on a regular basis. The ball used is however not a commercially available ball, it is a calibration ball made specifically for R&A Rules Ltd. As the ball is used as a calibration ball for equipment testing, for each ball the manufacturing process is expected to be accurate and repeatable which is a necessary feature when gathering data for FE analysis.

### 3.1 Small Core Sample Preparation

The initial proposal for testing the core material was to test in both compression and tension. It is advantageous to test in both tension and compression for polymers as these deformation modes provide different material data [18][30] yet are relatively simple in comparison to equi-biaxial and planar material tests. Johnson [12] reported that across the core of the ball there was a substantial difference in material properties. The tensile samples produced spanned the full diameter of the ball therefore could not be used to characterise the different areas of the core (Figure 3.1-1). It was thought that cylindrical core compression samples could be produced, tested and the results would be used to characterise the varying material properties throughout the core. The full ball was clamped in the three-jaw chuck, as shown in Figure 3.1-2, and the milling machine was programmed to remove material from the ball through a circular motion. The cutting tool was displaced by 19mm in the z-direction cutting the ball material and leaving a sample similar to the representation in Figure 3.1-3.
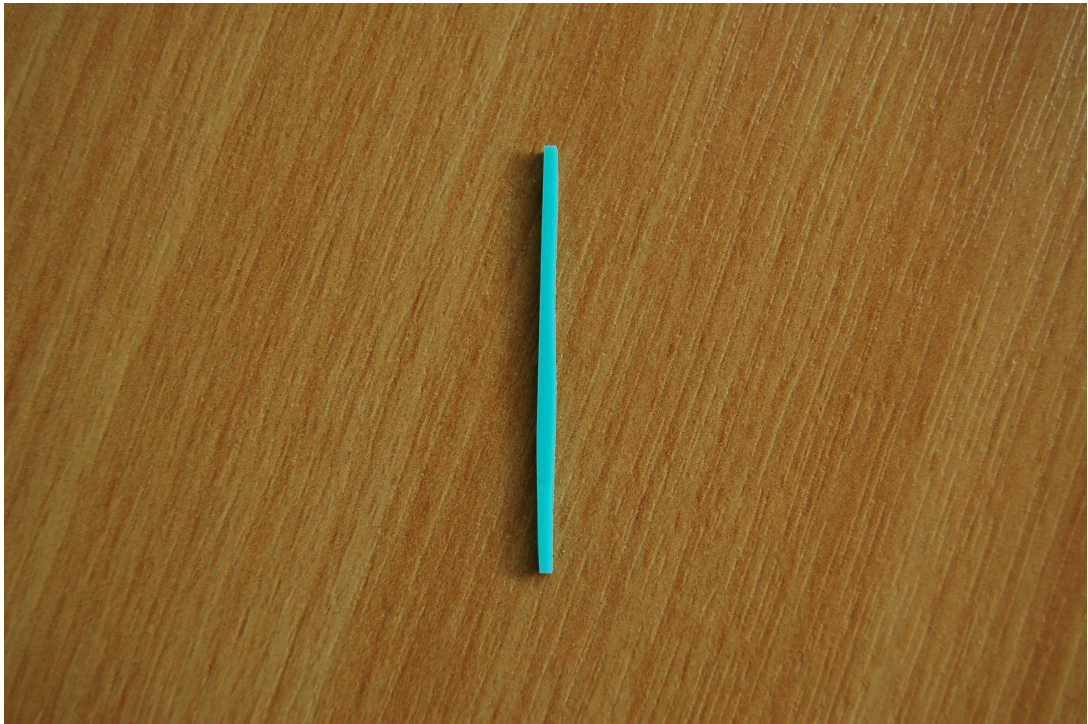
**Figure 3.1-1 – Tensile specimen produced from ball core.**



**Figure 3.1-2 – Complete golf ball secured in 3-jaw chuck for milling.**
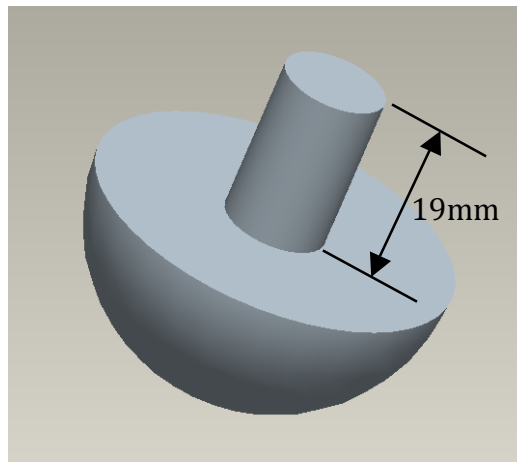
**Figure 3.1-3 – CAD representation of golf ball core midway through milling process.**

The protruding cylindrical section, shown in Figure 3.1-3, was reversed and used to clamp the ball in the three-jaw chuck and the material removal process was repeated on the remaining hemisphere of ball material. This left a cylinder of approximate length 38mm after the cover and excess core material was removed. This cylinder was then sectioned to produce compression samples of 12mm diameter and 5mm height. The 38mm cylinder that remained from the original machining phase still had curvature on the top and bottom faces. In order to produce outer samples of cylindrical geometry the spherical top and bottom faces were flattened using sand paper of various grades, starting with low grade to remove material and moving to higher grade to polish the face of the samples. Various methods of sectioning the cylinder were investigated but the most accurate and reliable method involved marking points a set dimension to the top face and connecting said points, creating a cut line parallel to the top surface. A scalpel was then used to section the sample along the marked cut lines. A typical sample can be seen in Figure 3.1-4.

Figure 3.1-4 – Typical cylindrical core compression sample.

The cylinder of core material was divided and labelled as shown in Figure 3.1-5 leaving a centre sample (C), two samples known as inner samples (i1/i2) and another two outer samples (o1/o2).
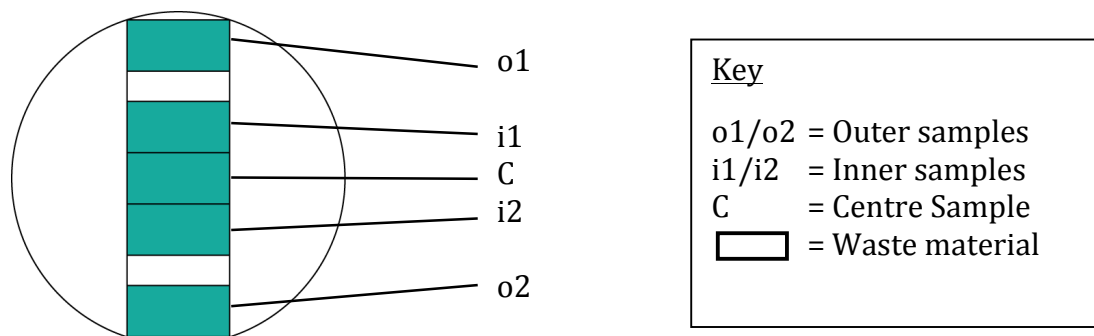


o1

i1
C
i2

o2

Key

o1/o2 = Outer samples
i1/i2   = Inner samples
C        = Centre Sample
⬜ = Waste material

Figure 3.1-5 – Location of compression samples through core radius.

The dimensions of the samples were selected in order to keep the ratio of diameter to height consistent with the ASTM standard sample size (29mm x 13mm) that was used by Quintavalla [20]. The disadvantage of this was that there was material between the inner and outer samples that was not of correct

geometry to conform to the ASTM standard and therefore discarded. Various sample diameters were investigated, the aim being to reduce it to as small a value as possible. Having small diameter samples would reduce the height of each sample allowing for more samples through the thickness of the core. Another area of concern with regards to the diameter of the samples refers back to the manufacturing process. As this resultant cylinder was used to clamp the ball for the second half of the machining phase, it had to be suitably thick to support the ball. It was decided that a diameter of 12mm was thin enough to produce 5 core compression samples of suitable geometry but thick enough to support the ball when clamped for machining. If a smaller diameter were chosen, the cylinder shown in Figure 3.1-3 was not thick enough to support the second phase of machining and the sample would snap.

### 3.2  Cover Sample Preparation

Cover samples were machined from complete golf balls using the same milling apparatus previously described. A three-jaw chuck was used to hold the ball securely whilst the mill was in operation (Figure 3.1-2). A centre line was marked on the ball, using a stencil, and aligned with the jaws on the clamping mechanism. The mill was positioned so that the cutting tool touched the top of the ball. From this position the mill was moved downward in the z-direction. The mill was programmed to remove 18.8mm of material from the top half of the ball. The ball was then rotated 180 degrees and the flat surface placed on an aluminium tower previously machined to the correct height (Figure 3.2-1).

**Figure 3.2-1 – Part machined ball supported on specifically manufactured support.**

The cutting tool was manoeuvred so that it was touching the top of the ball. Another 18.8mm were removed by the cutting tool leaving a disc of cover and core material approximately 5mm thick. Removing the cover from this disc was a relatively simple procedure, which involved cutting the cover material at one point and peeling it away from the core material. Figure 3.2-2 shows the cover material sectioned before peeling from the core providing a sample with suitable geometry to perform tensile tests on.
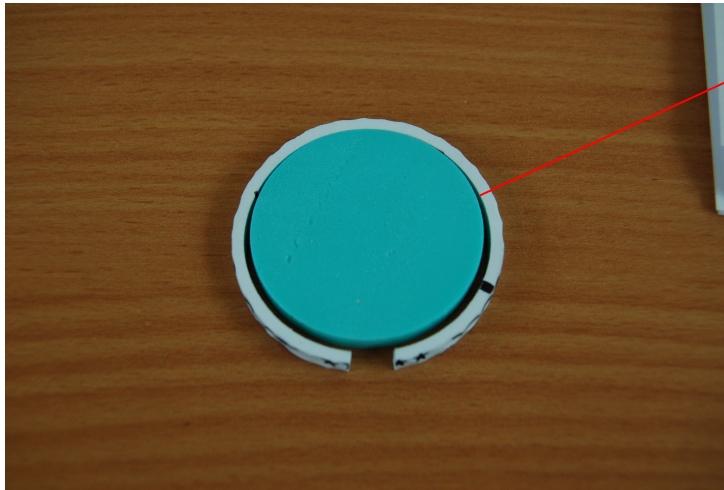
Cover sample removed from disc.

**Figure 3.2-2 – Cover tensile sample removed from machined core.**

As discussed previously the test standards for polymer materials are somewhat different to metal materials. As the aim of this test was to obtain material data for a state of pure tensile strain, it is documented in [24] that the most significant requirement is that the sample should be much longer in the stretch direction than it is in the width and thickness direction. The results of finite element analysis performed [24] on the specimen geometry show that the sample has to be at least 10 times longer than the width or thickness [24].

Due to the geometry of the golf ball components (core, cover etc.) it has not been possible to produce compression or planar samples for the cover. Monk [31] made attempts at characterising the cover material in compression but due to curvature and size of the samples is was problematic to gather any useable material data. Another complication of testing the cover in compression is the presence of dimples. Dimples are small indentations on the ball that alter the aerodynamic properties of a golf ball. They naturally cause complications in

compression testing because they result in the sample having varying thickness. Planar tests measure material shear behaviour [30] but require a wide flat sample. It hasn't been able to obtain a testable sample of correct geometry due to the curvature of the cover.

## 3.3    Experimental Procedure

### 3.3.1    Compression

It was decided during the testing phase that it would be more advantageous to focus on the core testing, both in FE analysis and verification. Since the core of the chosen two-piece golf ball is, by far, the largest component it was important to validate its behaviour before focussing on cover material properties. Initial testing also focussed on near normal impact, during which cover properties are deemed to play less of a role. A Zwick uniaxial test machine was set up for compression with the appropriate compression platens attached. The first stage was to calibrate the machine's position. The compression plates were moved into contact and a grip-to-grip separation of 0mm was entered. This allowed a starting position to be set relative to the 0mm grip-to-grip separation. Due to the uncertainty in the sample geometry it was decided to pre-load the sample to 100N, this would ensure that the top and bottom faces were parallel and the contact area was consistent. In order to prevent the sample from bulging and allow it to expand in the lateral direction, PTFE tape (BS 7786: 1995 Grade L) was introduced between the sample and the compression platens (Figure 3.3-1).
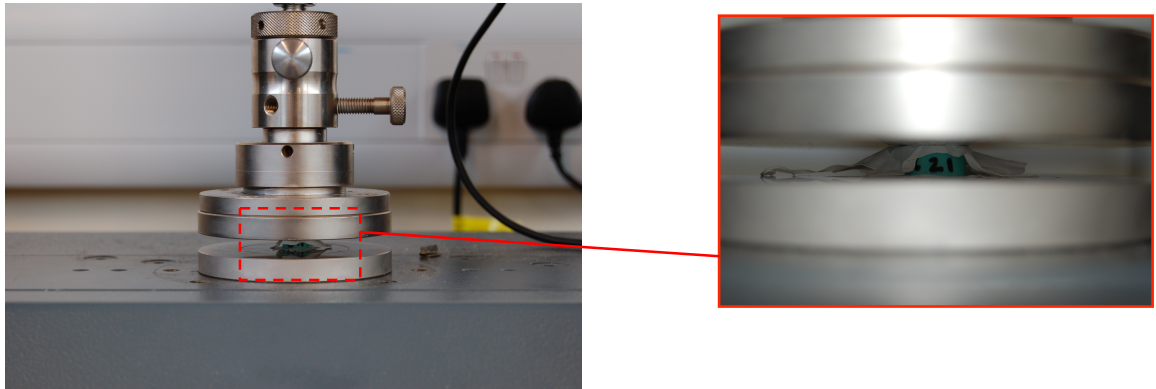
**Figure 3.3-1 – Compression test set-up. Detailed image showing position of PTFE tape.**

A compressive strain of 20% was applied based on the sample height. A strain magnitude of 20% was selected in line with Quintavalla [20]. During golf ball impact, strain greater than 20% is only seen at impact velocities close to 50m/s so for this part of the study 20% strain was deemed sufficient. The initial strain rate was 0.008 $s^{-1}$, this rate was chosen as it matched the strain rate used by Mase and Kersten [16]. It should be noted at this point that the strain rates experienced in golf ball impact can range from 400 $s^{-1}$ up to close to 1000 $s^{-1}$ based on a total contact time of 0.5ms and strains up to 20% however in this preliminary study the strain rates range from 0.0008 $s^{-1}$ to 0.08 $s^{-1}$

Cyclic compression was utilised in the experiment and 6 cycles were selected to allow any stress softening to take place. It is reported that the stress-strain graph for polymer materials stabilises after between 3 and 20 repetitions [24]. Given the time scale of the individual tests it was decided to run each sample through a programme of 6 conditioning cycles. The TestXpert software supplied

with the Zwick uniaxial test machine gave output of force, time, tool separation, standard travel, indentation travel and work. From these values the stress-strain curves were obtained. Engineering stress was calculated by dividing the reaction force acting on the plate by the initial cross-sectional area of the sample. The strain was calculated by dividing the change in sample length by the original, measured, sample height. Although equi-biaxial tension is preferred to compression [18][24], producing equi-biaxial test specimens and measuring strain in two dimensions was not possible due to sample geometry and equipment availability. Every care was taken to avoid the "bulging" effect and allow pure compressive strain to be captured, however it is probable that there was some material shearing present.

### 3.3.2 Tension

Due to sample geometry restrictions discussed previously, it was decided to perform tensile tests on the cover of the ball at this stage and not the core. The sample geometry allowed a 20mm gripping area at each end of the sample, which still allowed the correct length to width and thickness ratio for pure tensile strain. Pilot tests revealed that the sample was prone to slipping in the grips as the tensile force increased. To prevent the slipping from occurring medium grade sand paper was introduced between the clamp and sample (Figure 3.3-2). Lines were marked on the sample and aligned with bottom of the clamps to monitor any slippage that may have occurred.
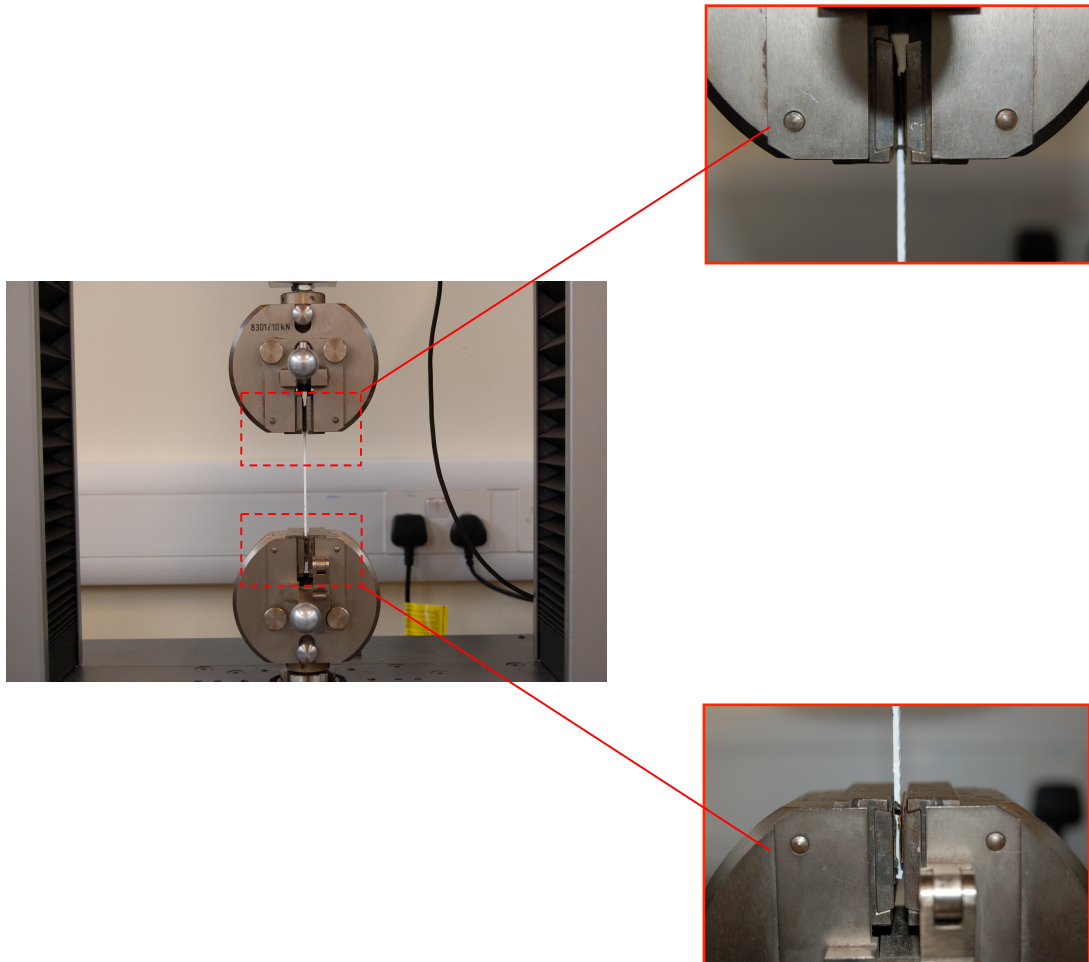
**Figure 3.3-2 – Experimental set-up for tensile tests on ball cover.**

A tensile 5N pre-load was applied to the sample to ensure there were no visible kinks.

In pilot tests, the ionomer cover snapped during the 20% strain cycles. From this result it was decided that the tensile testing would strain the sample to 5% through 6 cycles to see if there were any signs of plastic deformation. A gauge length of 40mm was marked on the specimen and re-measured at the end of the test. The overall sample length was also measured before and after the test. A strain rate of $0.008s^{-1}$ was selected in agreement with the compression tests. As

the data collected was for material model calibration and not representative of the strain rates observed in golf ball impact the actual rate used was not of concern. The emphasis was more on collecting data at a range of low strain rates.

### 3.3.3 Stress Relaxation

The tensile and compression tests described above are used to characterise the non-linear elastic response of a material, this is known as the hyperelastic response. As discussed in Chapter 2, polymer materials exhibit viscoelastic behaviour. Material relaxation data is necessary data to characterise viscoelasticity in ABAQUS using the Prony series expansion discussed previously (Equation 2.2-4).

An ideal relaxation test would involve a step change in strain and monitor the change in reaction force with respect to time. In practice, however, this step change is extremely difficult to achieve. The maximum strain rate possible from the Zwick apparatus used in this study was 16.66 mm/s. Before the relaxation characteristics of the specimen were investigated 3 conditioning cycles were performed. Each cycle strained the specimen to 20% at a rate of $0.008s^{-1}$ as used previously for the conditioning cycles. The relaxation test involved straining the specimen to 10% at a rate of 16.66 mm/s (which was the fastest deformation rate obtainable from the apparatus) and holding at that value for 300s. The load was then removed and the sample allowed to recover for 300s. A 20% strain was applied at a deformation rate of 16.66 mm/s and held for 300 s. During the

maintained strain the reaction force on the compression platens was monitored with the respect to time. At a rate of 16mm/s, the 10% strain was reached in approximately 0.3s. Given the hold time of 300s, it is reasonable to assume that the rate used to apply the load is instantaneous. Figure 3.3-3 displays a plot of plate displacement against test time.
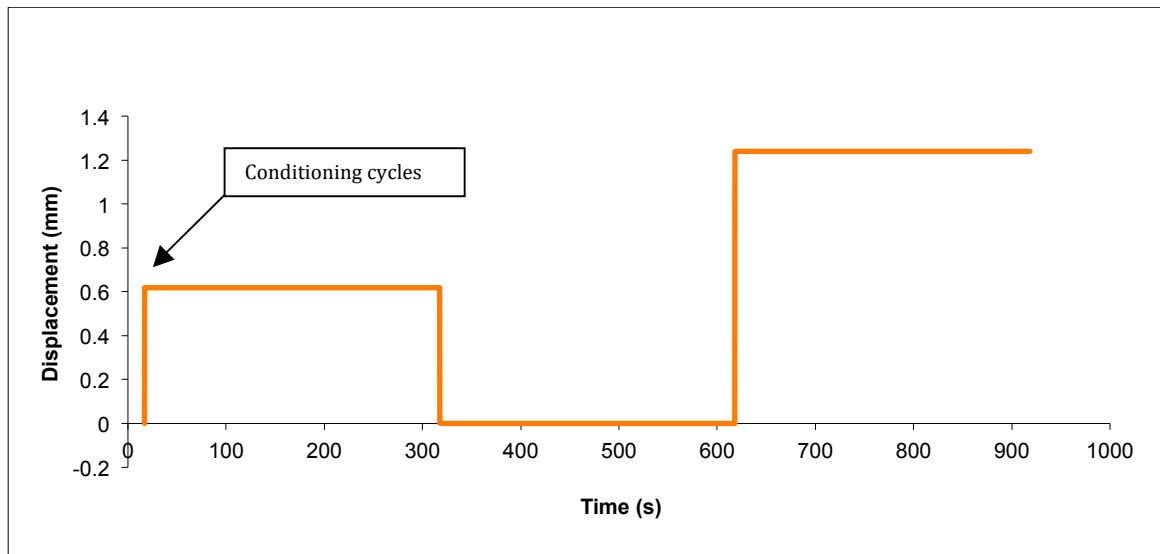


Figure 3.3-3 - Time-displacement graph for a relaxation test.

A test run time of approximately 1000 seconds meant that it was not possible to perform repeatability tests due to time constraints. Compression samples from the centre, inner and outer of the core were investigated.

The cover was also tested in relaxation following the procedure described above, with the only difference being the deformation mode. For the cylindrical core samples, the test was performed in compression and for the cover samples the test was performed in tension. Another major difference between the core and cover tests was with regard to the strain levels used. Based on previous

tensile results for the cover, the cover samples experienced 5% strain followed by 10% strain instead of a 10% strain followed by a 20% strain. This was to avoid plastic deformation of the cover material.

## 3.4   Summary

This Chapter introduced the tests carried out as part of the first phase of experimental investigation. A methodology for producing small cylindrical test specimens from a variety of locations within a golf ball core was developed. This allows multiple sets of material data to be characterised for the golf ball core, capturing the material heterogeneity present. A method for obtaining cover tensile samples was also reported. The data provided by the tests explained above will be illustrated and discussed in the following Chapter. The compression data will be used to calibrate hyperelastic material models, examine material rate dependence and quantify property differences between outer inner and centre samples for the core. The relaxation tests would provide information on whether the material is linear or non-linear viscoelastic and the data will be used to calibrate the Prony series model if deemed to be suitable. If the core could be accurately modelled, the tensile data from the cover tests would be used to calibrate material models to represent the cover of the ball.

# 4 Results and Discussion of Experimental Investigation - Phase 1

Having performed a variety of material tests, reported in Chapter 3. Chapter 4 presents and discusses the results obtained.

## 4.1 Small Sample Compression Test Results

### 4.1.1 Mullins Effect

As discussed in Chapter 2, it was expected that Mullins stress softening would be evident in the compression tests. The samples were processed through a programme of six load-unload cycles, with the aim of sufficiently softening the sample to a stabilised state. The aim was to establish a stabilised material response for material calibration. Figure 4.1-1 shows the results from a typical small sample cyclic compression test, exhibiting the Mullins effect.
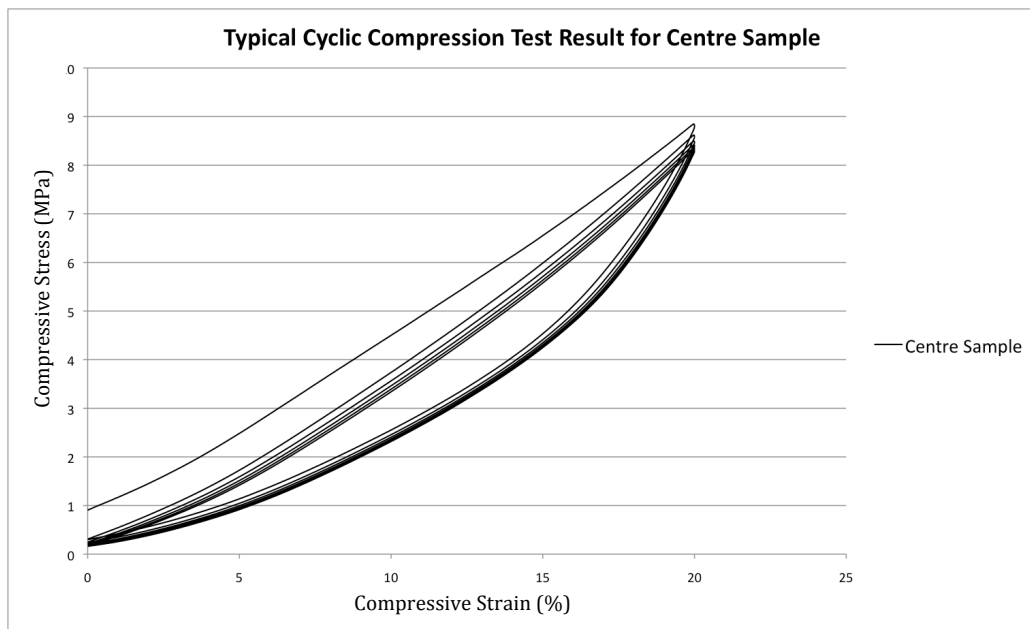


**Figure 4.1-1 – Stress-strain plot from cyclic compression tests.**

It can be seen that the data starts at approximately 1MPa, this is due to the initial 100N pre-load that was applied to the sample. The sample gradually softens with each cycle, as the internal structure changes [12] and converges towards a consistent stable hysteresis loop. Figure 4.1-2 is a representation of the stress- strain curve convergence through the six loading cycles.
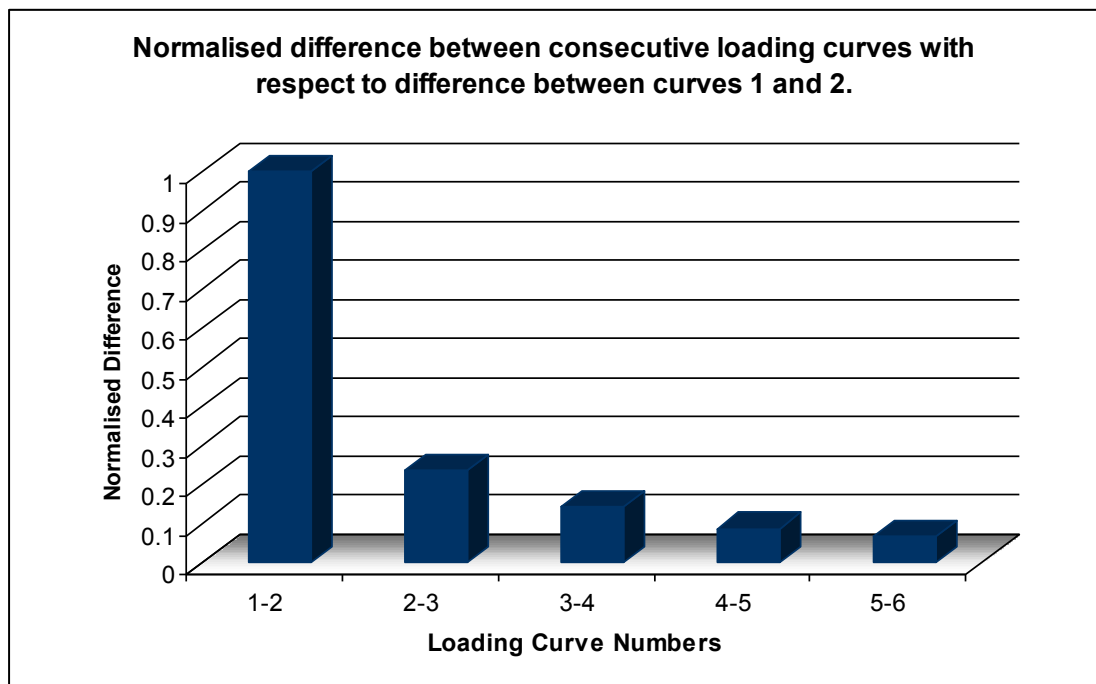


**Figure 4.1-2 - Convergence of loading curves for core compression samples.**

If the difference between loading curves one and two is taken to be 1, the differences between curves two/three, three/four, four/five and five/six are examined in relation to this original normalised difference. The difference between two curves is calculated using the following formula:

$$d = \frac{1}{N} \sum |y_2 - y_1|,$$

<div align="right">**.....Equation 4.1-1**</div>

Where $d$ = difference, $N$ = number of points , $y_2$ = y value of a point on the secondary curve and $y_1$ = y value of a point on the primary curve. This therefore refers to stress (at a particular strain) as a difference.

The relative differences between curves four/five and five/six indicate that the sample has softened sufficiently and converged to a final stable solution. This result agrees with the literature [24] that states the response of a polymer material should stabilise between three and twenty load cycles.

### 4.1.2   Comparison of Centre, Inner and Outer Core Samples.

Mullins effect was observed in all samples from the three locations within the core. Figure 4.1-3 shows the loading curves from the centre samples compared with the results from the inner and outer samples.
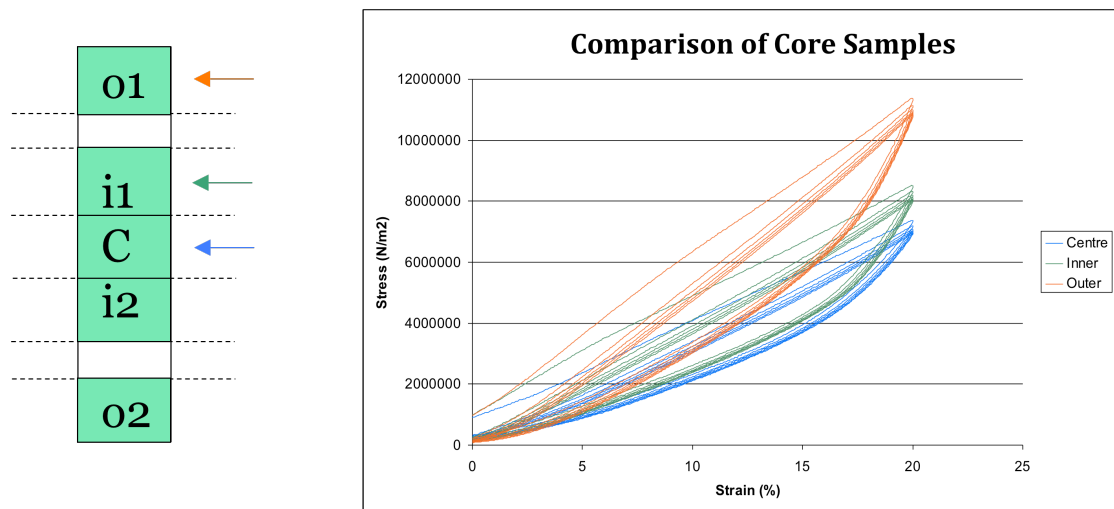
**Figure 4.1-3 - Stress strain plots for centre, inner and outer samples.**

The behaviour shown in Figure 4.1-3 is in agreement with published literature ,Johnson [12], and clearly shows the stiffening of the samples with increased distance from the centre of the ball core. This result further highlights the material heterogeneity present in the golf ball core and emphasises the potential need to include this variation into future FE models of the golf ball.

### 4.1.3 Core Repeatability

Having performed compression tests on small cylindrical samples obtained from three different golf ball cores of the same model, one of the primary concerns was the repeatability of the samples material behaviour between golf ball cores. As the balls are manufactured specifically for calibration it was expected that the centre, inner and outer samples removed from the cores would be fairly consistent with one another. The repeatability, as it is later referred to, is a measure of how repeatable the samples removed from similar locations in different golf ball cores are. Samples were prepared from three separate golf ball cores, the method, location and size of these samples was kept

consistent in order to compare the stress-strain responses. Figure 4.1-4 shows the repeatability, in terms of stress strain response, of samples removed from the centre of the core. Only one centre sample was available from each ball due to their position within the core. The data presented is from the sixth loading/unloading cycle. It was decided to use this data set as the stress strain function would have suitably stabilised to a final solution as shown in Figure 4.1-2, which represents a typical result experienced for all samples.
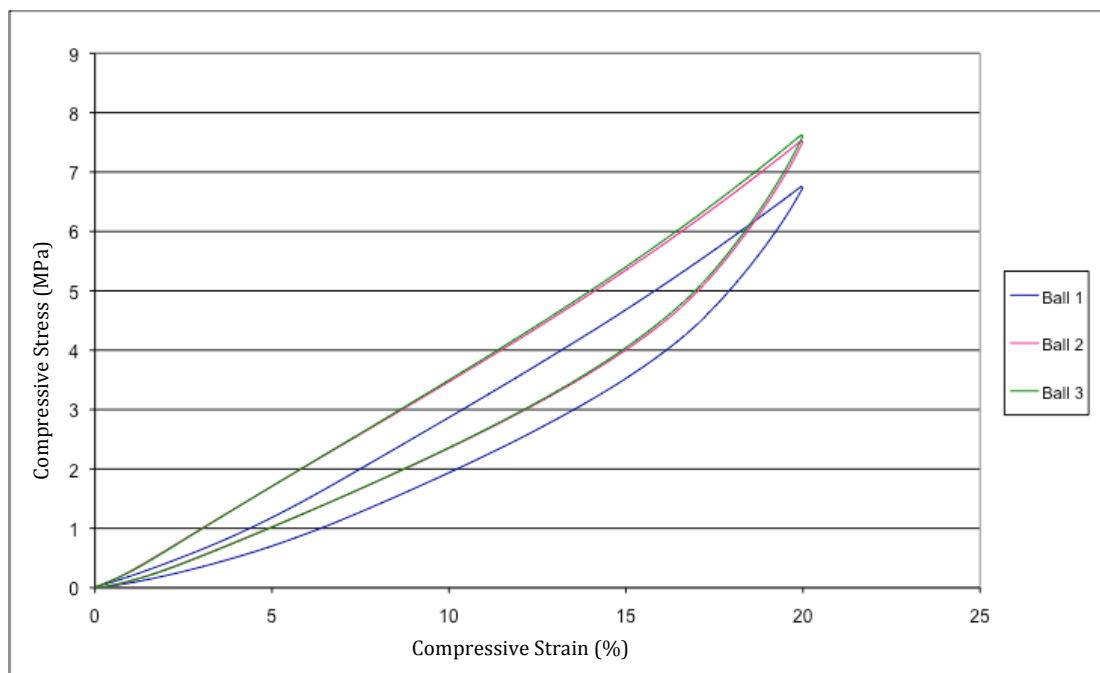


**Figure 4.1-4 - Repeatability of small centre samples between balls.**

Figure 4.1-4 shows that the sample removed from Ball 1 produces a stress strain curve substantially different to that of Balls 2 and 3. This error was thought to have been the result of poor experimental practice or a manufacturing difference with Ball 1 as the results from Balls 2 and 3 are consistent with each other. The data gathered from this compression test was for use in material model calibration so a data set that best represented the

overall behaviour was selected. The data from Ball 2 was selected to represent the behaviour at the centre of the core.

The comparisons that can be drawn for the small samples from the inner and outer locations are somewhat different to the centre samples. This is due to there being two inner and two outer samples produced from each ball. The manufacturing process that golf ball cores experience suggests that the properties at a certain radius from the centre of the ball should be similar. To confirm this, the two inner samples from one core were compared with each other to examine repeatability within the core and the six inner samples from the three cores were compared against each other to examine repeatability between balls. Figure 4.1-5 shows the loading curves of all six small core samples from the inner location, plotted on the same graph. The naming convention used in the legend of Figure 4.1-5 refers to the ball number and sample location. Due to the production method of the compression samples there were two inner and outer samples per ball, as discussed in Chapter 3. The number assigned to the location was used primarily for identification.
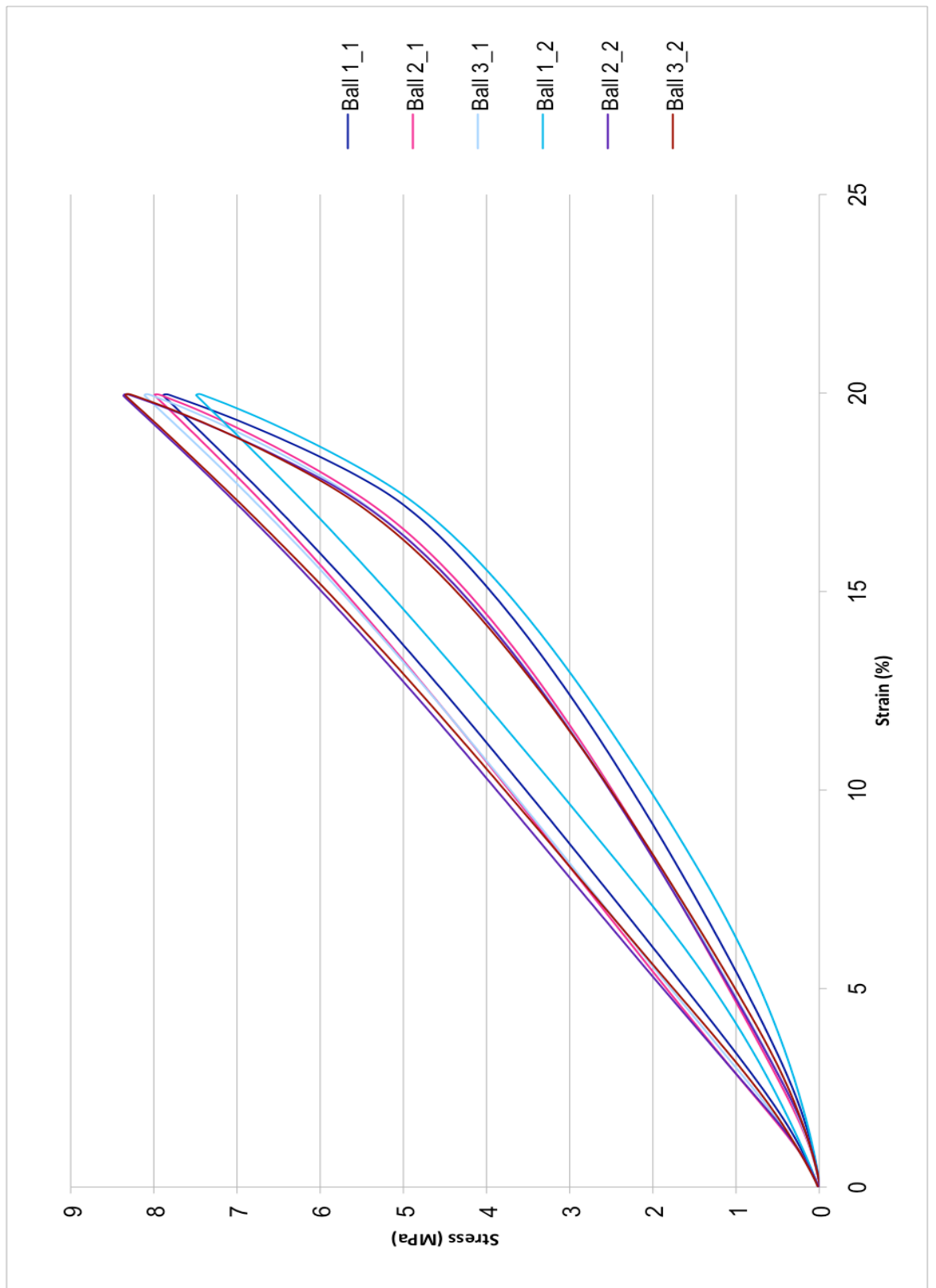
**Figure 4.1-5 - Variation of inner sample stress strain response for balls and location.**

Comparisons are going to be made at three locations in three balls. It aims to investigate the repeatability of the inner and outer samples within one core and also examine the repeatability of similar samples from different balls. Examining Figure 4.1-5 it can be seen that the inner samples are, in general, fairly repeatable. As highlighted in Figure 4.1-4 (centre samples), ball 1 produces responses that are noticeably softer to the others. This behaviour was also observed in the inner sample tests shown in Figure 4.1-5. It was initially assumed to be experimental inaccuracy however based on the results shown in Figure 4.1-5, it suggests that there may be manufacturing difference, in terms of the internal structure of ball 1.

As with the centre sample investigation, one set of data from the inner samples was chosen to calibrate the material model. It was therefore a requirement that this data set represented the average response of data set. Sample 2_1 (Ball 2, location 1) was chosen as it represented the average stress-strain response. The small differences observed can be attributed to manufacturing errors and experimental error. Figures 4.1-6 to 4.1-8 show the inner sample responses from each of the three balls to establish if the samples are repeatable in terms of location within the core of each individual ball. Hence in Figure 4.1-6 the loading curves from the inner samples from ball 1 at locations $i_1$ and $i_2$ are plotted on the same graph for comparison. Similar plots from Ball 2 and Ball 3 are given in Figures 4.1-7 and 4.1-8 respectively.
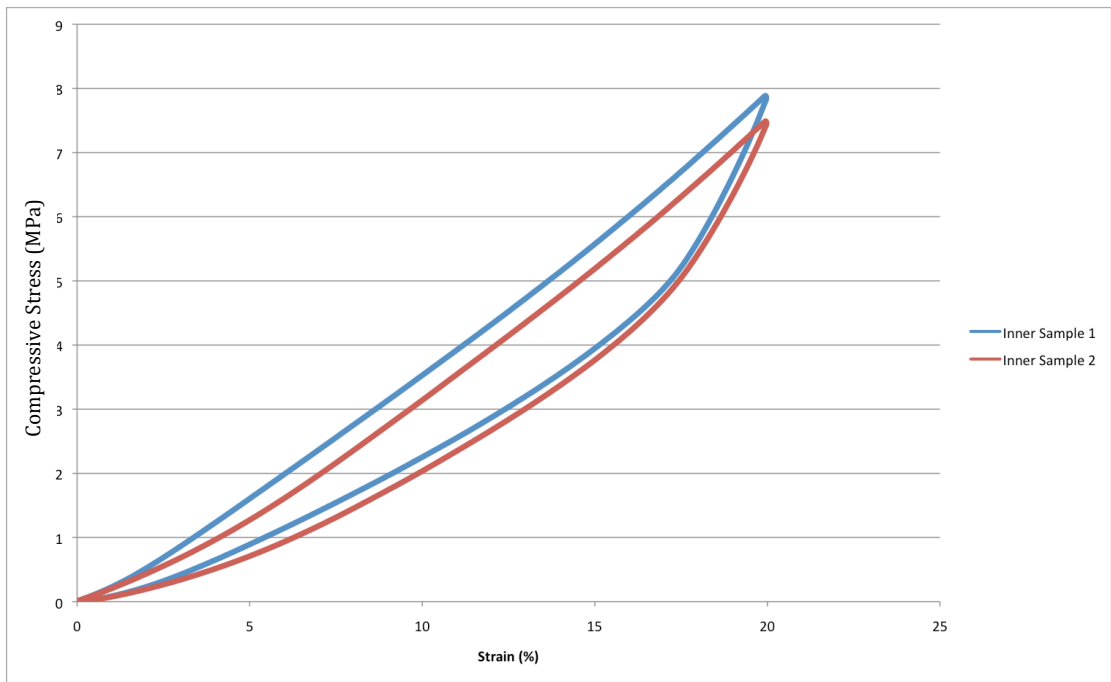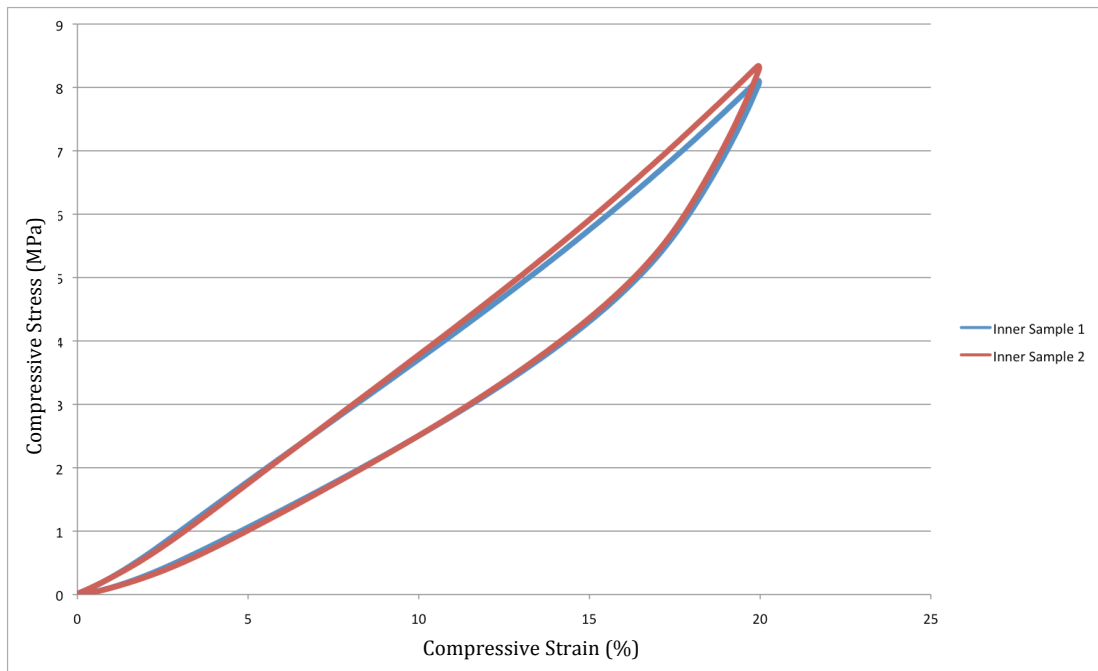
**Figure 4.1-6 - Inner sample responses from Ball 1.**
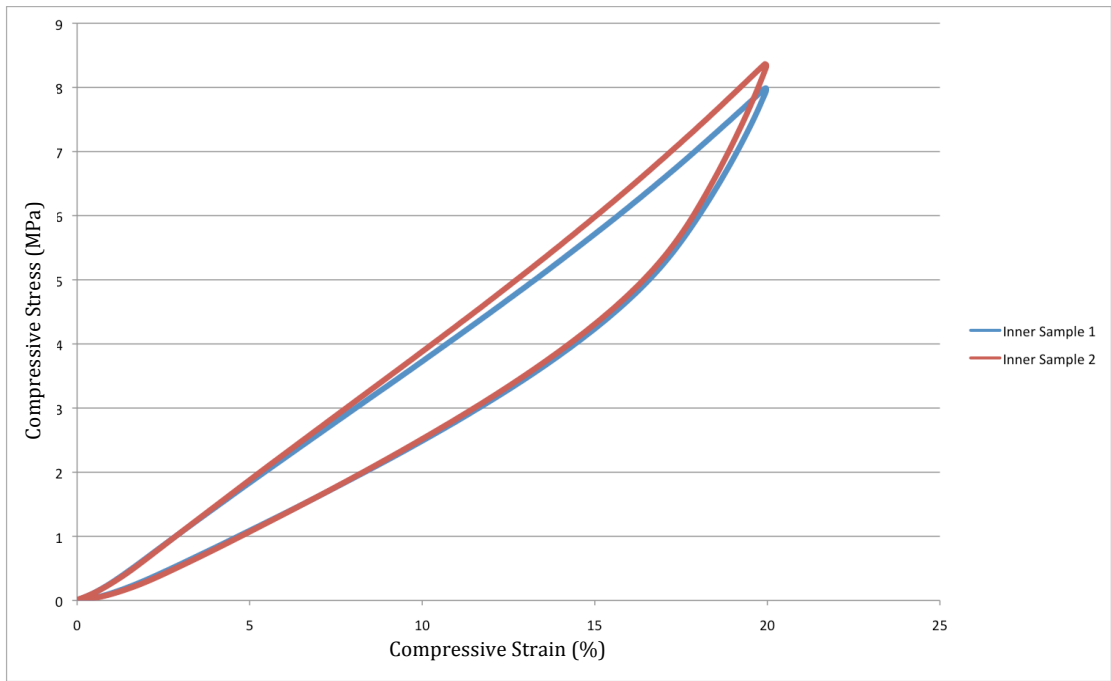


**Figure 4.1-7 - Inner sample responses from Ball 2.**

**Figure 4.1-8 - Inner samples responses from Ball 3.**

The above figures highlight that although there are slight differences in the response of the inner samples they are generally quite repeatable. The naming convention employed does not assume that all samples from location 1 are comparable. It merely gives an indication of differing samples for experimental purposes. There is no way to know the orientation of one core to another, in other words there is no way of ensuring that the direction and position of the inner samples are consistent with one another. The distance from the centres, however, is known to be equal between samples. As previously stated, these slight errors can be associated with experimental and manufacturing uncertainties. The properties at certain points throughout the core could be a result of heat dissipation differences. The moulds that shape the ball core experience an applied pressure and heat, this heat then dissipates through the ball during the curing process. It is also considered that the orientation of the

core in the manufacturing process may have an effect on the properties of the removed sample. Figure 4.1-9 shows that if one core (providing samples $i_1$ and $i_2$) is rotated through 90 degrees in relation to another core (providing samples $i_1^*$ and $i_2^*$) the inner samples will be further from the heat source hence will experience less heat energy throughout the manufacturing process.
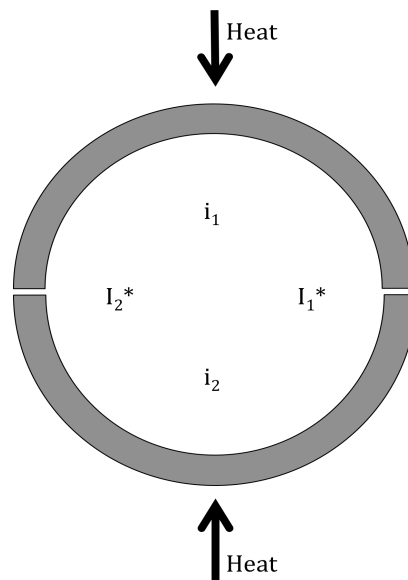


**Figure 4.1-9 – Diagram depicting application of heat to golf ball moulds during manufacture.**

If the internal structure of the ball is slightly different, the rate at which the heat dissipates through the core will vary also leading to material property differences.

The outer samples (locations $o_1$ and $o_2$ in Figure 4.1-3) were examined using the same procedure as applied to the inner samples. Figure 4.1-9 shows the responses of the six samples, it was expected that the outer samples would be the most repeatable as they are nearest to the heat source and less dependent on the dissipation of heat through the core of the ball.
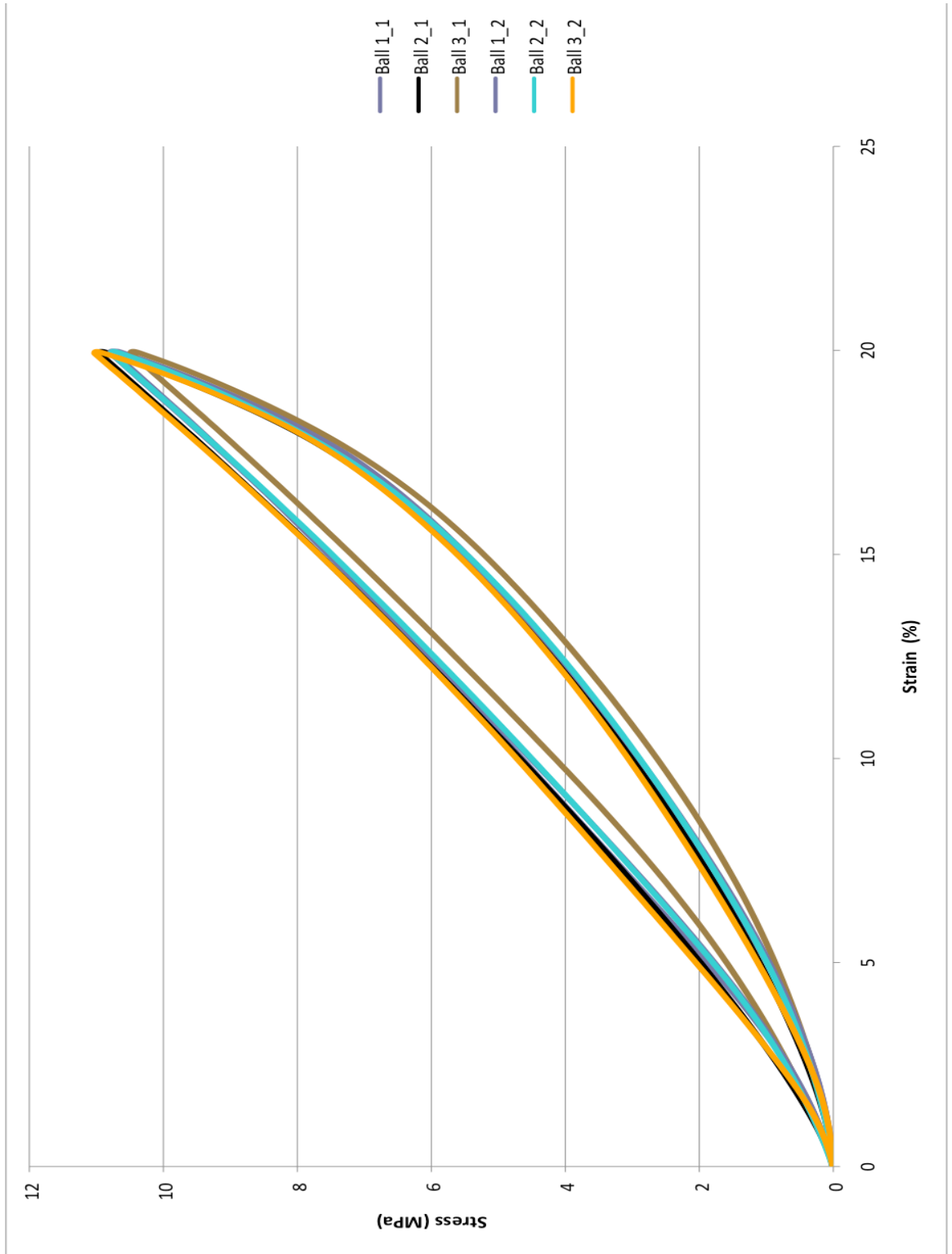
**Figure 4.1-10 - Variation of outer sample stress-strain response for balls and location.**

Figure 4.1-10 clearly shows the increased average stiffness of the samples due to the exposure of higher temperatures for longer durations. As expected, the samples are, in general, more repeatable. There is less variation between stiffest and least stiff samples. Interestingly, the outer samples from Ball 1 are repeatable with the outer samples from Balls 2 and 3, with an exception in regards to the outer sample from Ball 3, location one which is less stiff than the others. Again this is likely to be a result of the curing experienced by the core or manufacturing and experimental uncertainty. The data from sample 1_1 was selected for material model calibration as its response represented the overall response of the outer samples data set, as in it fell within the range of stiffness values.

As with the inner samples the outer samples were investigated for repeatability of the load cycle in terms of location within the core. Figure 4.1-10 shows the response for the two outer samples produced from Ball 1.
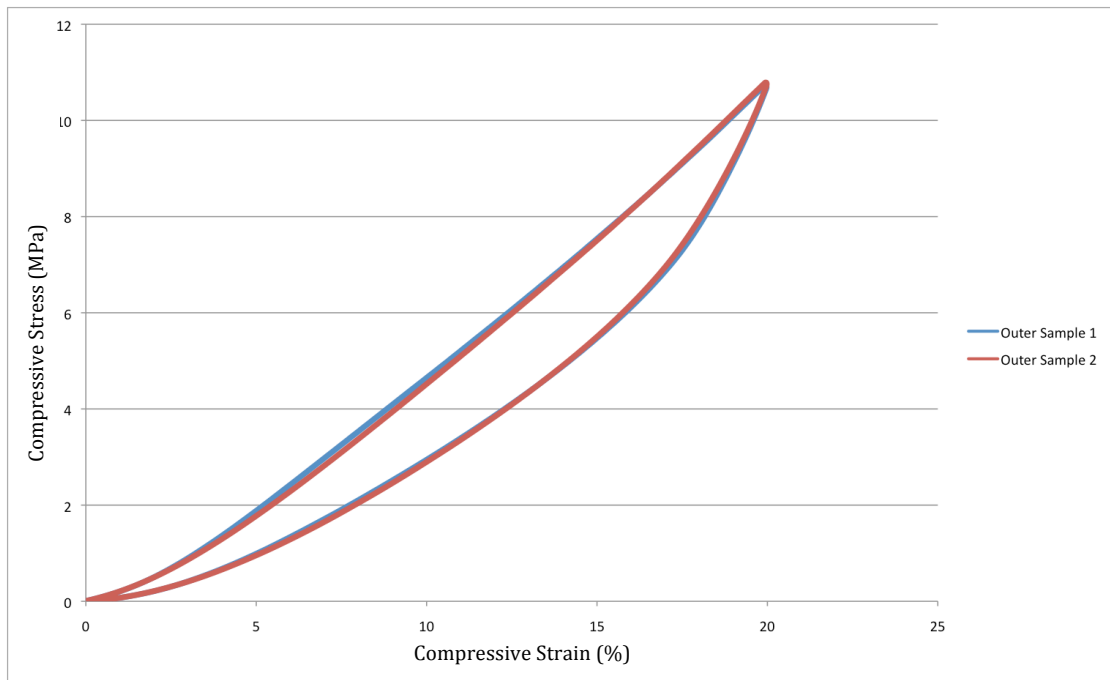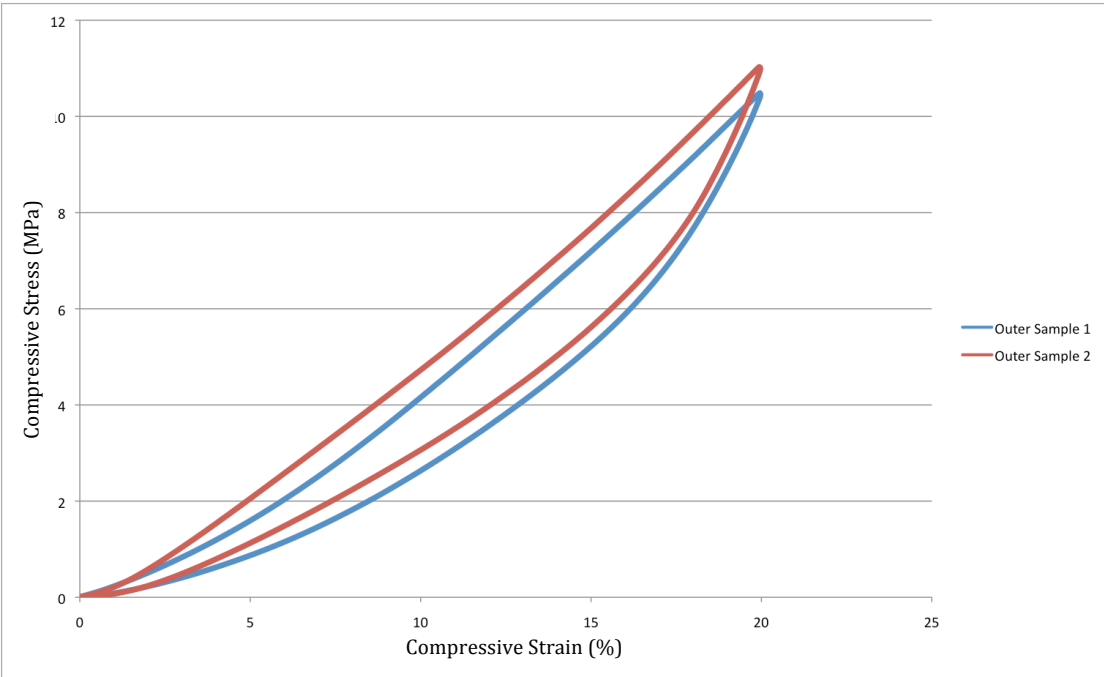
**Figure 4.1-11 – Outer sample responses for Ball 1.**

As expected, the results from the outer samples tend to be more consistent than the results reported for the inner samples. This increase in consistency over the inner samples is likely to be a result of less material between the sample and the core moulds, as discussed previously.

The results given in Figure 4.1-12 contradict the trend shown in Figures 4.1-10 and 4.1-11. Referring back to Figure 4.1-9 it can be seen that sample "Ball 3_1" produces a response that is noticeably less stiff than the other 5 outer samples. Therefore it would point to this difference being associated with the preparation of sample "Ball 3_1" or experimental uncertainty and not a true representation of material behaviour. Ignoring this one sample, the other five show good repeatability as expected from their proximity to the heat source.
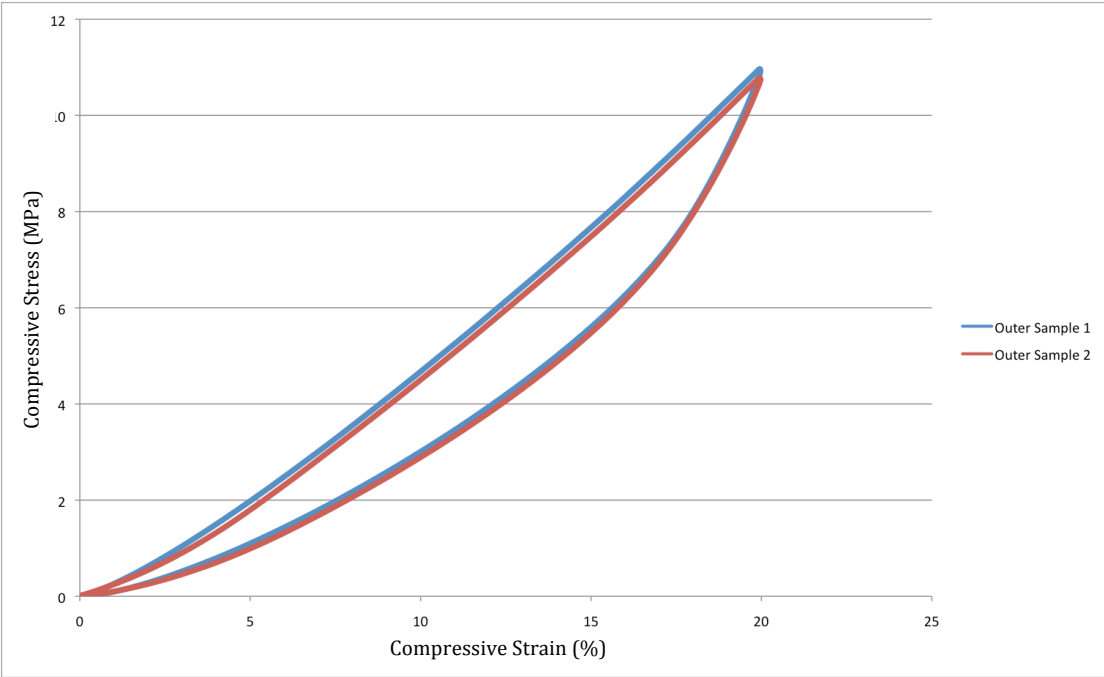
**Figure 4.1-12 - Outer sample responses for Ball 2.**



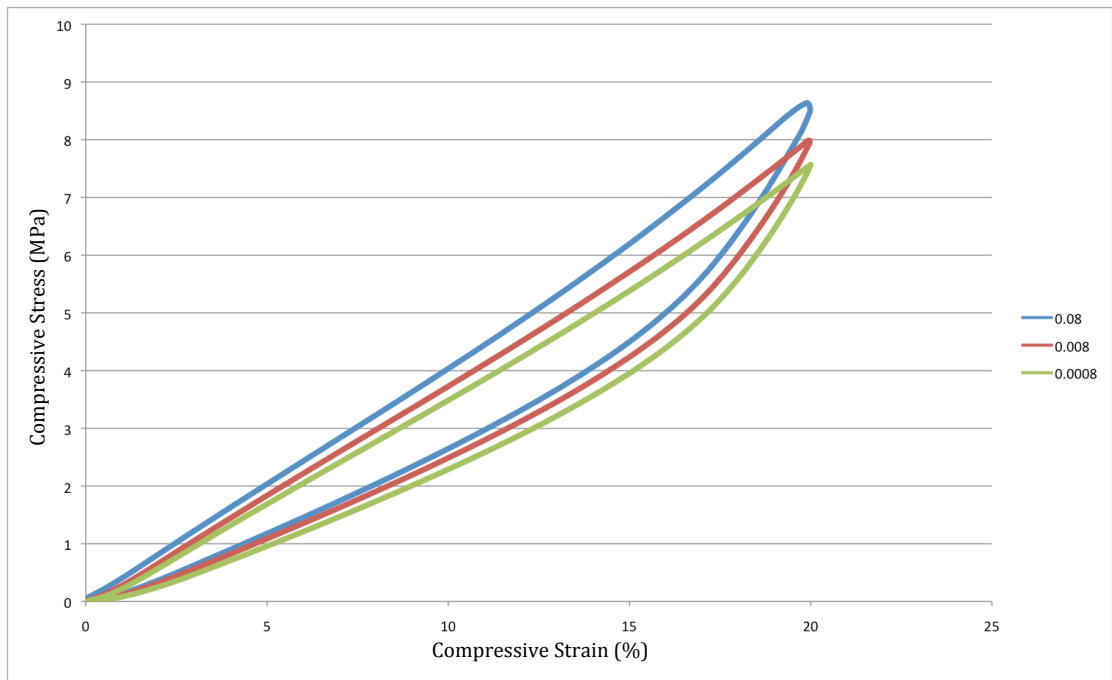**Figure 4.1-13 - Outer sample responses for Ball 3.**

### 4.1.4 Rate Dependence

As discussed in previous Chapters, a common characteristic of the materials used in golf ball construction is their rate dependence. Rate dependence simply means that the stress-strain response of the material differs depending on the rate at which the sample is loaded. The centre, inner and outer core samples were loaded at strain rates of $0.0008s^{-1}$, $0.008s^{-1}$ and $0.08s^{-1}$. In order to determine and display the rate dependence of the samples the results from the three loading rates were plotted against one another. Figures 4.1-13 to 4.1-15 display the outcomes.
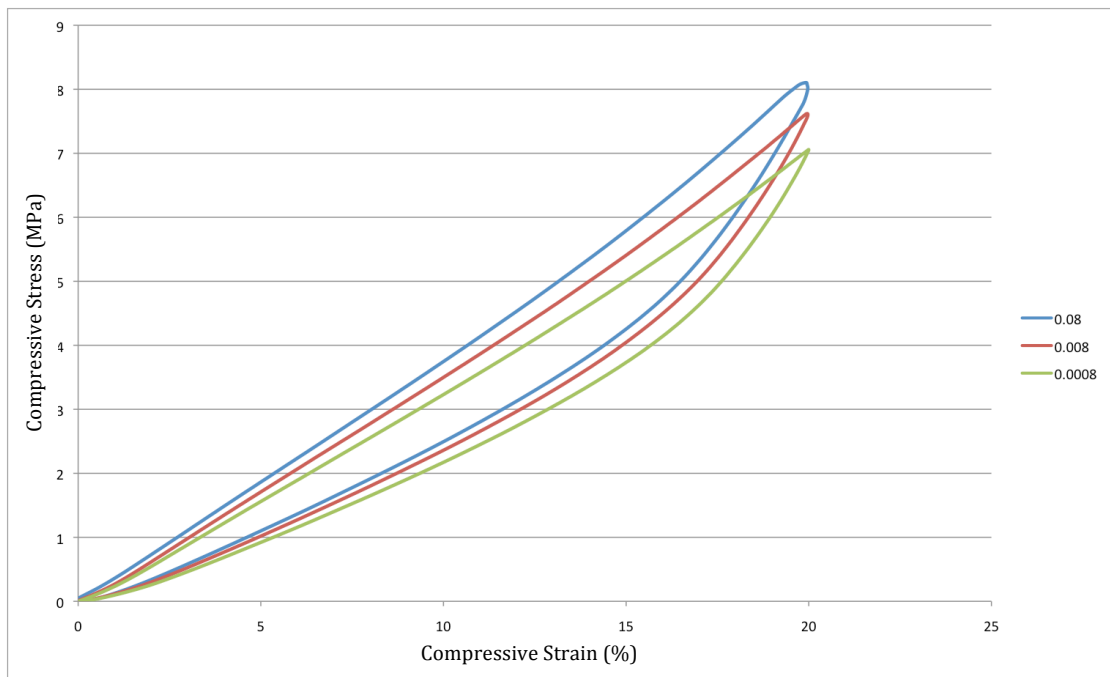


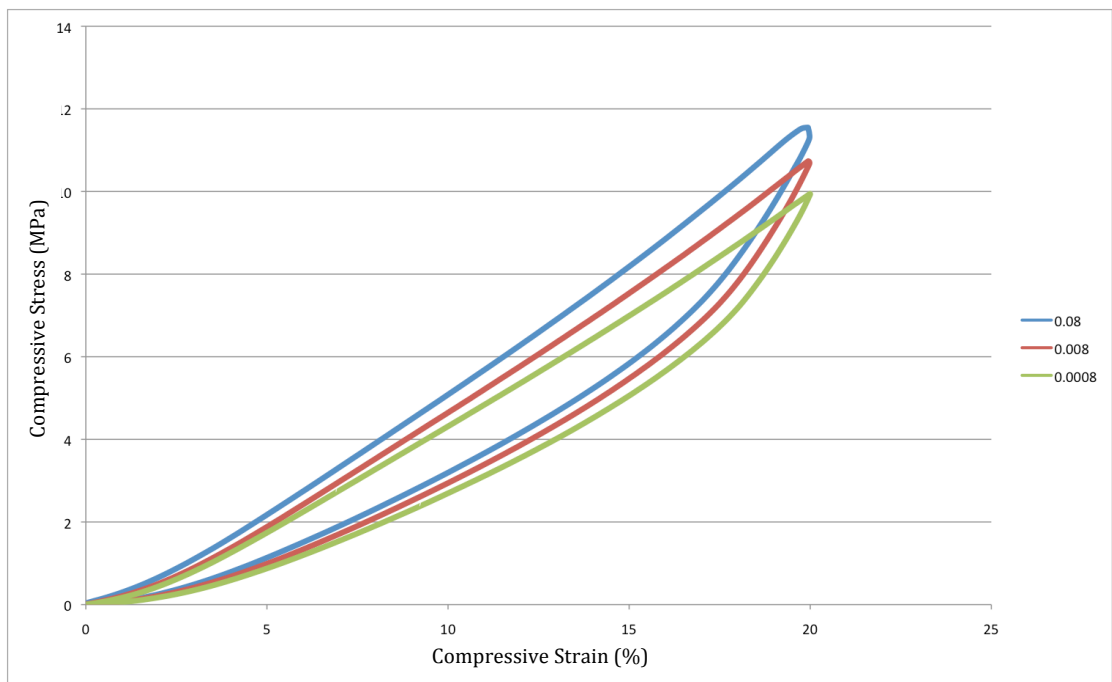**Figure 4.1-14 - Rate dependence of centre core samples for Ball 2.**

**Figure 4.1-15 - Rate dependence of inner core samples for Ball 2.**



**Figure 4.1-16 - Rate dependence of outer core samples for Ball 2.**

The rate dependence of the material is shown in the above figures. As expected the response at the fastest strain rate showed the stiffest behaviour. This was the case for all three balls.

## 4.2 Cover Sample Tensile Tests

The bulk of this testing phase was focussed on obtaining enough accurate and reliable data to successfully characterise the core material from the ball but a few simple tests were carried out on the cover material to determine whether the model used by Tanaka et al [13] was suitable. As discussed previously, Tanaka described the cover material with a single hyperelastic material model. This would suggest that under cyclic loading the loading and unloading paths would follow each other. Using the procedure outlined in Section 3.3 of this thesis the results displayed in Figure 4.2-1 were obtained.
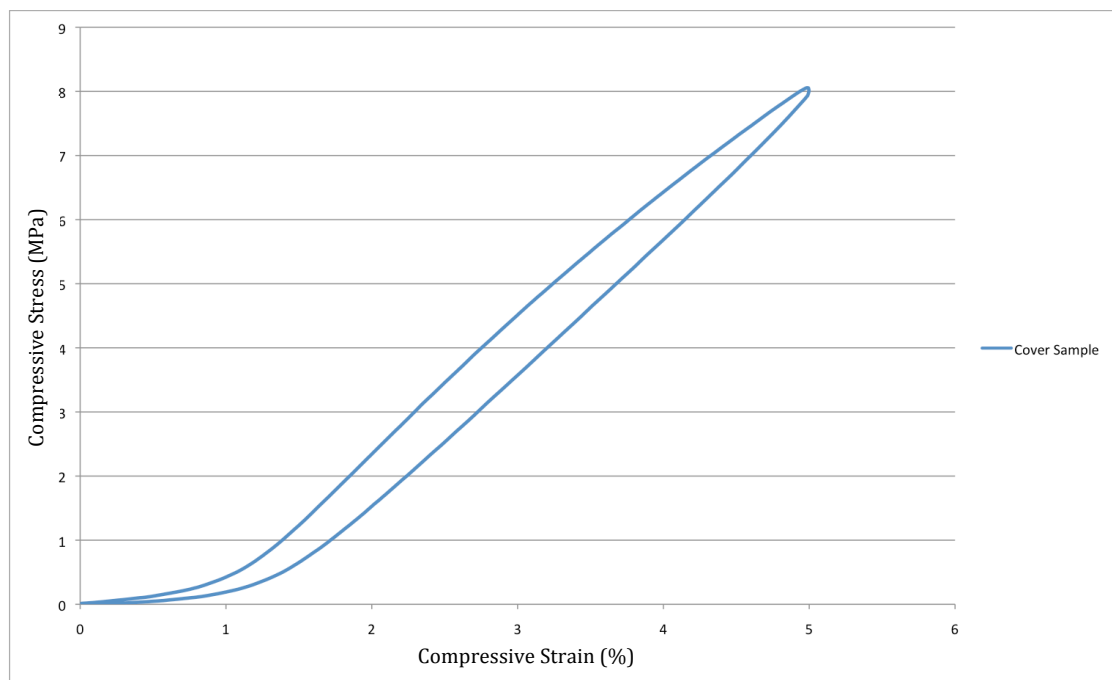


**Figure 4.2-1 - Typical material response for cover sample tensile tests.**

The hysteresis that is clearly present in Figure 4.2-1 suggests that a purely hyperelastic model is not sufficient for characterising the cover of the golf ball. Whether or not the inclusion of this is necessary is not yet known but from a

57

fundamental viewpoint, the model used to accurately describe the behaviour of the cover should include some degree of viscoelasticity.

## 4.3 Small Sample Relaxation Tests

As previously discussed in Chapter 3 relaxation tests were carried out in order to characterise the viscoelastic response of the material. Figure 4.3-1 shows the typical stress relaxation of a core sample. The blue line shows the stress response of the sample versus time and the red-dotted line shows a plot of the applied sample strain versus time.
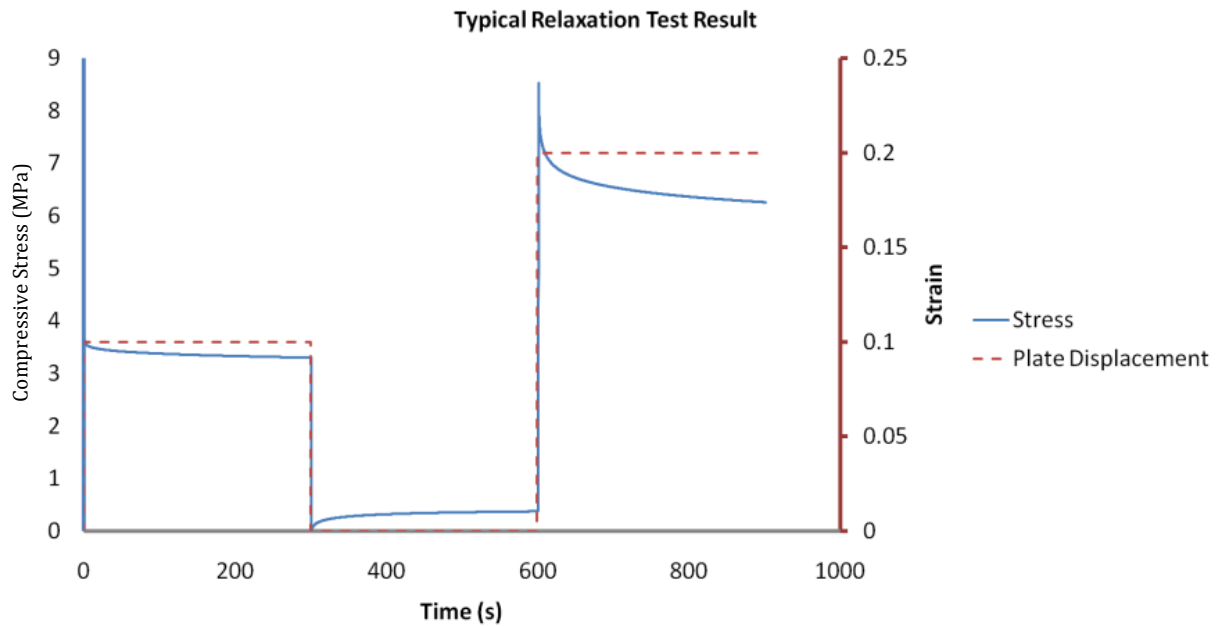


**Figure 4.3-1 - Typical results from core sample relaxation test.**

A description of the test is provided in Section 3.3 but to recap, a strain of 10% is applied to the sample and maintained for 300 seconds, during which the stress within the sample decreases. The applied strain is calculated based on

sample height and entered in the form of compression platen displacement whereas the stress is calculated from the reaction force the sample exerts on the compression platen. The area used for stress calculations is the initial cross sectional area of the sample therefore the stress calculated is engineering stress. This reducing stress with regards to time is known as relaxation. The compression platen is returned to the initial position and the sample is allowed to recover for 300s. A further strain of 20% is then applied to the sample and maintained for 300 seconds. As discussed previously, linear viscoelastic material models do not capture strain amplitude dependence [30]. Figure 4.3-1 shows that when the applied strain is doubled, the resultant stress does not. An applied strain of 10% yields a stress of 3.8 MPa whereas an applied strain of 20% results in a stress of 8.5 MPa. This shows that the resultant stress does not vary linearly with the applied strain. This characteristic suggests that the material is not displaying linear viscoelastic material behaviour therefore requires a more advanced non-linear viscoelastic material model to accurately represent the behaviour across a wide range of strain values and rates. Another observation that suggests a non-linear model may be better suited to the application regards the path of which the relaxation curve follows. The relaxation path linear viscoelastic materials follow is independent of strain magnitude [19]. This means that the relaxation path of the sample when a strain of 10% is maintained would be the same as the relaxation path when a strain of 20% is maintained. Looking at the results displayed in Figure 4.3-1 it can be seen that the relaxation paths differ depending on strain magnitude. To confirm this, the relaxation curves were normalised to a constant starting value and

plotted against each other. This was achieved by dividing the stress-values by the initial stress-value resulting in a starting value of unity for both cases. Figure 4.3-2 shows the result.
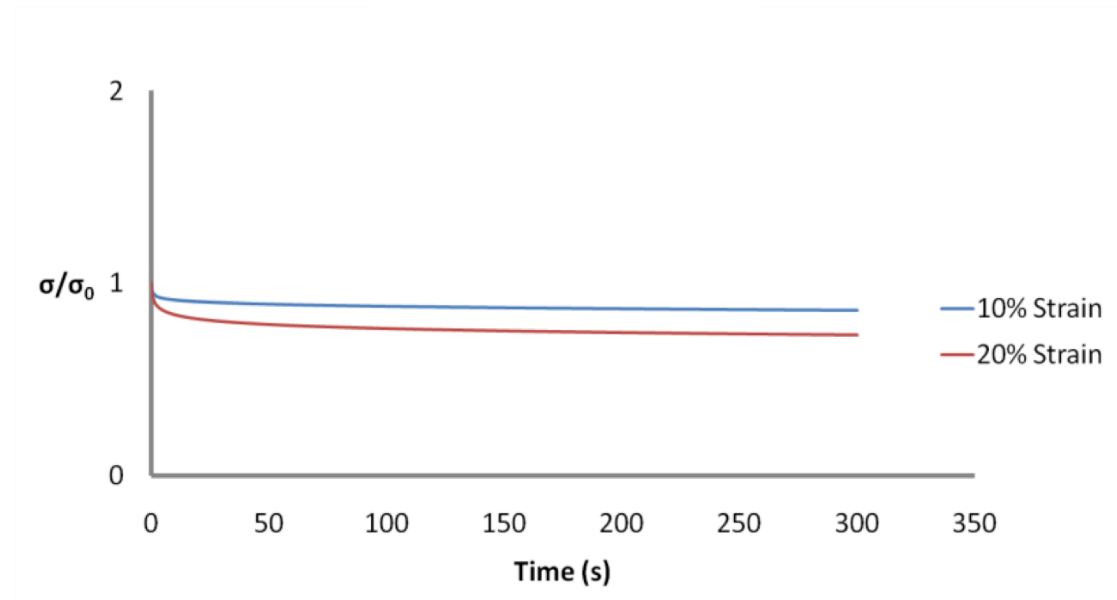


**Figure 4.3-2 - Comparison of normalised small sample relaxation curves.**

The scale of this difference is not critical; the important point is that there is a difference present between the relaxation curves, which confirms the non-linear nature of the material behaviour. With this material information and the goal of creating an FE model capable of predicting the core behaviour at quasi-static compression test strain rates along with the behaviour at impact speeds of 50m/s experienced in the golf ball impact event with the golf club, it was decided to investigate various non-linear viscoelastic material models.

## 4.4 Summary

The results of the experimental procedures outlined in Chapter 3 have been reported and discussed above. The repeatability of the small sample

experiments was shown to be fairly reliable although contained some rogue values. This variability was thought to be a result of manufacturing differences due to the heat energy dissipation through the core material or uncertainty within the experimentation.

Previous tests/analysis presented in the literature assume purely hyperelastic behaviour for the golf ball cover however the outcomes from the cover sample tensile tests contradict this modelling technique and show conclusively that viscoelastic behaviour is present in the cover material. Whether this change will yield more accurate results than already published is yet to be established but the presence of hysteresis in the cover under cyclic loading is clearly apparent and should be considered when developing a fully representative material model for use in finite element analysis.

The relaxation tests were initially carried out to provide data to calibrate the ABAQUS Prony series [18] however the results highlighted that a non-linear viscoelastic material model may be more suited to the material and golf ball application. The following Chapter discusses the modelling techniques employed; the material models investigated and presents results from finite element analysis on various golf ball core components.

# 5 Finite Element Analysis of The Small Cylindrical Samples, Golf Ball Core and Material Model Calibration

The finite element method dates back to the 1950's and the basic premise is very simple. No matter how complex a shape is it can be discretised into a number of small elements finite in size. These elements are then arranged in a specific order to allow continuous displacement from element to element. The resultant displacement field can then be approximated and from the magnitude of the displacement, strain and stress can be found. There are now many commercial finite element codes available on the market, which all vary in their level of functionality and ease of use. There are also many more in-house codes being continuously developed. The finite element method is now so widely used that it is considered standard practice within the field of structural engineering, and to this end the fundamentals of FE shall not be discussed herein. The most complicated element of the modelling process in this work is the modelling of the materials involved in the construction of the golf ball. As discussed, the materials show non-linear viscoelasticity, strain-rate dependence and strain dependence. The user defines these materials with specific material models containing various material parameters. In this thesis all material models, besides the linear elastic models, which were standard rubber properties, have been calibrated with actual material data obtained from golf ball cores. This process is described in detail in the following Chapter.

There are various commercially available FE codes currently available, based on previous experience and published literature the author chose to use ABAQUS v6.7 [32] as it provides both an implicit and explicit solver within its graphical interface. It was decided that both implicit and explicit solvers may be required, implicit for the low strain-rate compression tests and explicit if high strain-rate impacts were to be investigated. In ABAQUS all parts and assemblies can be constructed within ABAQUS [32] negating the need for external modelling software and it allows contact and large deformation modelling. Based on this it was decided that ABAQUS was the correct choice to perform the FE modelling required in this thesis.

The approach used for the finite element modelling presented in this thesis starts with the production of parts. These parts define the geometry of an item and detail the mesh used. The assembly module is then used to position the parts in relation to each other. The interactions between the various parts in an assembly are defined in the interaction module. To assign material properties to parts the user enters material data in the property module. Boundary conditions describe the motion of parts and are defined separately. With assembly, mesh, boundary conditions and material data in place the FE model is ready to simulate.

To summarise, any FE model consists of, a minimum, three areas: the model geometry which is meshed with finite elements, the material model and a set of loading and boundary conditions constraining the model. This Chapter details

the modelling techniques, material models and boundary conditions employed for the FE section of the work.

## 5.1 Boundary Conditions

### 5.1.1 Symmetry

With a spherical geometry it is beneficial to introduce symmetry boundary conditions as they reduce the amount of computational power required therefore reducing the time taken to simulate each model. Symmetry boundary conditions allow the user to model a portion of an object, in this study an eighth of a ball model was sufficient to study the deformation of the full core. Separate symmetry boundary conditions were applied to face A, B and C, as shown in Figure 5.1-1.
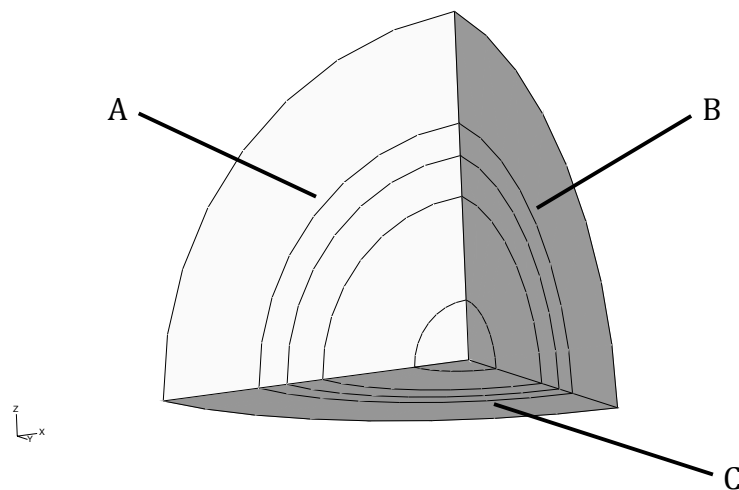


**Figure 5.1-1 – ABAQUS eighth of a ball core model.**

When the user applies a symmetry boundary condition ABAQUS applies constraints to represent this symmetry. For example, if symmetry in the Y-

direction was applied to a suitable face, ABAQUS would apply the constraints U2=UR1=UR3=0, where U represents displacement along a specified axis and UR represents rotation around a specified axis. This constrains the face so that movement in the 2-direction (i.e. the Y-direction) is zero, rotation around the 1-axis (UR1) is zero and rotation around the 3-axis (UR3) is zero. Figure 5.1-2 is a graphical representation of the constraints in place when Y symmetry is activated in ABAQUS.
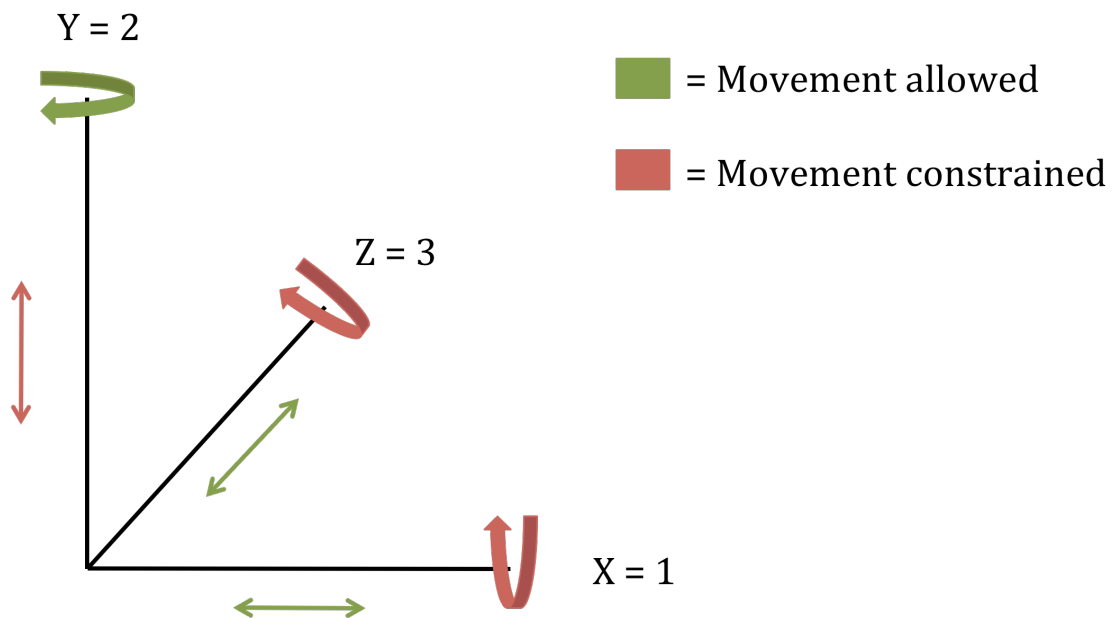


**Figure 5.1-2 - Graphical representation of Y symmetry boundary conditions in ABAQUS.**

Hence referring to figure 5.1.2, on face A symmetry in the x-direction was applied (U1=UR2=UR3=0), on face B symmetry in the y-direction was applied (U2=UR1=UR3=0) and on face C symmetry in the z-direction was applied (U3=UR1=UR2=0).

### 5.1.2 Platen Displacement and Simulation Steps

Each model involved the sample experiencing compressive loading from an analytically rigid plate, which will be discussed further in the following sections. Boundary conditions were used to describe the plates' motion throughout the analysis. An analysis consists of various simulation steps with each step having a defined time. A typical series of steps used in this work would include an initial step by default, a "contact" step to define the plate coming into contact with the sample, a "compress" step to define the plate compressing the sample, an "unload" step to define the plate releasing the compressive force and finally a "release" step to remove the contact between the two parts in the model. Displacement boundary conditions can be applied to the compression plate during each step to define its motion and because this displacement is applied over a defined time the rate of displacement is also known. The majority of simulations investigated in this work are comparable to experimentally obtained data therefore the step time and displacement can be taken from the experimental results and entered directly into ABAQUS. Figure 5.1-3 shows a complete simulation assembly, before meshing, for the core.
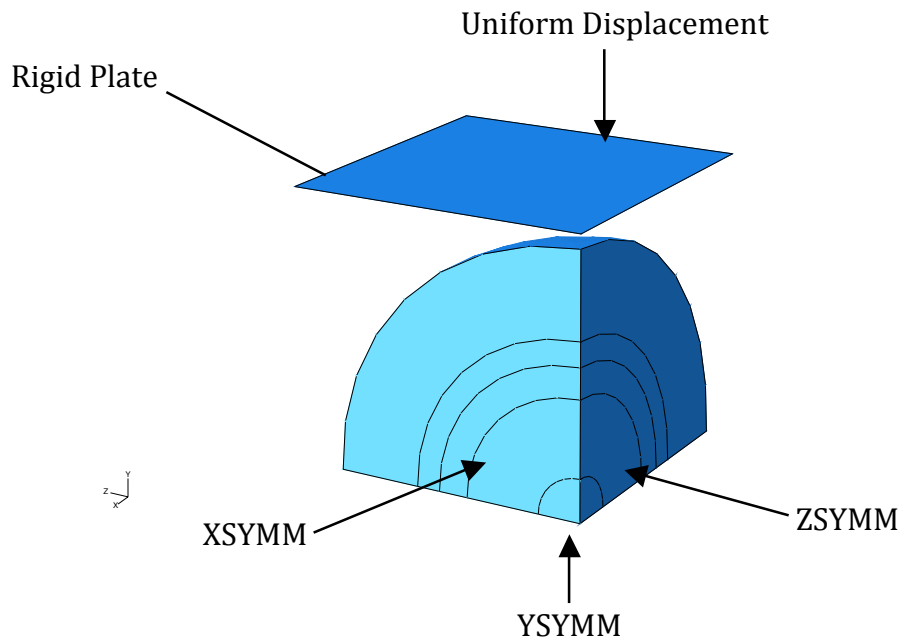
**Figure 5.1-3 - ABAQUS assembly, prior to meshing, for core compression simulation.**

### 5.1.3   Interactions

If the above simulation was solved in ABAQUS the plate would penetrate through the ball as no interaction has been defined in the model. Interactions allow the user to specify what separate parts within an assembly come into contact and where that contact will be. In the above model, 2 surfaces are defined on separate parts, the outer surface of the core and the bottom face of the plate. The user can control the behaviour of this contact and how it is discretised. For all the analysis in this thesis, surface-to-surface was the chosen discretisation method as it establishes relationships based on the defined surface rather than the nodes within the surface. Additionally, the user has to set the interaction property, which defines the mechanics of the contact. Throughout the work only two interaction properties were used, defined as "Friction" and "Frictionless". In both, the normal behaviour constraint

enforcement method was default and the pressure-over closure "hard" contact [18]. The tangential behaviour varied between interaction properties. For "Friction" the tangential behaviour friction formulation was "rough" meaning that no slip would occur between the parts. For "Frictionless" the tangential behaviour friction formulation was "frictionless" meaning that the samples were allowed to slide, without penalty, across each other.

## 5.2 Geometry and Mesh of Finite Element Models

The model geometry refers to the overall shape of the parts, how they are assembled, partitions and meshes. The geometry of each sample will be discussed individually. This section details the modelling methodology employed. Initially a linear elastic model of a spherical core was created primarily to check boundary conditions, specifically the interaction and contact between the finite element parts. A model of the small cylindrical compression sample is detailed in Section 5.2.2 and a heterogeneous ball core model described in Section 5.2.3.

### 5.2.1 Spherical Linear Elastic Model

The first stage of the modelling procedure was to ensure that the boundary conditions described previously had been applied correctly and also validate the contact and finite element mesh. It is advantageous to simplify the material model for this stage to reduce the possible sources of error. The initial simulation was therefore run with a linear elastic material model applied defined by a Young's modulus and Poisson's ratio. This material model differs

from the more complex material models discussed, as it does not represent any energy loss or non-linearity.

The model consists of 2 parts. The spherical part is a three-dimensional deformable, revolution of a quarter circle and the compression plate a two-dimensional analytically rigid plate. The finite element mesh for the ball is shown in Figure 5.2-1.
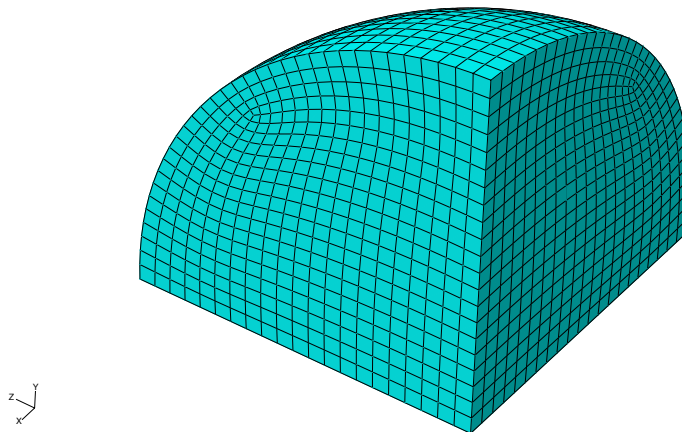


**Figure 5.2-1 – Finite element mesh for the initial linear elastic simulations.**

The mesh shown in Figure 5.2-1 consists of 8381 8-node linear brick elements with reduced integration, C3D8R. The advantage of the linear elastic material model is that it requires less computational power therefore the number or elements can be increased without having too much effect on the overall simulation time. As the simulation was only being used to check the functionality of the geometry, mesh and boundary conditions there was no need to perform mesh convergence studies. The mesh was verified for element geometry quality using the ABAQUS mesh verification function and showed no

warnings or errors associated with element geometry. Ideally when applying a mesh it is advisable to keep each elements aspect ratio 1 (e.g. a cube) however in practice this is not always achievable. As a rule when using linear brick elements an aspect ratio of 2 is acceptable and when using quadratic brick elements and aspect ratio of 5 is acceptable [38].

As mentioned previously, the materials used in this simulation displayed linear elastic properties, ABAQUS has pre-defined models to define this behaviour. The user is required to enter Young's' modulus (E) and Poisson's ratio ($v$) within the property module in ABAQUS. As this simulation is only intended to validate the contact and mesh, standard rubber parameters were used, E = 20MPa and $v$ = 0.49. Figure 5.2-2 displays the output von Mises stress plot from the analysis.



19mm
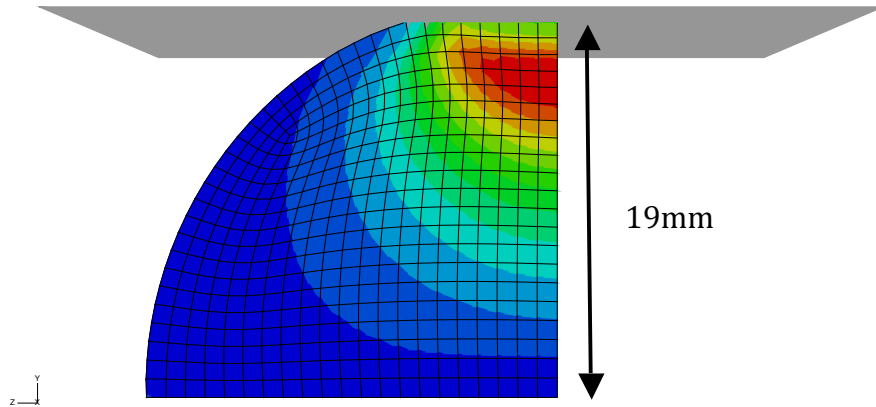
**Figure 5.2-2 – Von Mises stress plot from initial linear elastic simulation (10% strain).**

The model was examined to ensure that one part had not penetrated the other and the displacement of the top surface nodes of the ball equalled the applied displacement of the plate. The boundary conditions applied held the ball in

place yet allowed deformation in the compression direction and allowed the Poisson effect.

The second stage of the linear elastic modelling investigation involved introducing a secondary layer to the ball and applying a different set of material parameters to the section. The ball part can be sectioned in ABAQUS through a process known as partitioning. In order to model the ball cover, a small partitioned section was produced near the outer surface of the ball. This partitioned area was assigned slightly stiffer rubber parameters, E = 50 MPa and ν = 0.49, again assuming a linear elastic material. The objective was to ensure the model solved with various sections of differing material properties. Figure 5.2-3 shows the output stress plot from the analysis.
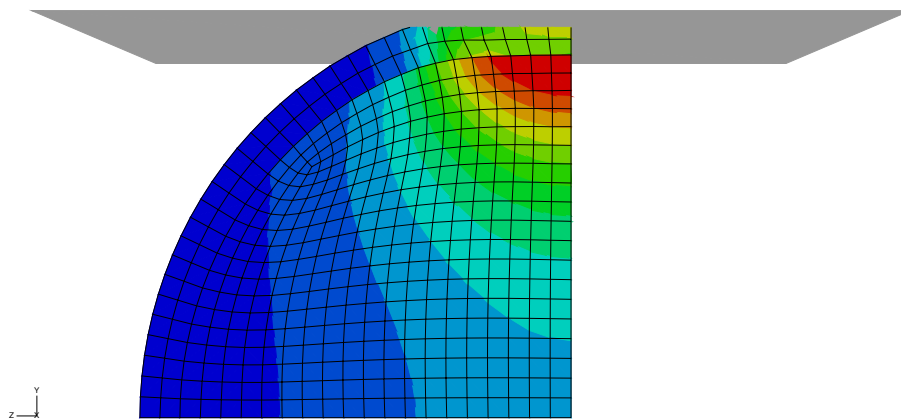


Figure 5.2-3 – Stress plot for 2 layer linear elastic simulation.

This model, again, solved satisfactorily in terms of contact and displacement. As described previously the applied displacement matched that of the top surface nodes. The stress field has a step change at the boundary indicating the different

material property regions. The values of the stress cannot be validated because the properties applied were for a generic rubber. The aim was to model a difference between layers to see differing stress fields, which have been observed. It was decided to focus on mesh density and convergence studies when the more complex material models were applied.

Having established that the model was behaving satisfactorily in terms of boundary conditions and displacements, the next logical step was to begin characterising the more complex material models used for viscoelastic materials and apply them to the geometry already modelled.

### 5.2.2  Small Cylindrical Compression Sample Model

As the material models required for these analyses are more advanced they will be discussed separately in Section 5.3. Referring to the compression samples described Section 3.1 the overall modelling techniques were simpler due to the cylindrical geometry. The "small sample" was a three-dimensional deformable part experiencing compressive loading from an analytically rigid plate. This is similar to the analysis of the "ball" part discussed previously. Figure 5.2-4 shows the mesh applied to the sample.
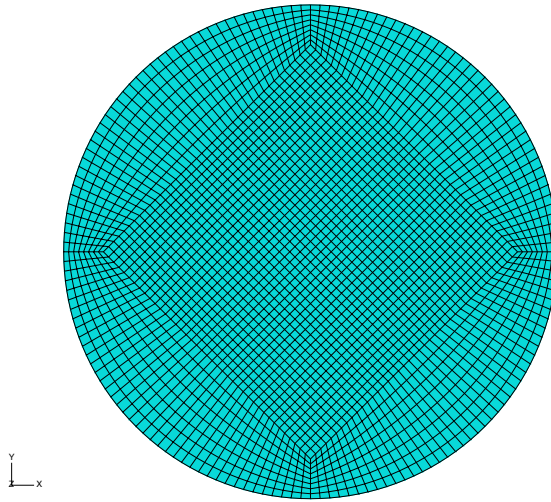
**Figure 5.2-4 – Top face of cylindrical sample showing sample mesh.**

Due to the circular cross section of the sample the face had to be partitioned to yield a suitable mesh. A large square was positioned in the centre of the circular face and straight lines connected the corners of the square to the circumference of the sample. Maximising the size of the square guarantees that the majority of elements have ideal aspect ratios. Figure 5.2-5 shows the FE model after partitioning before the mesh was applied.
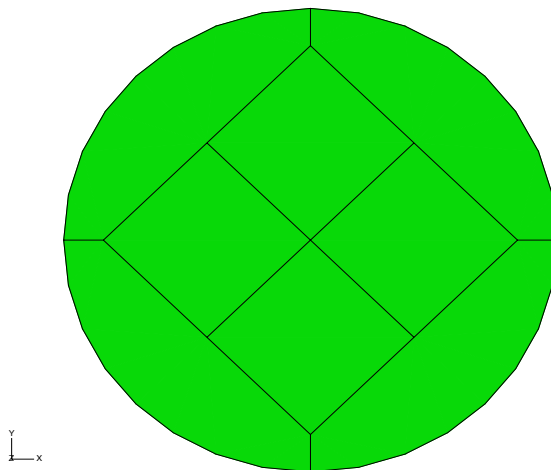


**Figure 5.2-5 - Diagram showing position of part partitions.**

The mesh used consisted of 25920 C3D8H elements. The C3D8H element is an eight-node linear brick element, hybrid, constant pressure element and commonly used for incompressible materials to avoid volumetric locking [38]. The reasonably short simulation time, approximately thirty minutes on a quad core 32-bit Windows desktop, allowed full modelling of the sample without the need for symmetry boundary conditions. The only boundary condition applied to the sample was on the bottom face and specified that the sample could not move along the z-axis but was free to expand laterally along the x and y-axes, to capture the Poisson's effect. The boundary conditions applied to the compression plate were similar to those applied in the initial linear elastic core models, the only difference being the overall displacement. Figure 5.2-6 shows the FE assembly for the small sample simulations.
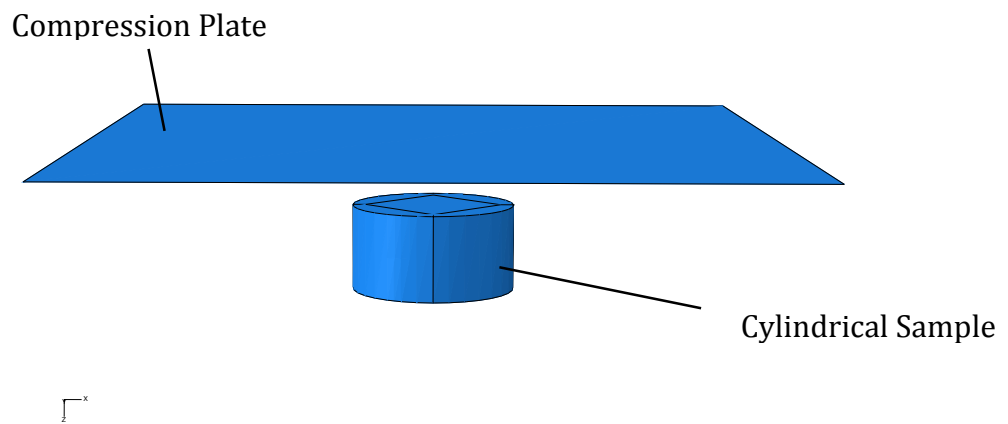
Compression Plate

Cylindrical Sample

**Figure 5.2-6 - Small sample model assembly.**

### 5.2.3 Heterogeneous Core Model

The third model constructed was the heterogeneous core model. This was identical to the model discussed in Section 5.2.1, the only changes being the

partitions applied. The quarter hemisphere was partitioned creating "shell" sections. These "shell" sections were geometrically matched to the initial machined cylinder of material discussed in Section 3.1. The location and sizes of the partitions used in this model can be seen in Figure 5.2-7, which also relates the partitioned sections to the original machined cylinder.
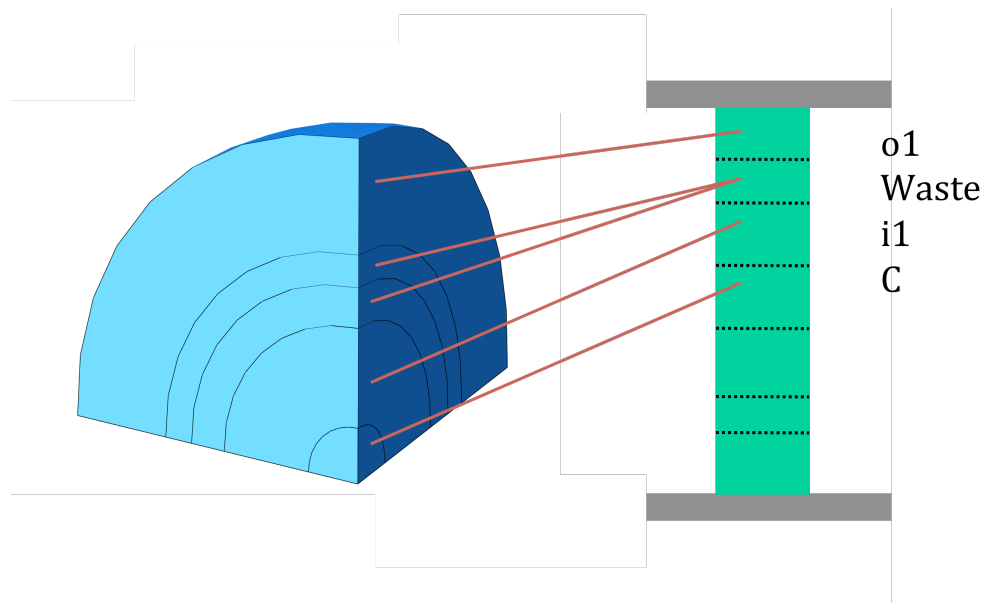


**Figure 5.2-7 - Size and location of FE sections and relative material sections from original sample.**

Referring to Figure 5.2-7 it can be seen the small samples sections produced can be related to specific areas in the FE model. The "waste" section that resulted from the manufacture of the small samples to a specific geometry was separated into two sections. It was assumed that the parameters for this waste section would be bounded by the parameters describing the inner and outer materials. As the removed material was not of testable geometry the properties had to be approximated. It was decided that the "waste" section would be divided into two equally sized sub-sections with the inner and outer material models applied to the sub-sections adjacent to the inner and outer sections respectively. This provided a suitable approximation of the behaviour. The boundary conditions

applied were consistent with those described in the linear elastic model. The plate displacement values were taken directly from experimental displacement values. For comparison purposes, full cores were tested in compression during the experimental phase. The plate displacement values from the compression apparatus was read directly and entered into ABAQUS to define the simulation plate displacement.

When doing any FE analysis it is important to find a balance between accuracy and computational time. Various meshes were investigated as part of the study with a compromise being made with regards to accuracy and simulation time. The mesh was refined to a point where increasing the number of elements did not have an effect on the accuracy of the model. The final mesh is shown in Figure 5.2-8 below.
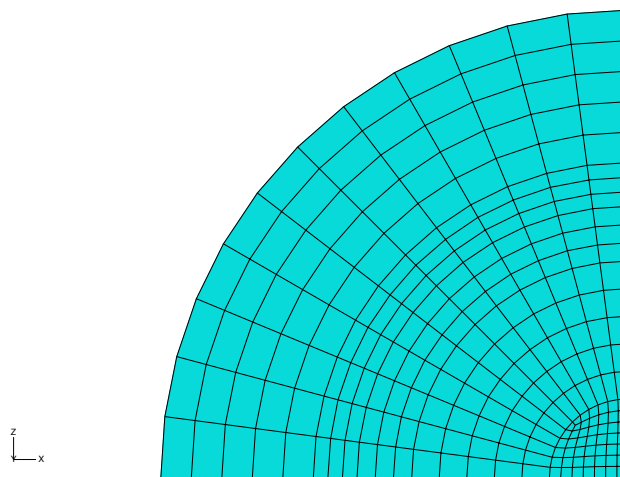


**Figure 5.2-8 - Heterogeneous model mesh.**

The mesh shown in Figure 5.2-8 consists of 2052 8-node linear brick elements of type C3D8. ABAQUS has the option to verify a mesh after it has been applied

which highlights errors and warnings with regards to element geometry. The above mesh resulted in 0 analysis errors and 1 analysis warning when verified using the ABAQUS mesh verification tool. Figure 5.2-9 shows the mesh warnings. Highlighted elements show the location of the analysis warning and the detailed view shows the element geometry that has resulted in an analysis warning.
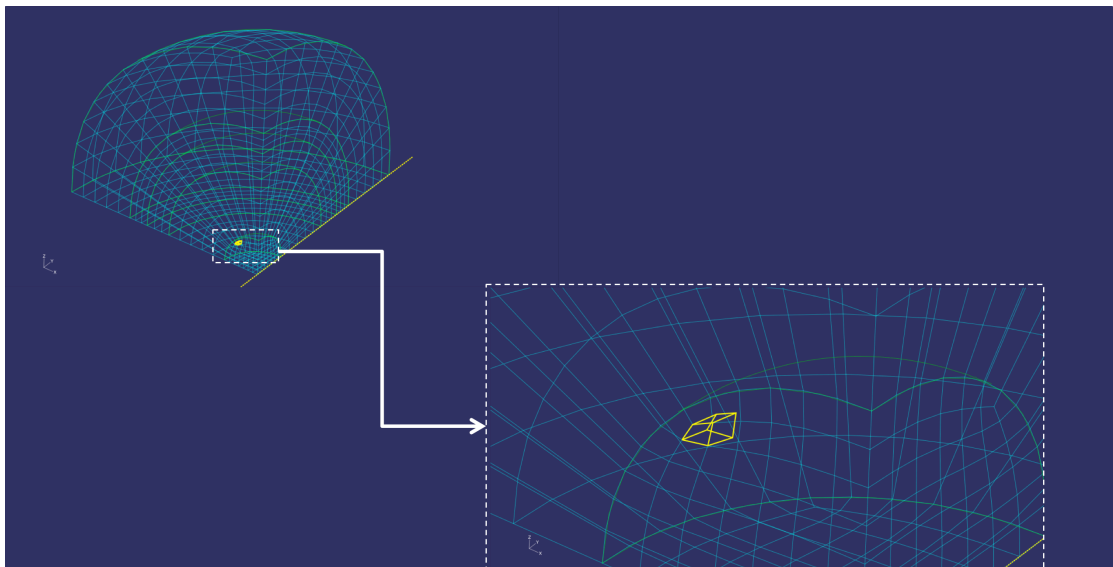


**Figure 5.2-9 - Results of ABAQUS mesh verification.**

## 5.3 Material Characterisation

The material models required to model the polymers used in golf ball construction are somewhat more complicated than linear elastic and linear viscoelastic models. Initially, the structure of the material models will be discussed and the reasons behind the selected networks. The characterisation of the individual model will be discussed afterwards.

### 5.3.1 Non-Linear Viscoelastic Material Models.

As previously discussed in Section 2.2.2 the material models chosen to be investigated were all non-linear viscoelastic models meaning that the mathematical models used to describe the behaviour of the spring and dashpots (see Figure 2.2-3) in the material model are all non-linear. The first material model examined was the Bergström-Boyce (BB) model [23], which is an advanced non-linear model for rubber like materials. The model incorporates non-linear strain dependence, non-linear viscoelastic flow, hysteresis, Mullins effect and temperature effects [19]. The BB model is a three-element model as shown in Figure 5.3-1 with the elastic response Network A) defined by the 8-chain model. The 8-chain model (also known as the Arruda-Boyce model) is a hyperelastic model that uses three material parameters; shear modulus, bulk modulus and limiting stretch. ABAQUS formulates hyperelasticity in terms of a "strain energy potential," (U) which defines the strain energy stored in a material per unit reference volume (volume in the initial configuration) as a function of the strain at that point in the material [33]. The strain energy potential of the 8-chain model takes the form:

$$
U = \mu \left\{ \frac{1}{2}\left(\overline{I_1} - 3\right) + \frac{1}{20\lambda_m^2}\left(\overline{I_1^2} - 9\right) + \frac{11}{1050\lambda_m^4}\left(\overline{I_1^3} - 27\right) \right.
$$
$$
\left. + \frac{19}{7000\lambda_m^6}\left(\overline{I_1^4} - 81\right) + \frac{519}{673750\lambda_m^8}\left(\overline{I_1^5} - 243\right) \right\} + \frac{1}{D}\left( \frac{J_{el}^2 - 1}{2} - \ln J_{el} \right)
$$

<div align="right">.....Equation 5.3-1</div>

where $U$ is the strain energy per unit volume; $\mu$ is the shear modulus, $\lambda_m$ is the locking stretch and $D$ is the volumetric parameter. The shear modulus is related to the initial shear modulus with the following expression:

$$\mu_0 = \mu(1 + \frac{3}{5\lambda_m^2} + \frac{99}{175\lambda_m^4} + \frac{513}{875\lambda_m^6} + \frac{42039}{67375\lambda_m^8}).$$

.....Equation 5.3-2

Bergström [34] suggests estimating the initial shear modulus as one-third of the Young's Modulus due to the incompressibility of elastomers. The volumetric parameter, $D$, is related to the initial bulk modulus, $K_0$, using the following relationship:

$$K_0 = \frac{2}{D}.$$

.....Equation 5.3-3

Bergström [34] indicates that the initial bulk modulus is difficult to calculate for elastomers, again due to their incompressibility, and suggests that a value of 500 times greater than their shear modulus can be assumed. The locking stretch, $\lambda_m$, can be calculated from the limiting chain stretch ($\lambda_{lim}$), which is the point in a uniaxial compression test where the stress increases without limit [34], using the following equation,

$$\lambda_m = \sqrt{\frac{1}{3}\left\{\lambda_{\text{lim}}^2 + \frac{2}{\lambda_{\text{lim}}}\right\}}$$

$\overline{I_1}$ is the first deviatoric strain invariant defined as:

$$\overline{I_1} = \overline{\lambda_1^2} + \overline{\lambda_2^2} + \overline{\lambda_3^2}$$

where the deviatoric stretches $\overline{\lambda_i} = J^{-\frac{1}{3}}\lambda_i$. $J$ is the total volume ratio and $J_{el}$ is the elastic volume ratio which relates the total volume ratio to the thermal volume ratio ($J_{th}$) with the following relationships.

$$J_{el} = \frac{J}{J_{th}} \quad \text{and}$$
$$J_{th} = (1+\varepsilon^{th})^3 .$$

The linear thermal expansion strain, $\varepsilon^{th}$, is obtained from the temperature and the isotropic thermal expansion coefficient [33].

The advantages of the 8-chain model are that it is always stable and can be calibrated with one dataset [19]. Due to these properties and the restrictions of what experimental data could be gathered, it was expected that this might be a suitable model to define Network A.

Network B, which describes the viscous response of the material, consists of both a spring and dashpot, which use separate mathematical models to describe their behaviour. The 8-chain model, as used in Network A, defines the spring and the viscoelastic flow is defined by Bergström-Boyce (BB) flow model [23]. This viscoelastic flow rate for the BB flow model is given by:

$$\dot{\gamma}_B^v = \dot{\gamma}_0 (\overline{\lambda_B^v} - 1 + \xi)^C \left[ R(\frac{\tau}{\tau_{base}} - \hat{\tau}_{cut}) \right]^m$$

<div align="right">.....Equation 5.3-7</div>

where $\dot{\gamma}_0 \equiv 1/s$ is a constant introduced to ensure dimensional consistency, $R(x) = (x + |x|)/2$ is the ramp function introduced to increase the numerical efficiency of the material model for cases when regions of the FE mesh is not undergoing significant deformations, $\hat{\tau}_{cut}$ is a cut off stress below which no flow will occur, $\overline{\lambda_B^v}$ is the viscoelastic chain stretch, $\tau_{base}$ is the flow resistance, $C$ is the strain exponential, $m$ is the stress exponential, $\xi$ is the strain adjustment factor and $\tau$ is the effective stress driving the flow [23].

### 5.3.2 Material Model Calibration

To calibrate the material models using the experimental data gathered, the MCalibration software [35] from Veryst Engineering was utilised. MCalibration takes an initially guessed set of parameters, which describe the springs and dashpot, and alters them to reduce the error between the material model prediction and experimental data. In place of using creep or relaxation data, rate dependence is captured by using stress-strain curves at three strain rates thus negating the need for lengthy relaxation tests. As mention previously in Chapter 3, the strain rate chosen for the core compression tests was 0.008 $s^{-1}$, in agreement with Mase and Kersten [16]. In order to capture significant rate dependence it was decided to increase and decrease this strain rate to 0.08 $s^{-1}$ and 0.0008 $s^{-1}$ respectively thus providing a data range covering three orders of magnitude. It was thought that this range would be enough to capture the rate dependence of the materials. The data points of these three curves were saved as text files and directly read by MCalibration.  A typical data set for the small samples is shown in Figure 5.3-2.
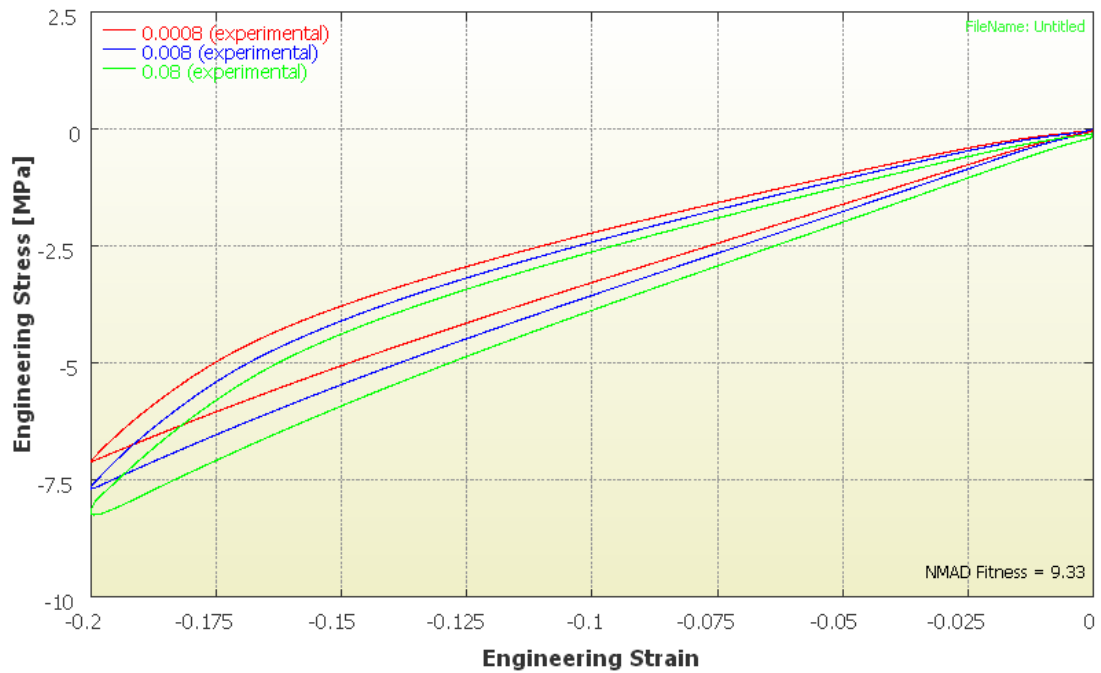
**Figure 5.3-1 – Experimental data set read into MCalibration software.**

The user selects the desired material model, in this case the Bergström-Boyce (BB) model, and defines a series of material parameters as a starting point for the optimisation. This optimisation takes the initially guessed parameters and plots the stress strain response based on these parameters. The difference between this predicted plot and the experimental plot is quantified using the NMAD (normalized mean absolute difference) defined by:

$$NMAD = 100 \frac{\left\langle \left| \sigma^p - \sigma^e \right| \right\rangle}{\left\langle \left| \sigma^e \right| \right\rangle} \quad ,$$

where $\sigma^e$ is the predicted stress, $\sigma^e$ is the experimental stress and $\langle . \rangle$ is the average operator. The user specifies what material parameters can be varied and changes accordingly to reduce the NMAD error, ideally to 0.

The BB Model uses nine material parameters highlighted in Table 5.3-1.

| Symbol | Umat Name | Unit* | Description |
|---|---|---|---|
| $\mu$ | mu | S | Shear modulus of network A |
| $\lambda$ | lambdaL | - | Locking stretch |
| $\kappa$ | kappa | S | Bulk Modulus |
| $s$ | s | - | Relative stiffness of network B |
| $\xi$ | xi | - | Strain adjustment factor |
| $C$ | C | - | Strain exponential |
| $\tau_{Base}$ | tauBase | S | Flow resistance |
| $m$ | M | - | Stress exponential |
| $\tau_{cut}$ | tauCut | S | Cut-off stress for flow |

*Where: - = dimensionless, S = Stress

**Table 5.3-1 – Summary of parameters used by the BB Model**

Various example characterisation runs had been completed whilst learning to use the software, so the initial parameters were taken from an example for a similar material. Figure 5.3-3 displays the results from a typical optimisation of the BB Model for the small core samples.
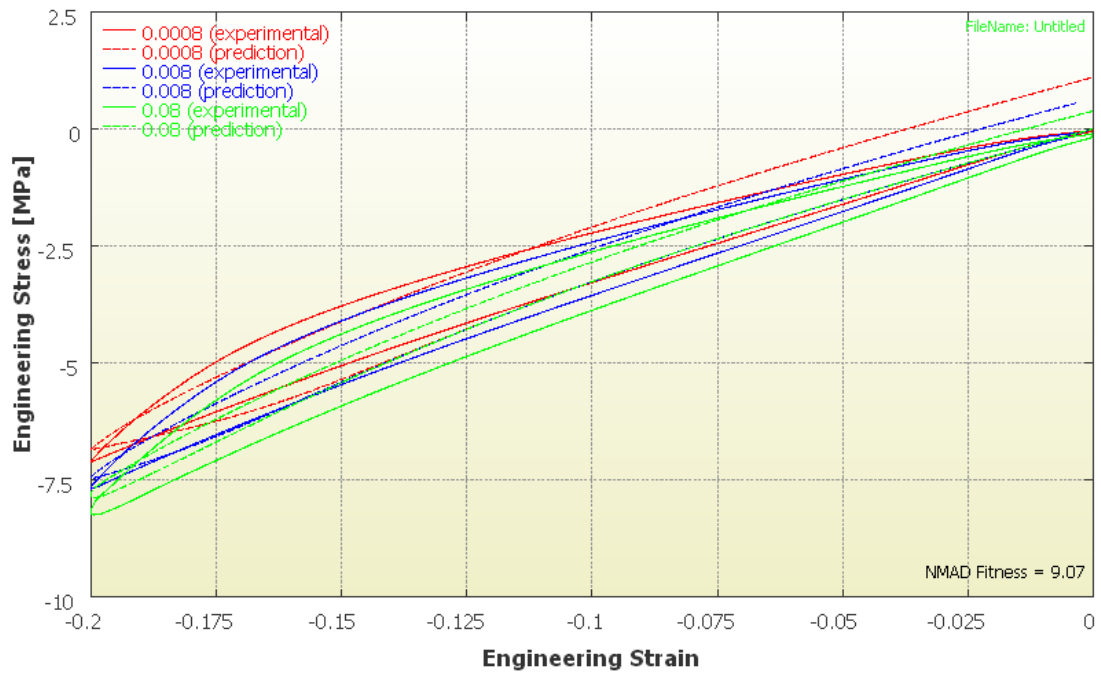
**Figure 5.3-2 – Typical result from optimisation of the BB Model for the small core samples.**

Figure 5.3-3 shows the material model predictions and the experimental data in one plot. It can be seen that the BB Model gives a normalised mean absolute difference (NMAD) of 9.07 and the model is not accurately predicting the overall shape. The predictions all under estimate the peak stress, and predict a permanent offset when the strain returns to the starting position. To increase the accuracy of the material model, the mathematical models that describe the springs and dashpot were investigated. Based on various example problems that modelled rubber materials with similar stress strain curves to the gathered experimental data, it was decided to replace the eight chain model in Network A with the Yeoh model [33]. The strain energy density of the Yeoh model is a third order polynomial in the first strain invariant that is reported to give good predictions of stress at large strain and can also be characterised with one data set.

$$U = C_{10}(\bar{I}_1 - 3) + C_{20}(\bar{I}_1 - 3)^2 + C_{30}(\bar{I}_1 - 3)^3$$
$$+ \frac{1}{D_1}(J_{el} - 1)^2 + \frac{1}{D_2}(J_{el} - 1)^4 + \frac{1}{D_3}(J_{el} - 1)^6 \quad,$$

where U is the strain energy per unit reference volume, $C_{i0}$ and $D_i$ are temperature dependent material parameters. The initial shear modulus ($\mu_0$) and bulk modulus ($K_0$) are given by:

$$\mu_0 = 2C_{10} \text{ and}$$

$$K_0 = \frac{2}{D_1} \quad.$$

For the Yeoh model Bergström suggests that typically [19]:

$$C_{20} \approx -0.01 C_{10} \text{ and}$$

$$C_{30} \approx -0.01 C_{20}.$$

In order to change the spring and dashpot models that describe various networks in the material model, the parallel network (PNM) model has to be used. The PNM model allows the user to specify the mathematical models for individual springs and dashpots and is completely customisable. It was decided that the BB Model would be used as a template as it provided a reasonable

starting point for the prediction of the material behaviour. The structure of the material model would stay the same, a three-element model with two networks. Bergström-Boyce flow would still be used to describe the dashpot and the Neo-Hookean (NH) hyperelastic model would be used to define the spring in Network B. The strain energy potential of the Neo-Hookean model is represented in the form:

$$ U = C_{10}(\overline{I}_1 - 3) + \frac{1}{D_1}(J_{el} - 1)^2 \quad , $$

where the symbols have the definitions discussed above. The NH model was chosen as a starting point because it is reported as being simple and stable. This gave a three-element model, as shown in Figure 5.3-1 where Network A consisted of the Yeoh hyperelastic model and Network B consisted of a Neo-Hookean spring and Bergstöm-Boyce flow dashpot.
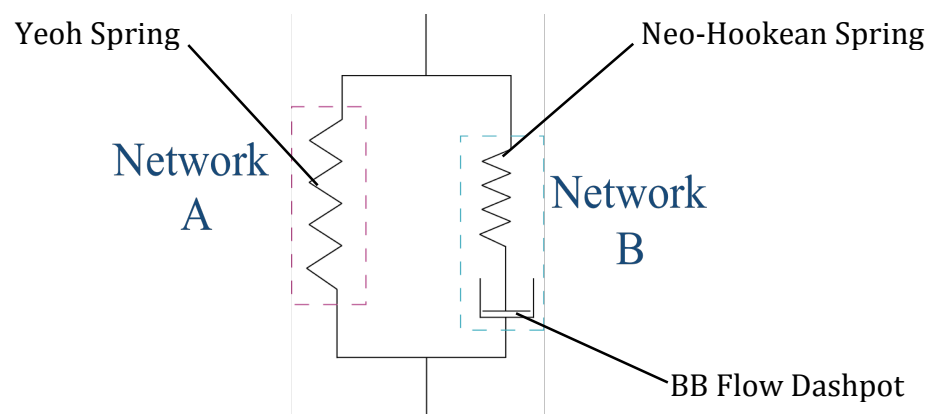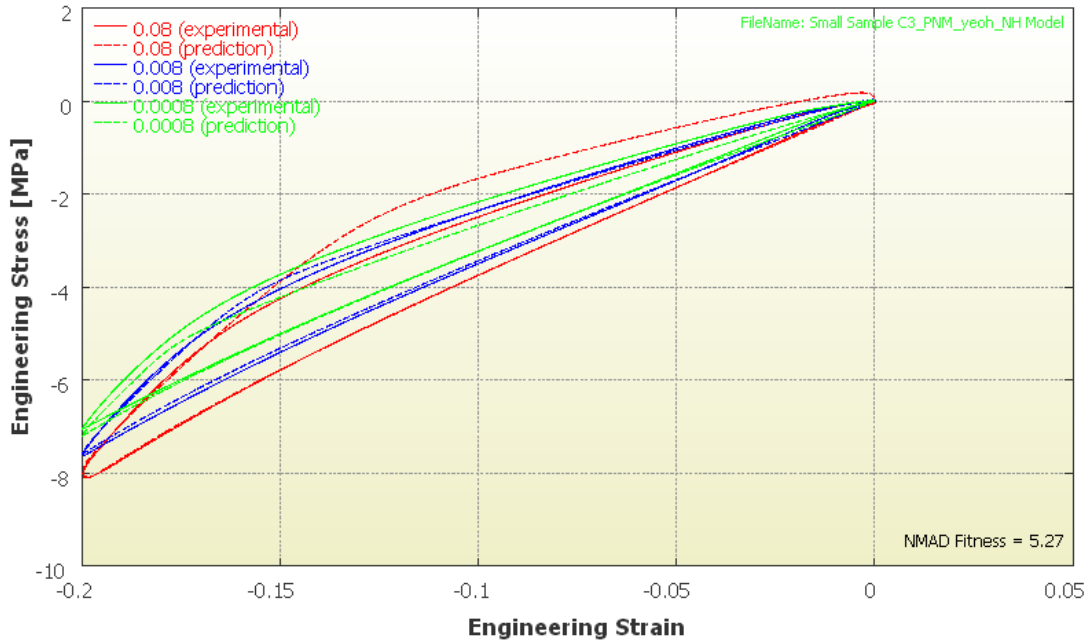


**Figure 5.3-3 - PNM Material Model with specifically selected elements**

The results of the optimisation are shown in Figure 5.3-4 and given separately for the three strain rates in Figures 5.3-5, 5.3-6 and 5.3-7.



**Figure 5.3-4 – Typical results from optimisation of the PNM model (Yeoh and Neo-Hookean) for the small core samples.**

It can be observed that the overall shape of the prediction is better matched to the experimental data and the NMAD fitness has been reduced to 5.27. It should be noted that this NMAD fitness is the overall statistical fitness for all three strain rate data sets. Individually the NMAD fitness value for the 0.08/s strain rate is 7.006, the NMAD fitness for the 0.008/s strain rate is 1.891, and the NMAD fitness for the 0.0008/s strain rate is 6.921. This difference in accuracy is expected as 0.08 and 0.0008 are the upper and lower bounds of the experimental data. As there is one set of parameters describing the full model it would be expected that the fitness of the model at the upper and lower limits

88

would not be as accurate as the fitness of the function in the middle of the data

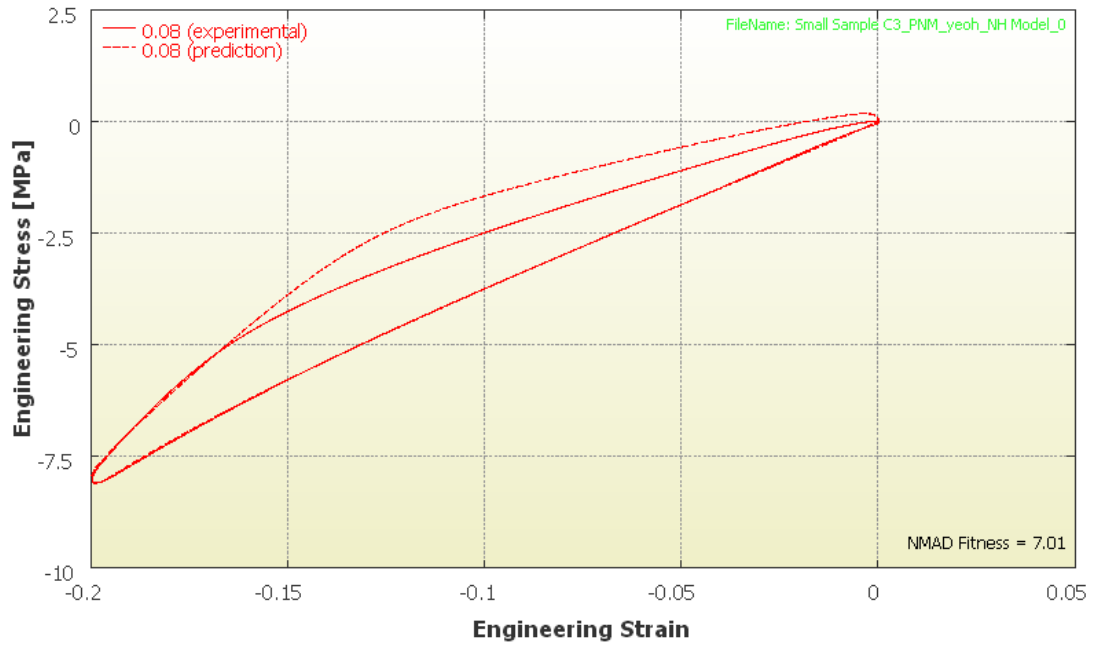range. Figures 5.3-5, 5.3-6 and 5.3-7 show the model fit at each strain rate.



**Figure 5.3-5 - NMAD fitness for small sample at 0.08s⁻¹.**
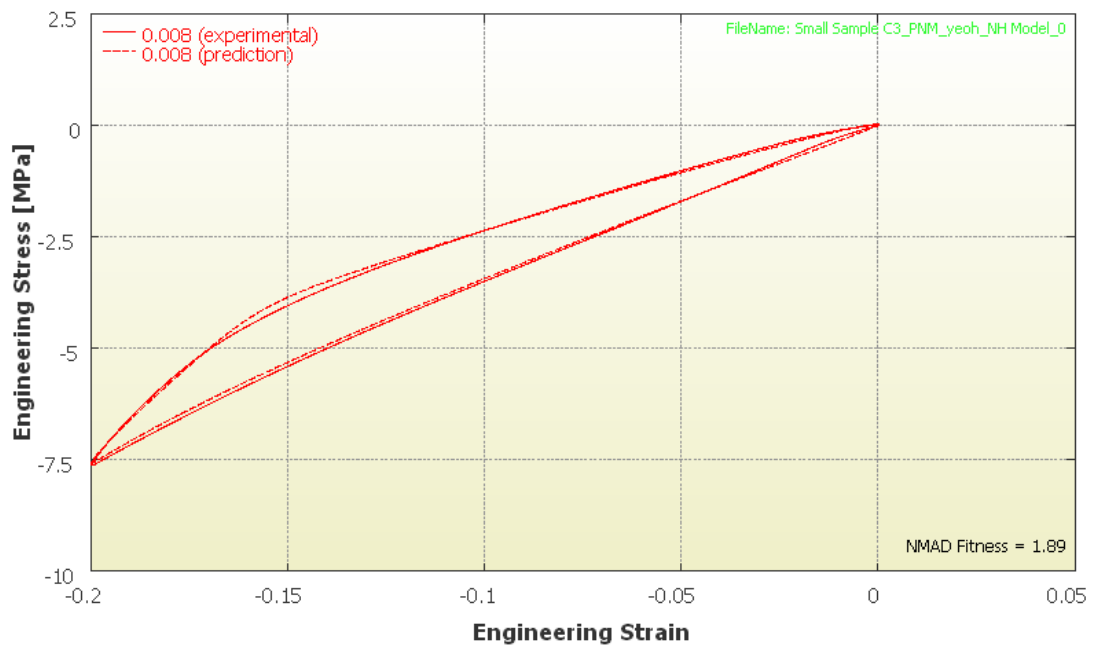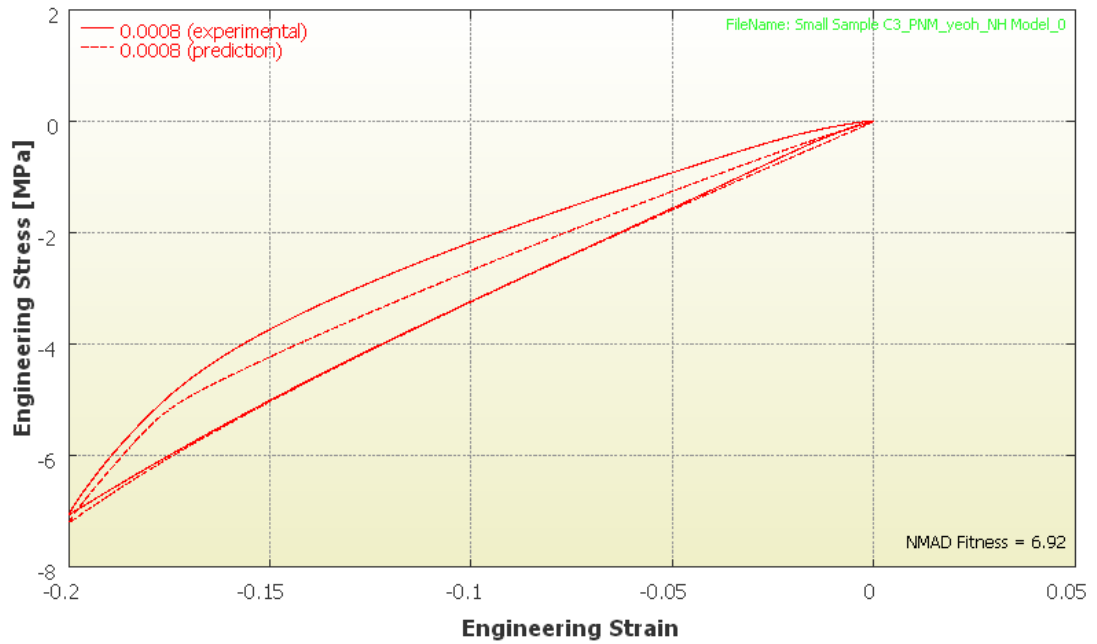


**Figure 5.3-6 - NMAD fitness for small sample at 0.008s⁻¹.**

**Figure 5.3-7 - NMAD fitness for small sample at 0.0008s⁻¹.**

As shown in Figure 5.3-4 the current PNM model fits the experimental data successfully. It was decided to investigate whether changing the spring in Network B from NH to Yeoh would yield better results. In theory it should provide a slightly more accurate result as the Yeoh model is more suited to the current application with its reported properties of being able to provide good stress predications at large strain but the strength of the NH model is its simplicity and stability. The spring in Network B was changed and the material model optimisation procedure repeated to see if the more complicated material model resulted in a significantly improved accuracy between predicted and experimental data. Figure 5.3-8 summarises the results and it can be seen that increasing the complexity has not noticeably increased the accuracy of the material model (NMAD = 5.27).
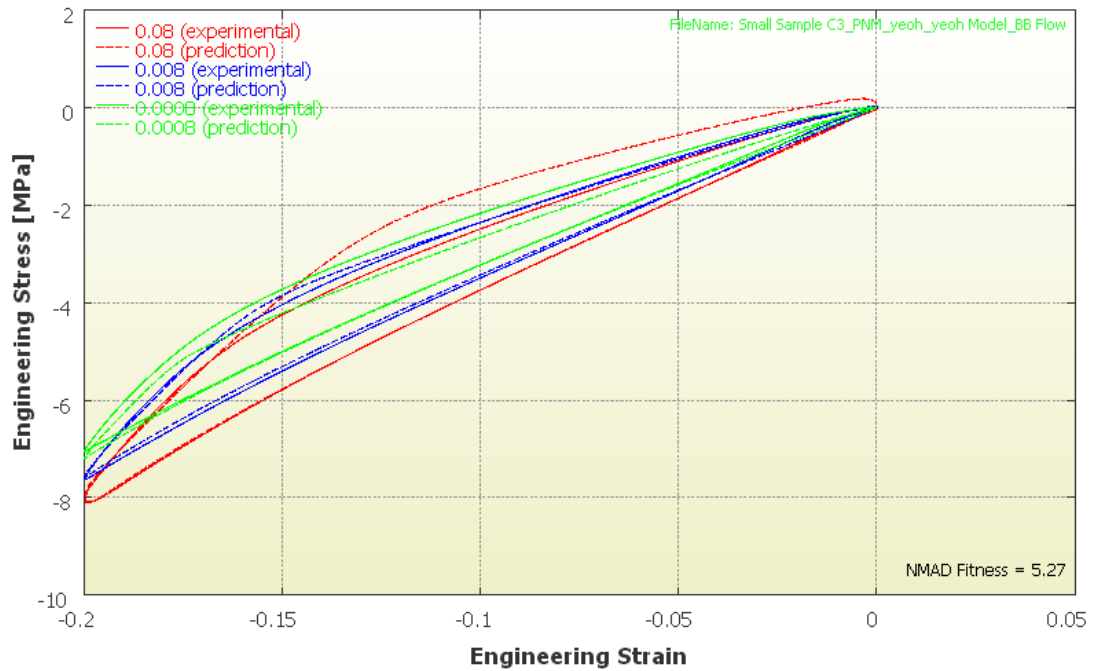
**Figure 5.3-8 - Typical results from optimisation of the PNM model (Yeoh and Yeoh) for the small core samples.**

Alongside altering the elastic response spring models, the PNM model allows the user to change the flow model used in Network B to describe the dashpot. In addition to the MCalibration software, for optimising material properties, Veryst Engineering provide the PolyUMod [36] material model library for use with ABAQUS. PolyUMod is a library of advanced material models for polymetric materials. PolyUMod has a variety of flow models available. This library of models was investigated and the models with suitable characteristics were selected for optimization. The initial flow model used was the Bergström-Boyce (BB) flow model, which resulted in appropriate accuracy [38] discussed above. To accurately isolate the effect of altering the flow model the elastic responses were kept consistent with the Yeoh and Neo-Hookean spring models.

The flow model was changed from the BB model to the Bergström-Boyce Network Dependent (BBND) Model. The BBND model is a modification to the original BB flow model in which the flow resistance stress is dependent on the network state through a factor, $f_v$. Most elastomer-like materials are experimentally shown to have less strain-rate dependence during unloading than during loading [23]. The flow rate for the BB flow model is given by:

$$\dot{\gamma}^p = \left[\lambda_L - 1 + \xi\right]^C \cdot \left(\frac{\tau}{f_p f_{\varepsilon^p} \hat{\tau}}\right)^m f_\theta \ ,$$

where $\lambda_L$ is the chain stretch, $\xi$ is the strain adjustment factor, $C$ is the strain exponent, $\hat{\tau}$ is the shear flow resistance and $m$ is the shear flow exponent. $f_p, f_{\varepsilon^p}, f_\theta$ are scalar factors only used when defining temperature dependent components, pressure dependence of the yield stress equation and yield evolution factor. As the defined material model does not include these values they can all be taken to equal 1. The BBND model follows the same form and is given by:

$$\dot{\gamma}^p = \left[\lambda_L - 1 + \xi\right]^C \cdot \left(\frac{\tau}{f_v f_p f_{\varepsilon^p} \hat{\tau}}\right)^m f_\theta \ ,$$
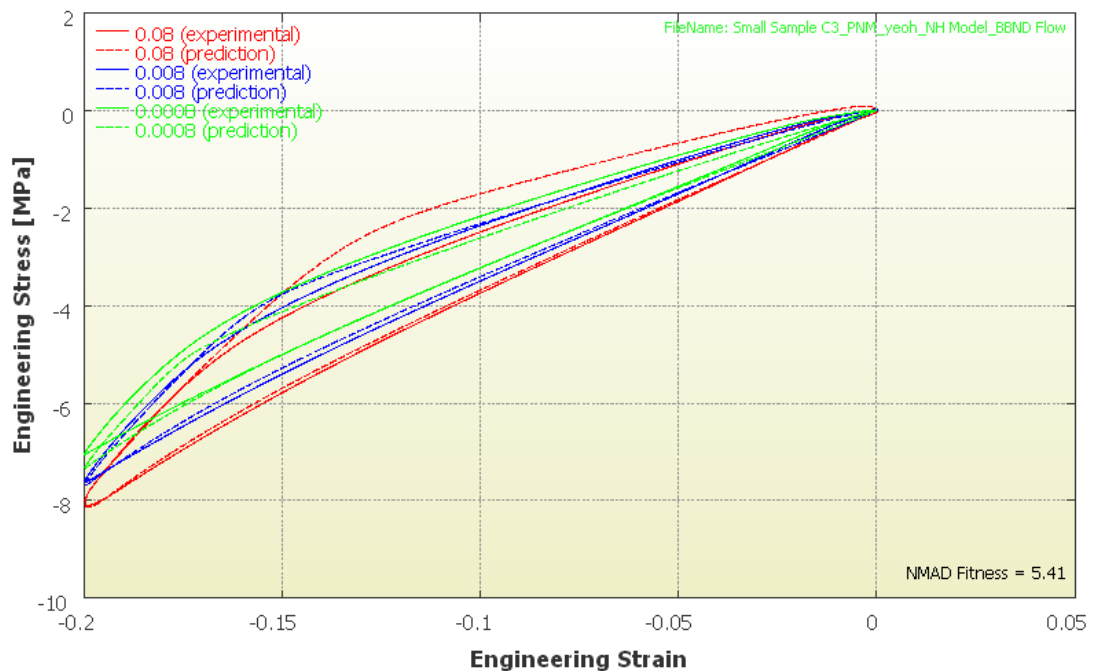
where $f_v = 1 + \alpha \varepsilon : \varepsilon_e$ , the true strain $\varepsilon = \ln[v]$ and the true elastic strain $\varepsilon_e = \ln[v_e]$.

This modified BBND flow model introduces the ability to capture this response. The model was calibrated with the same experimental data as used above and resulted in the fitness shown below in Figure 5.3-9.



**Figure 5.3-9 - Typical results from optimisation of the PNM model (Yeoh and Neo-Hookean) with BBND flow for the small core samples.**

It can be seen that the overall shape of the predictions is largely similar to the predictions of the BB flow model but the NMAD fitness is slightly worse at 5.41. It was therefore concluded that the original BB flow model displays more accurate predictions and has the advantage that it relies on one less parameter.

Another flow model available in the PolyUMod library that suits the application is the Power-Law flow with Strain-Dependence model. This is an extension of the power-law flow model in which the stress exponent is dependent on the plastic strain magnitude. The purpose of this model is to enable accurate predictions of elastomers both at small and large strains. The flow rate of this model is given by:

$$\dot{\gamma}^p = \left( \frac{\tau}{f_p f_{\varepsilon^p} \hat{\tau}} \right)^{m^{eff}} f_\theta \ ,$$

<div align="right">.....Equation 5.3-15</div>

where $m^{eff}$ is given by: $\quad m^{eff} = \left[ m_i - m_f \right] e^{\frac{-\varepsilon^p}{\hat{\varepsilon}}} + m_f \ ,$

<div align="right">.....Equation 5.3-16</div>

where $m_i$ is the strain exponent at small strains, $m_f$ is the strain exponent at high strains and where $\varepsilon^p$ is the true strain from the deformation gradient, $F^p$. Figure 5.3-10 shows the results of the model optimisation with the same experimental data used above.
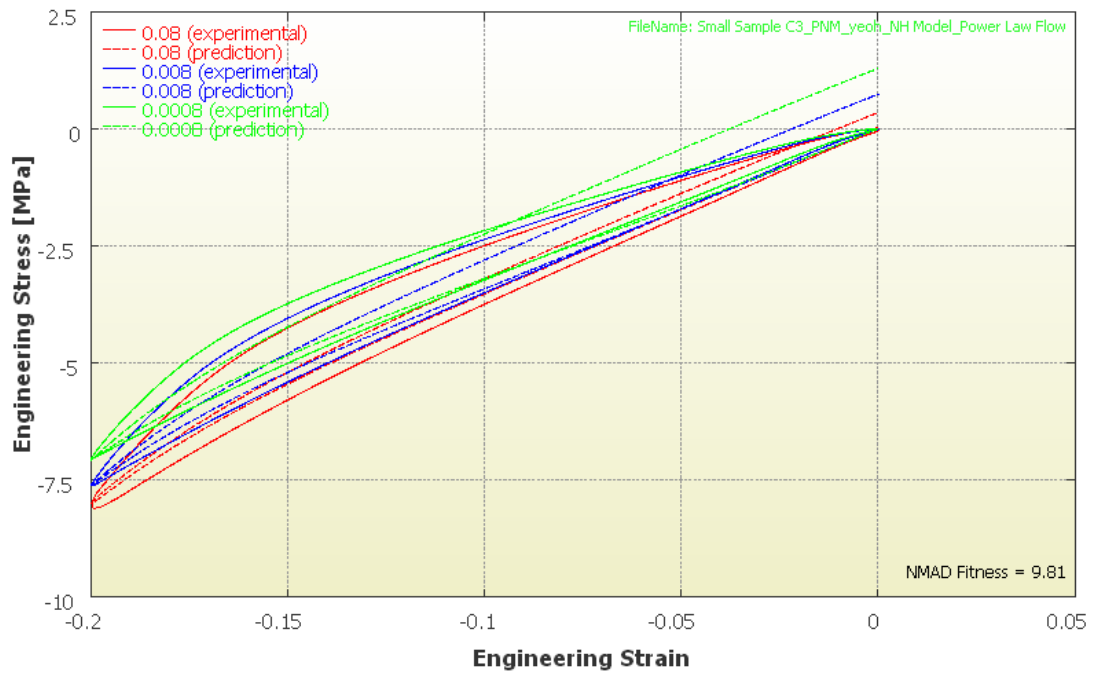
**Figure 5.3-10 - Typical results from optimisation of the PNM model (Yeoh and Neo-Hookean) with Power-Law Flow with Strain-Dependence applied for the small core samples.**

It can be seen that this model is not accurately predicting the overall shape of the data and results in a NMAD of 9.81.

Having investigated various options for the elastic response and examining various flow models the PNM consisting of a Yeoh spring in Network A and an NH spring and the BB flow model in Network B was chosen as the model to work with as it resulted in the most accurate predictions of the material behaviour and was not overly complicated. The parameters used by the PNM model are summarised in Table 5.3-2.

| Symbol | Value | Unit * | Description | |
|--------|-------|--------|-------------|---|
| EType | 5 | | Elastic component type | |
| C10 | 4.59831 | S | Linear term in $I_1$ | |
| C20 | -2.56041 | S | Quadratic term in $I_1$ | Network A |
| C30 | 9.03943 | S | 3rd order term in $I_1$ | |
| kappa | 500 | S | Bulk modulus | |
| EType | 2 | | Elastic component type | |
| mu | 8.56176 | S | Shear modulus | |
| kappa | 500 | S | Bulk modulus | |
| FType | 503 | | Flow model type | |
| xi | $1.34565e^{-10}$ | | Strain adjustment factor | Network B |
| C | -1.19373 | | Strain exponent | |
| tauHat | 7.64827 | S | Shear flow resistance | |
| m | 3.6217 | | Shear flow exponent | |

*where: - = dimensionless, S = Stress

Table 5.3-2 - Summary of parameters used by the optimized PNM material model.

## 5.4 Integration of Material Model with ABAQUS

### 5.4.1 Finite Element Analysis of Small Core Samples

Having developed a suitable PNM material model using the MCalibration optimisation software it was necessary to validate the material model through FE analysis. The parameters obtained through optimisation of the PNM model

with the experimental data were used to define the material in ABAQUS through a user material subroutine. The user material subroutine was utilised, as the default material models in ABAQUS are not flexible enough to define the non-linear viscoelastic material model. The user enters a series of parameters, which allow ABAQUS to recognise what material model is being used in the PolyUMod library and what material parameters are defining the model.

The first step towards integrating the material model and validating its accuracy was to model the small core samples, as described in previous Sections 5.1 and 5.2, apply the material model described in Section 5.3 and simulate a compression test with test conditions similar to the experimental set up. Initially the intermediate strain rate ($0.008$ s$^{-1}$) was simulated, as this would ideally yield the most accurate results. The parameters that describe the model were optimised with data at three strain rates, the most accurate prediction was expected to be at $0.008$s$^{-1}$ as this strain rate lay in the middle of the upper and lower bounds of $0.08$s$^{-1}$ and $0.0008$s$^{-1}$. Figure 5.4-1 show the FE results and experimental data for the uniaxial compression test carried out at $0.008$s$^{-1}$.
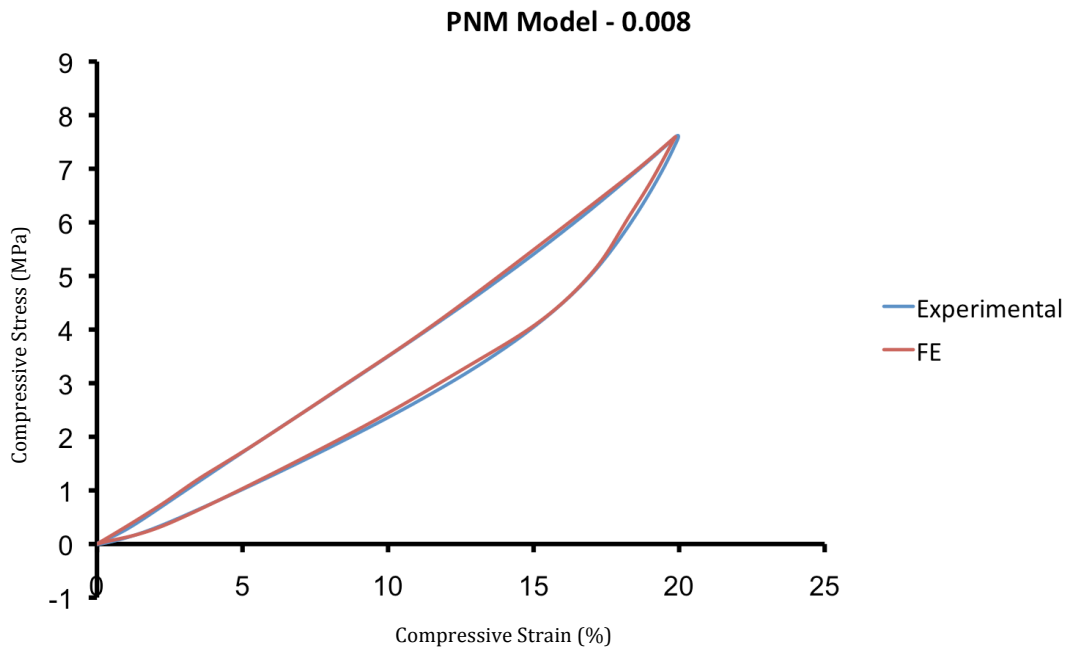
**Figure 5.4-1 - Finite element prediction of small sample behaviour at 0.008s⁻¹ strain rate.**

It can be seen that the simulation is accurately predicting the stress-strain response of the material under loading conditions similar to those experienced in reality. The peak stress is accurately predicted with a percentage error (Percentage Error = $\left| \dfrac{FE - Exp}{Exp} \right| \times 100$ , where FE = finite element prediction and Exp = experimental curve) of 0.25% and the loading curves of the experimental and finite element analysis follow the same path. The material hysteresis is slightly under predicted with a percentage error, between experimental and finite element, of 3.65%. Figure 5.4-2 shows the FE results for a simulation carried out at the upper bound of the experimental data, 0.08 s⁻¹.
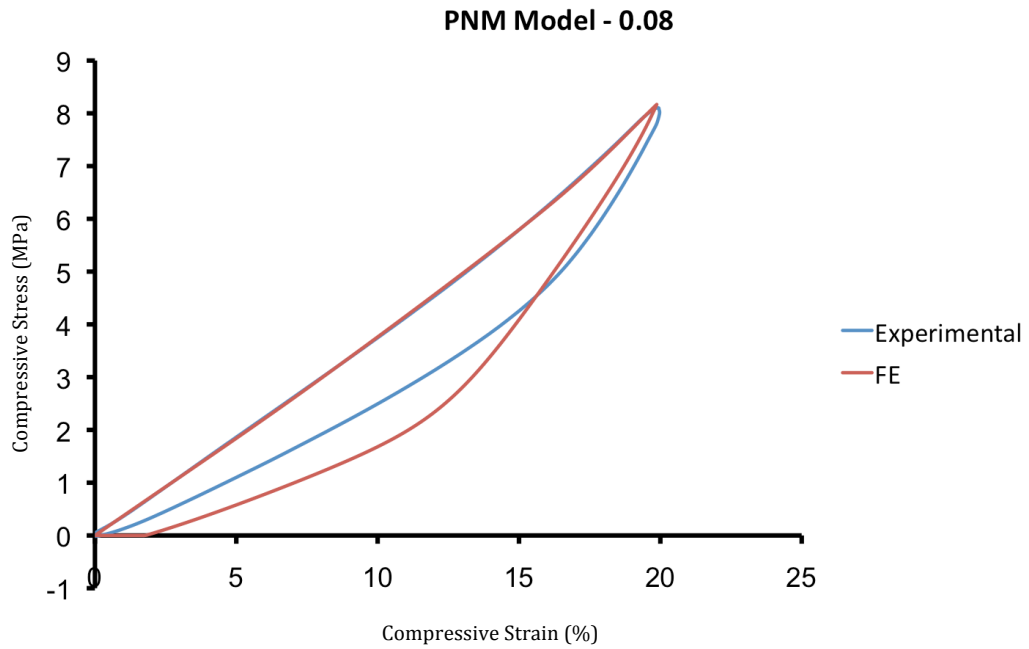
**PNM Model - 0.08**

*y-axis: Compressive Stress (MPa)*
*x-axis: Compressive Strain (%)*

Legend: Experimental, FE

**Figure 5.4-2 - Finite element prediction of small sample behaviour at 0.08s⁻¹ strain rate.**

It can be observed that the model accurately predicts the peak stress with a percentage error of 0.79% and the loading path is accurately predicted, however the model over predicts hysteresis by 37%. This can be explained by considering the issue of strain and strain rate dependence. The parameters used to describe the overall model cannot accurately predict the behaviour for all strain rates as the parameters used to accurately describe each model individually vary too much. It is important to realise that the 0.08s⁻¹ simulation is at the upper limit of the experimental data so the prediction will be far less accurate than the 0.008s⁻¹ simulation. Similarly, the predictions for the FE analysis carried out at the lower limit of the experimental data, 0.0008s⁻¹, will not be as accurate as 0.008s⁻¹. Figure 5.4-3 show the FE prediction against the experimental data for a small sample from the centre of the core under uniaxial compression at 0.0008s⁻¹.
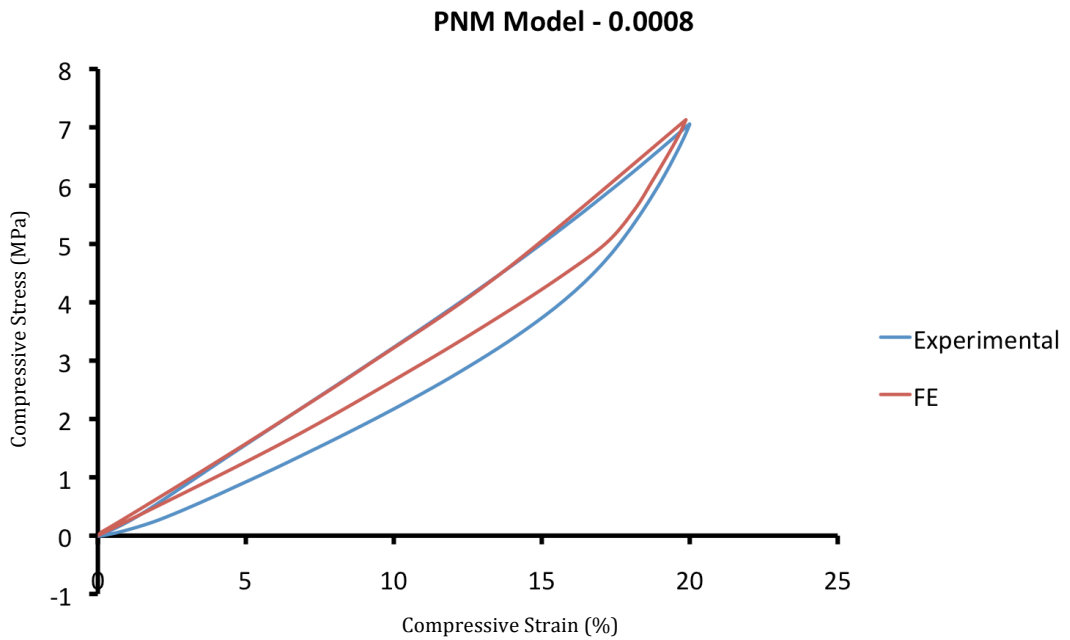
**PNM Model - 0.0008**

*Figure 5.4-3 - Finite element prediction of small sample behaviour at 0.0008s$^{-1}$ strain rate.*

The above figure shows that, again, the FE prediction for peak stress is good with a percentage error of 1.03% and the loading path is adequately captured. The hysteresis in this case it under predicted with a percentage error of 39.59%.

Although the errors associated with the hysteresis are quite large, the overall trend in hysteresis behaviour is captured by the finite element analysis. The experimental results demonstrated that the hysteresis observed increased with strain rate, meaning that at higher strain rates there is higher energy losses. The FE analysis agreed with this behaviour, albeit slightly exaggerated.

Having produced validated FE models for the small samples removed from the centre of the core, the procedure described above was also applied to the inner

and outer small core samples. Table 5.4-1 summarises the parameters used for each material model, the individual NMAD fitness values for the load cases and the overall NMAD fitness value of the model.

| Name | Description | Centre Material Model | Inner Material Model | Outer Material Model | |
|------|-------------|-----------------------|----------------------|----------------------|---|
| EType | Elastic component type | 5 | 5 | 5 | Network A |
| C10 | Linear term in $I_1$ | 4.59831 | 4.93436 | 5.79535 | |
| C20 | Quadratic term in $I_1$ | -2.56041 | -2.91677 | -0.147572 | |
| C30 | 3rd order term in $I_1$ | 9.03943 | 8.71616 | 6.35598 | |
| kappa | Bulk modulus | 500 | 500 | 500 | |
| EType | Elastic component type | 2 | 2 | 2 | Network B |
| mu | Shear modulus | 8.56176 | 9.69644 | 13.2611 | |
| kappa | Bulk modulus | 500 | 500 | 500 | |
| FType | Flow model type | 503 | 503 | 503 | |
| xi | Strain adjustment factor | $1.34565e^{-10}$ | $9.97371e^{-10}$ | $5.69181e^{-10}$ | |
| C | Strain exponent | -1.19373 | -1.22995 | -1.95069 | |
| tauHat | Shear flow resistance | 7.64827 | 8.0943 | 11.9916 | |
| m | Shear flow exponent | 3.6217 | 3.76919 | 5.01355 | |
| NMAD - 1 | Fitness of load case 1 – $0.08s^{-1}$ | 7.01 | 6.90 | 8.41 | |
| NMAD – 2 | Fitness of load case 2 – $0.008s^{-1}$ | 1.89 | 1.22 | 4.98 | |
| NMAD – 3 | Fitness of load case 3 – $0.0008s^{-1}$ | 6.92 | 6.54 | 8.12 | |
| NMAD – Overall | Overall fitness of three strain rates | 5.27 | 4.89 | 7.17 | |

**Table 5.4-1 – Summary of parameters used in heterogeneous ball model.**

## 5.4.2    Heterogeneous Ball Model

With three material models created, optimised and validated on a cylindrical geometry they were then applied to the full core (eighth spherical) model described in Section 5.2.3. This resulted in a representation of a heterogeneous golf ball core as shown in Figure 5.4-4.
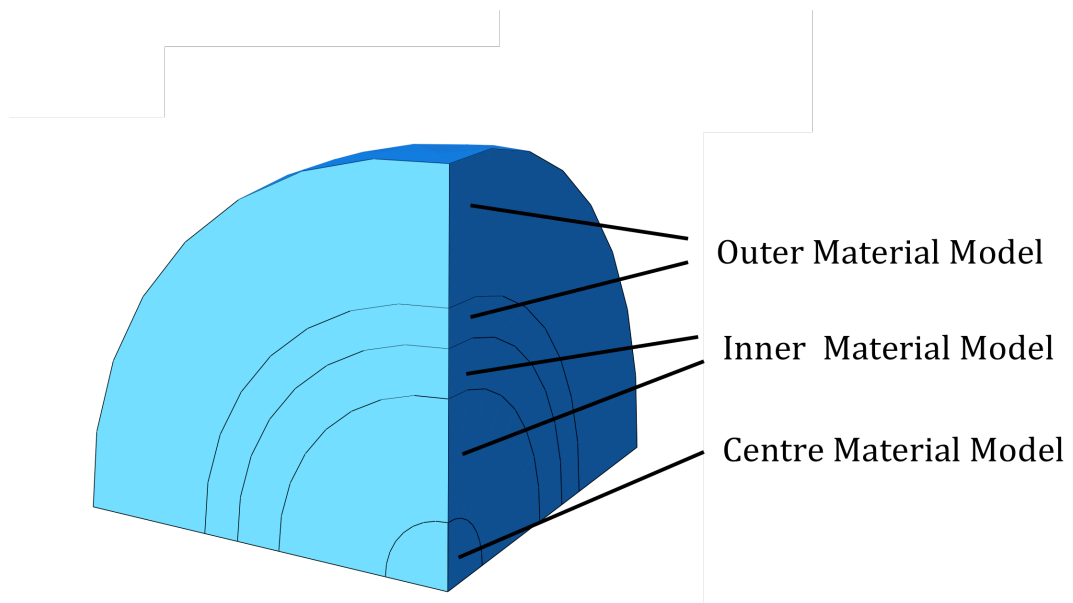


**Outer Material Model**

**Inner Material Model**

**Centre Material Model**

**Figure 5.4-4 – Material model assignments in the heterogeneous core model.**

A compression test of the model shown in Figure 5.4-4 was simulated in ABAQUS as described in Section 5.2.3. The reaction force on the compression plate and the displacement on the plate in the compression direction (y-direction) were requested as outputs from the simulation. The results of the FE analysis and the results from an experimental complete core compression test are plotted in Figure 5.4-5 as force versus displacement graphs.
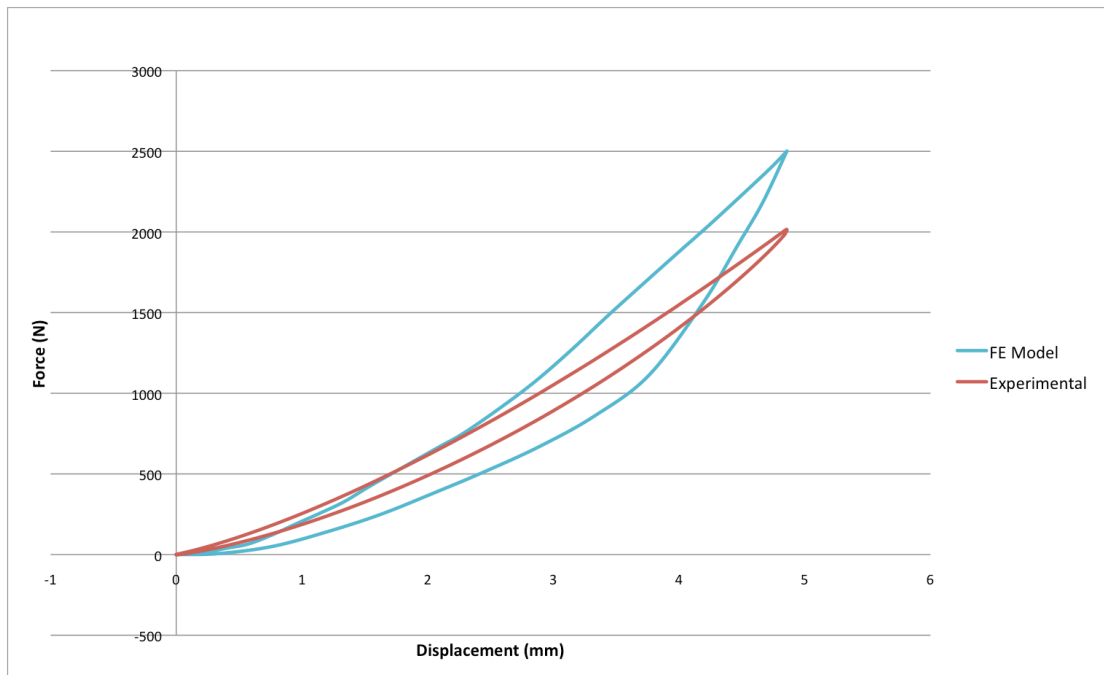
**Figure 5.4-5 - Plot of FE results and experimental results for core compression tests.**

It can be seen that the FE model is over predicting the peak force with a percentage error of 24.1% and over predicting the hysteresis with a percentage error of 163.1%. Based on these percentage errors, it was clear that the heterogeneous model was not capturing the correct behaviour of the core. The mesh density and element type were investigated and the results summarised in Figure 5.4-6.
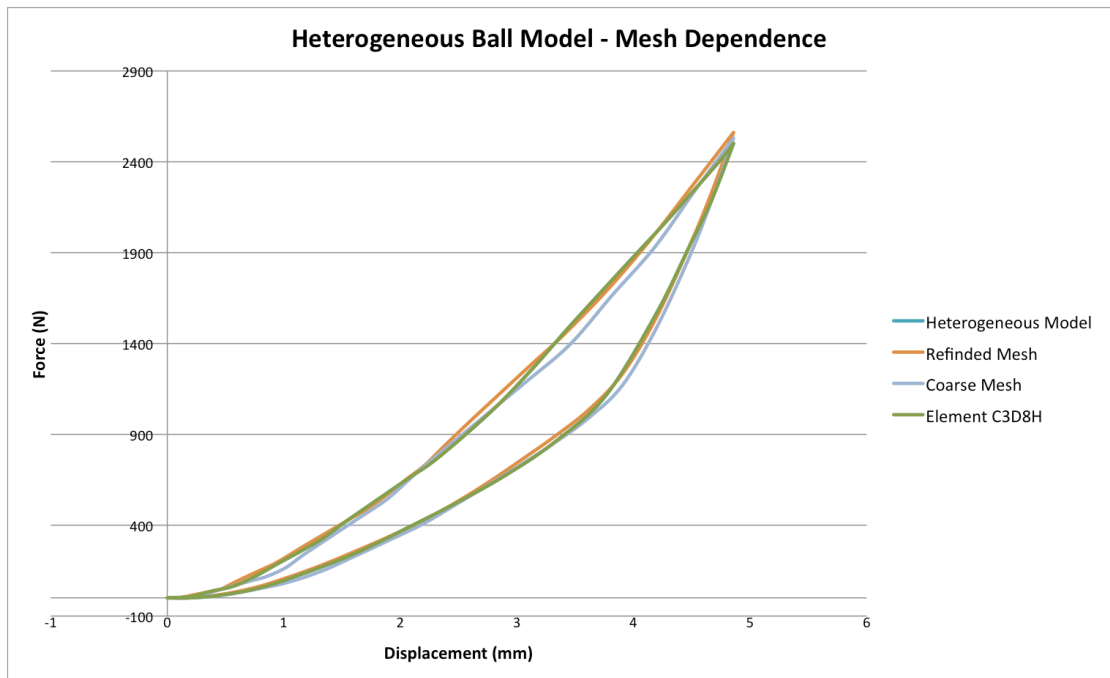
**Figure 5.4-6 - Results of element and mesh investigation.**

The "Heterogeneous Model" data set in Figure 5.4-6 corresponds to the "FE Model" data set in Figure 5.4-5. This model contained 2485 elements of type C3D8 [38]. The refined mesh and coarse mesh models kept the same element type but increased the number of elements to 4320 and reduced the number of elements to 800 respectively. Figure 5.4-6 shows that this had very little effect on the results of the simulation, therefore it can be concluded that mesh density is not affecting the solution. The element type was also investigated with the C3D8 elements being changed to the C3D8H elements, which are 8-node linear brick, hybrid with constant pressure often recommended for simulations of incompressible materials [38]. It is shown in Figure 5.4-6 that this alteration to the simulation again did not result in noticeable change to the force-displacement response.

On reflection there are fundamental differences between the FE model and the golf ball core. The FE model comprises of various material models with notably differing behaviour, the modelling technique introduces step changes in these properties that are not present in reality. The material properties in the physical object probably vary smoothly through the radius of the core. Having step changes between material models can often cause areas of high stress, which would artificially stiffen the sample increasing the force required to reach an specified strain.

The core model is further complicated by the geometry involved. With the small cylindrical samples, the load through the sample was constant due to a constant cross-sectional area. It is very difficult to obtain accurate strain rates for the core, as it does not have a constant cross sectional area, therefore deformation rates were used. Although the overall strain rate could be estimated, it was not possible to determine the experimental strain rates experienced by various sections of the ball. If certain sections of the FE model were experiencing strain rates higher than seen in reality this would artificially stiffen the material and over predict the hysteresis based on the behaviour of the material model shown previously in this Chapter.

The complications associated with the strains are also experienced when dealing with stress. Engineering stress and strain were obtained from the small samples and used to calibrate the material model but due to the constantly varying contact area between the compression platens and spherical core, force

displacement was chosen to represent the results. It was expected that the behaviour of the core would lie somewhere between the behaviour of the centre small samples and outer small samples as the core contained three material models however, because the small samples were expressed in stress strain and the core data was expressed in force displacement a comparison could not be made. To ensure that the FE results behaved as expected, three homogeneous core models were produced. If the material models were behaving in a truly representative manner the homogeneous core with centre properties would be softer than the homogeneous core with inner properties, which in turn would be softer than the homogeneous core with outer properties. Figure 5.4-6 shows the relative behaviour of the three homogeneous core models in FE and the heterogeneous FE model.
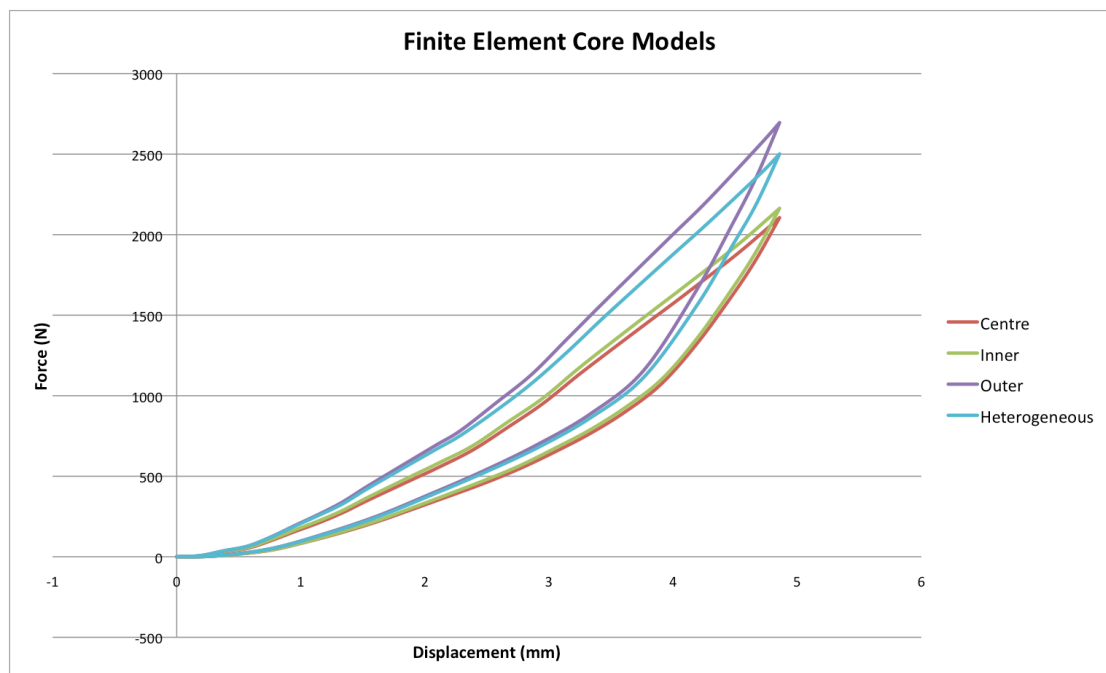


**Figure 5.4-7 – Relative behaviour of homogeneous and heterogeneous finite element core models.**

Figure 5.4-7 shows that the FE models are predicting the behaviour, in relation to each other, correctly. The homogeneous model comprising of centre properties results in the lowest reaction force at the specified displacement. The models follow the expected trend with the homogeneous sphere comprising of the outer material model, which is the stiffest, resulting in the highest reaction force for the specified displacement. Plotting the heterogeneous model along with the three homogeneous models is encouraging with regards to the material models as the force displacement curve lies between the inner and outer homogeneous curves.

In order to determine if the sample was able to predict the response for a change in strain rate the heterogeneous FE model was simulated at deformation rates an order of magnitude slower and faster than the original deformation rate. This was achieved by adjusting the duration of the compression boundary condition from 25.5s to 2.55s and 255s, to represent the faster and slower strain rates respectively. Figure 5.4-8 displays the results from the three simulations.
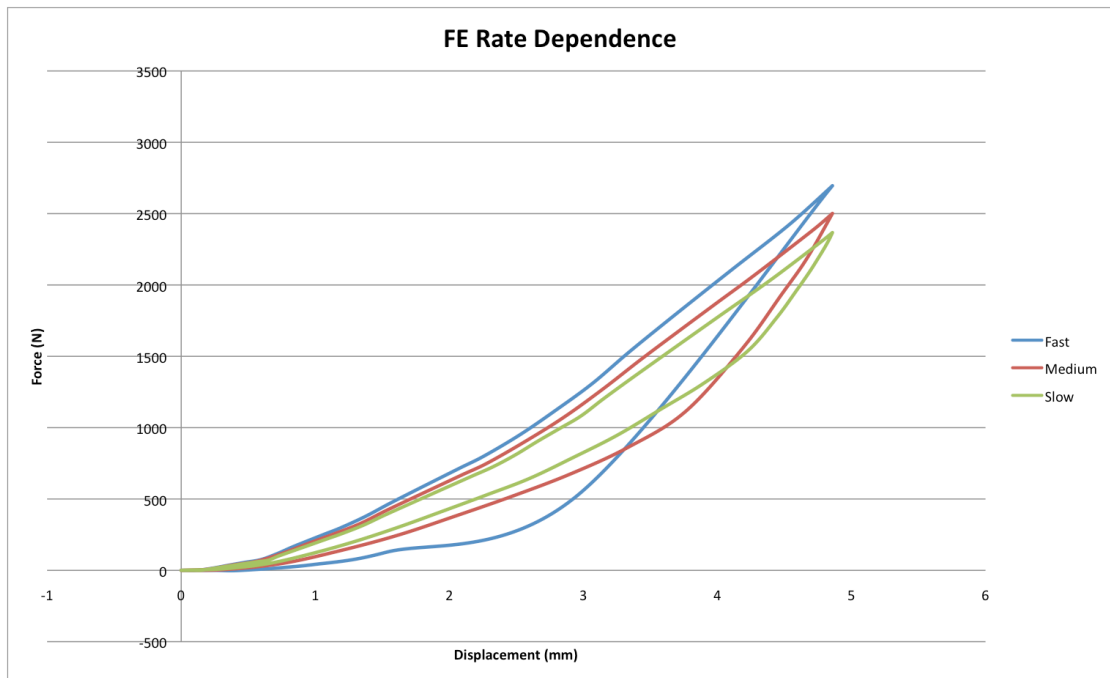
**Figure 5.4-8 - Rate dependence predictions from FE simulation.**

It is clear that the model is correctly predicting the overall core behaviour trend. It successfully predicts that the model results in higher forces at a fixed displacement with increased displacement rates although the increased strain rate visually has a detrimental effect on the shape of the hysteresis prediction.

## 5.5  Conclusions

The work described in this Chapter had a number of outcomes. The material model has been successfully calibrated with the experimental data and the FE simulations successfully predicted peak stress and captured the correct hysteresis, with respect to strain rate, behaviour. The material models were then applied to a representation of the heterogeneous core FE model. This model over predicted peak force by 24.1% and hysteresis by 163.1% but when compared to homogeneous spherical models of each material model, behaved as

expected (i.e. the heterogeneous model fell in the bounds of the centre and outer homogeneous FE models).

After further consideration it was concluded that there had been too many variables changed in one stage with regards to the development of the FE models. The simple homogeneous cylindrical geometry analysis had changed to a spherical heterogeneous analysis in one step, meaning that both geometry and material behaviour had changed. It was thought that introducing an intermediate stage, such as a heterogeneous model with cylindrical geometry would help the FE model development, hence a second experimental investigation was undertaken to try and bridge the gap between these two models with the aim of understanding the source of the errors. This experimental investigation is described in Chapter 6.

# 6   Experimental Investigation - Phase 2

Chapters 1 to 5 detail the experimental methodology of sectioning a complete golf ball core into five small cylindrical samples. Non-linear viscoelastic material models were evolved using the experimental data obtained from the small cylindrical samples and the resulting material models applied to a heterogeneous sphere in FE analysis. This investigatory phase was split into four distinct sections: ASTM samples, large cylindrical samples, wide cylindrical samples, known as "tree trunk" samples and full spherical core compression tests.

Between experimental phases 1 and 2 the calibration balls used had changed batch and the material of the ball core had been altered. The first point of concern was the difference in colour, it had been noticed that the small samples were a lighter shade of green than the ASTM and large cylinder samples. New and old cores were tested in compression under identical test conditions and it was noticed that the core consisting of older material was slightly stiffer than the new material. This difference is quantified in Section 6.4. Although this is not the ideal case, care was taken to avoid any erroneous results. Models calibrated with the small samples were compared to old core compression data and models calibrated with ASTM and large cylinder data were compared to new core compression data.

## 6.1 ASTM Samples

### 6.1.1 Sample Preparation

The ASTM samples are cylindrical samples of standard ASTM compression test geometry (29mm diameter by 13mm height) [25]. The aim was to have a testable sample of standard geometry and use the data gathered from a compression test to characterise the material models previously discussed. This material model would be applied to the complete core in FE to identify whether these "averaged" material parameters were sufficient to describe the behaviour of the core. Figure 6.1-1 shows a typical ASTM sample.
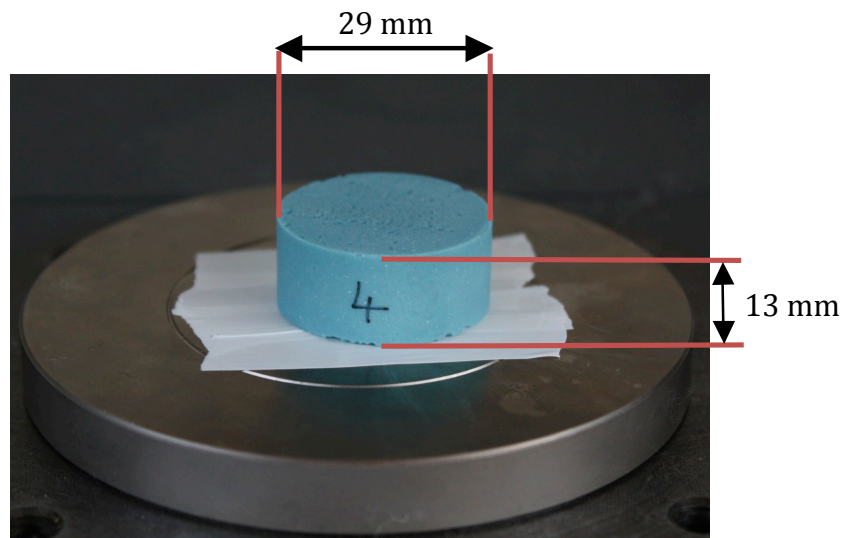


**Figure 6.1-1 - Typical ASTM sample.**

This standard geometry is not truly representative of the complete core material though as it does not include the stiffer material present at the outer radius of the core. However due to the practical considerations of machining and preparation, this was considered a good compromise. Figure 6.1-2 shows the material that is wasted through the production of the ASTM sample.
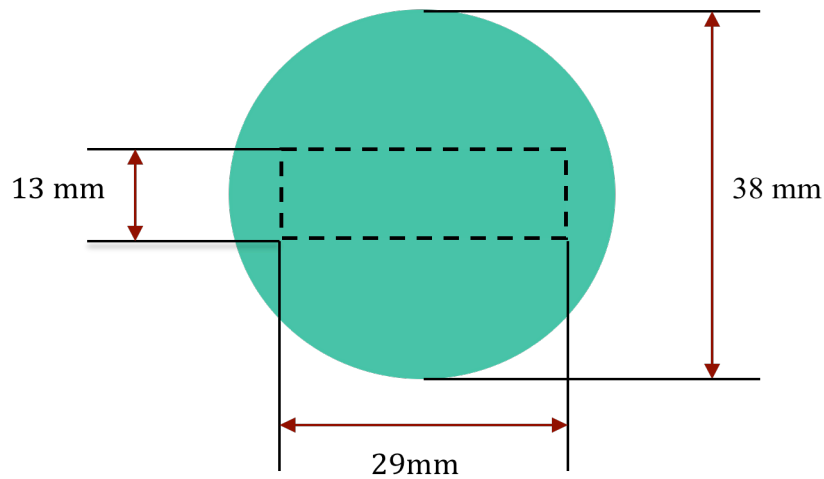
**Figure 6.1-2 - Location of ASTM samples in relation to the core.**

The production techniques for the ASTM samples were similar to that of the small compression samples but had a slightly more refined process. One of the main disadvantages of the previous method (Section 3.1) was the need to remove the remaining excess material that surrounded the machined cylinder. To avoid this, the following technique was introduced.

Initially, the complete ball was glued to a machined aluminium support for milling as shown in Figure 6.1-3. The aluminium support could then be clamped instead of clamping the ball itself, removing the need to rotate the sample midway through the machining process.

**Figure 6.1-3 – Complete ball glued to the aluminium support and example of the ball mid way through milling process.**

The top face of the sample could also be machined from this position meaning that sample preparation time was reduced as a result of less sample adjustment and CNC programming. Figure 6.1-4 shows the facing off stage of the manufacturing process.
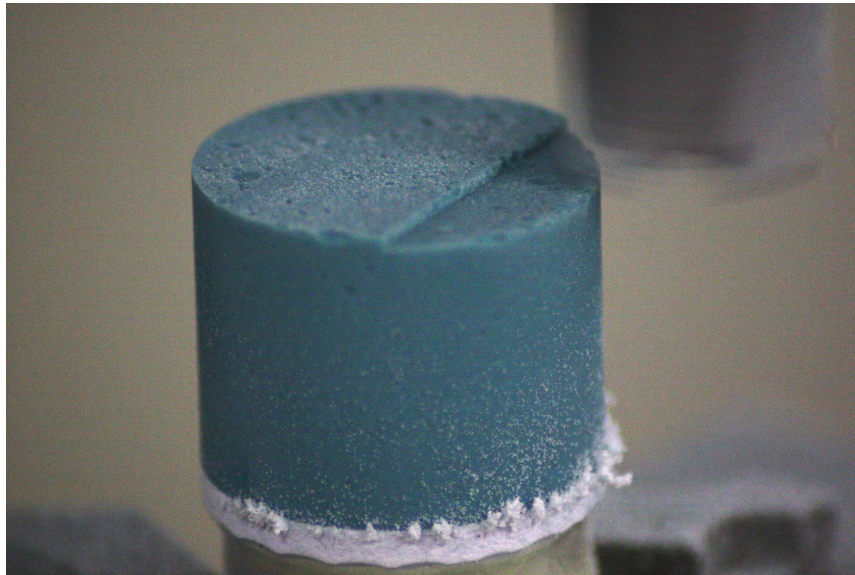
**Figure 6.1-4 – Machining of ASTM sample top face.**

The sample was separated from the cover that was attached to the aluminium support, simply by pulling, and inserted back into the three-jaw chuck to allow machining of the bottom face. The sample was supported using a pair of calibrated parallel edges. This ensured that the top and bottom faces were parallel to one other.

It was observed at this stage that machining the ball with the cover on caused the mill tool to blunt. This was possibly due to the impurities in the cover material so further machining was completed with no cover present. Removing the cover is a simply, yet time consuming, task that involves a series of incisions with a knife and separating the core and cover with pliers.

### 6.1.2 Experimental Procedure

The described ASTM samples were tested in compression to obtain suitable stress strain curves for material characterisation. The method followed that described previously in Chapter 3, Section 3.3.1. The maximum strain magnitude was 20% and strain rates used were 0.08 s$^{-1}$, 0.008 s$^{-1}$ and 0.0008 s$^{-1}$ again as described in Section 3.3.1. The preload and number of cyclic loads were as described previously. Eight samples with ASTM geometry were examined.

### 6.1.3 Results and Discussion

ASTM samples 1-4 had to be discarded due to non-parallel compression platens. On completion of the first phase of ASTM sample investigation it was discovered that the plates were not aligned correctly. This was believed to be too large a source of experimental uncertainty therefore the data was discarded. Figures 6.1-5 to 6.1-7 show the repeatability of the data from the sixth cycle for the remaining three samples at the three strain rates, 0.08 s$^{-1}$, 0.008 s$^{-1}$ and 0.0008 s$^{-1}$, mentioned in Section 6.1.2. To clarify, each sample (ASTM 5, 7 and 8) was tested at all three strain rates making nine tests in total. The order of the strain rates that the samples were tested at remained consistent throughout the testing phase to avoid possible sources of uncertainty with the data.
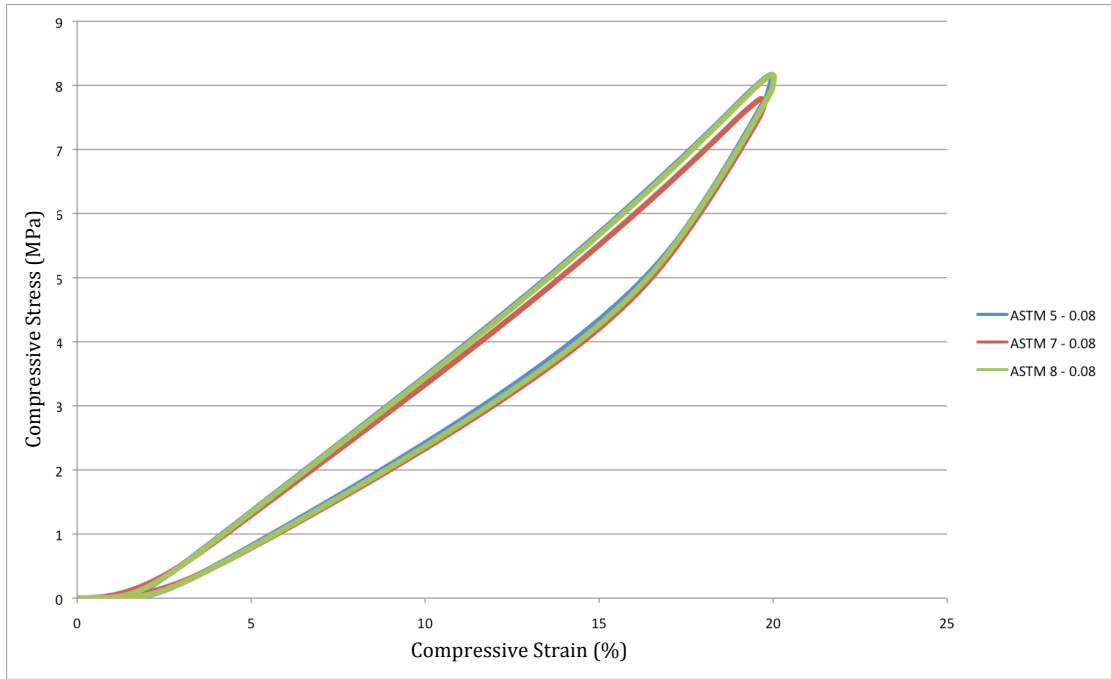
**Figure 6.1-5 - Repeatability of ASTM samples at 0.08 s⁻¹.**
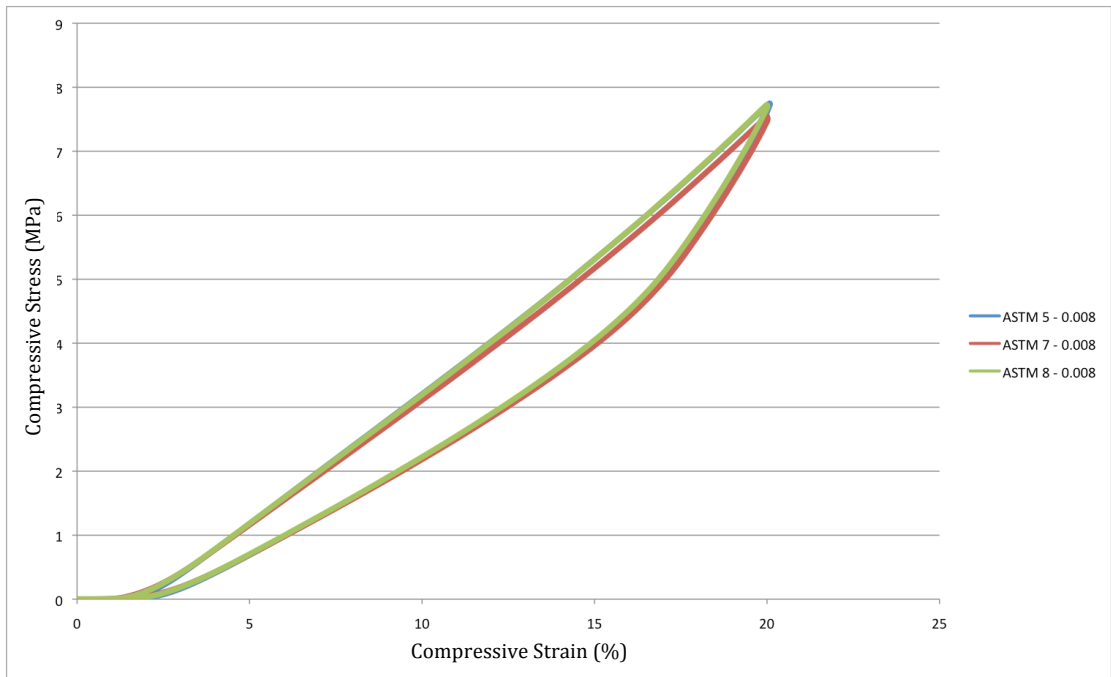


**Figure 6.1-6 - Repeatability of ASTM samples at 0.008 s⁻¹.**

116
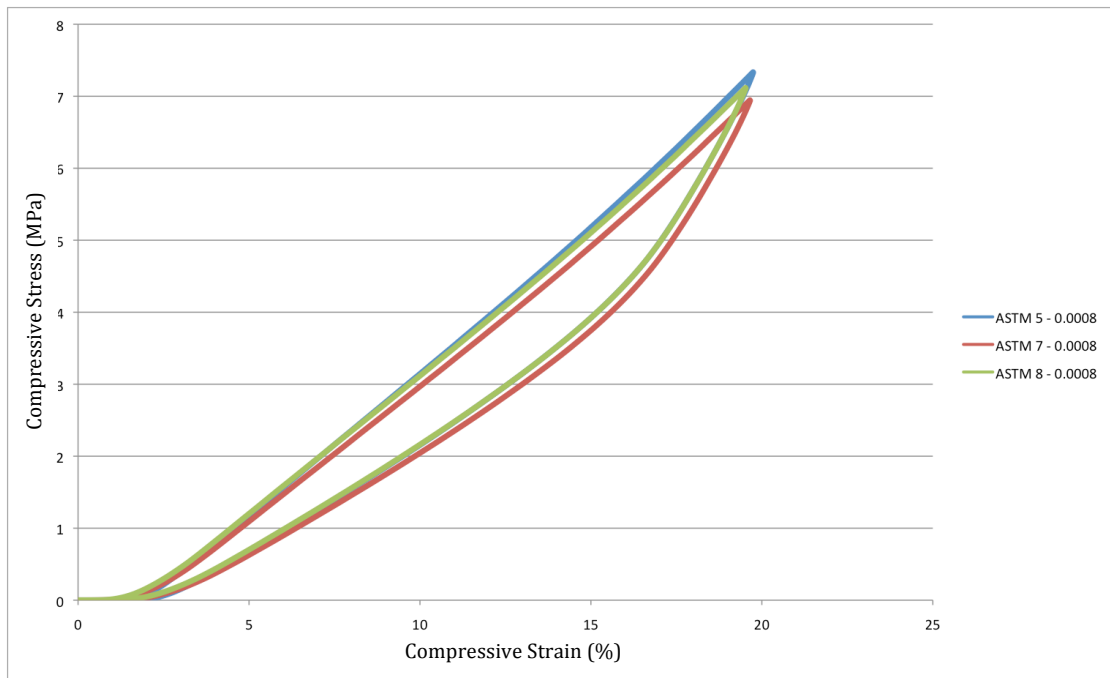
**Figure 6.1-7 - Repeatability of ASTM samples at 0.0008 s⁻¹.**

Figures 6.1-5 to 6.1-7 show that samples ASTM 5 and ASTM 8 have good repeatability whereas ASTM 7 is slightly softer at all three strain rates. As with previous tests, the nature of the manufacturing process of the cores and the method of sample preparation may result in an increased chance of experimental uncertainty. There is one very noticeable characteristic of the ASTM data, the experimental stress-strain curve seems to have very low tangent stiffness at small strains, and then reach an almost constant slope around a strain of 1.5% (or so). It was suspected [37] that this was a result of experimental slack and not a true representation of the material behaviour. Experimental slack is a term referring to the platens not being in full contact with the sample at the start of the test. If the sample faces are not parallel to the compression platen faces this can cause the sample to exhibit a reaction force not akin to the realistic material behaviour. Typically, elastomer responses do

117

not exhibit such a slow tangent stiffness [37] and it was thought that the behaviour reported was a result of the plates coming into contact with the sample edges before full contact was established. Due to time restrictions, further tests were not carried out to confirm the source of this behaviour but it was expected to be experimental error rather than true material behaviour.
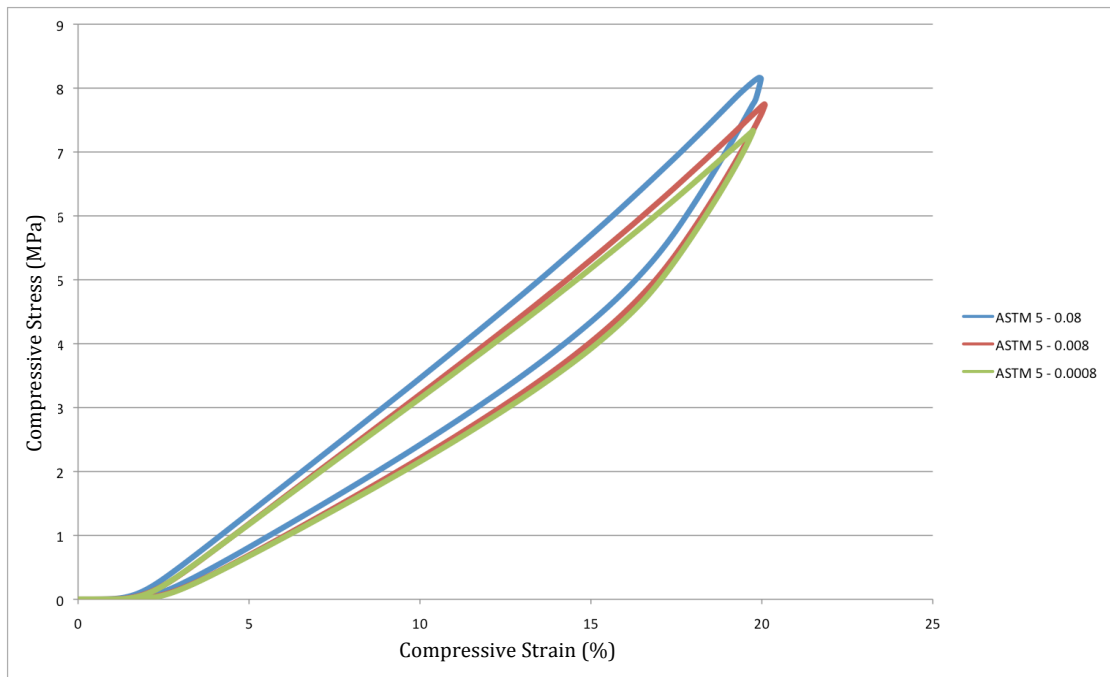


**Figure 6.1-8 - Rate dependence of ASTM Sample 5.**
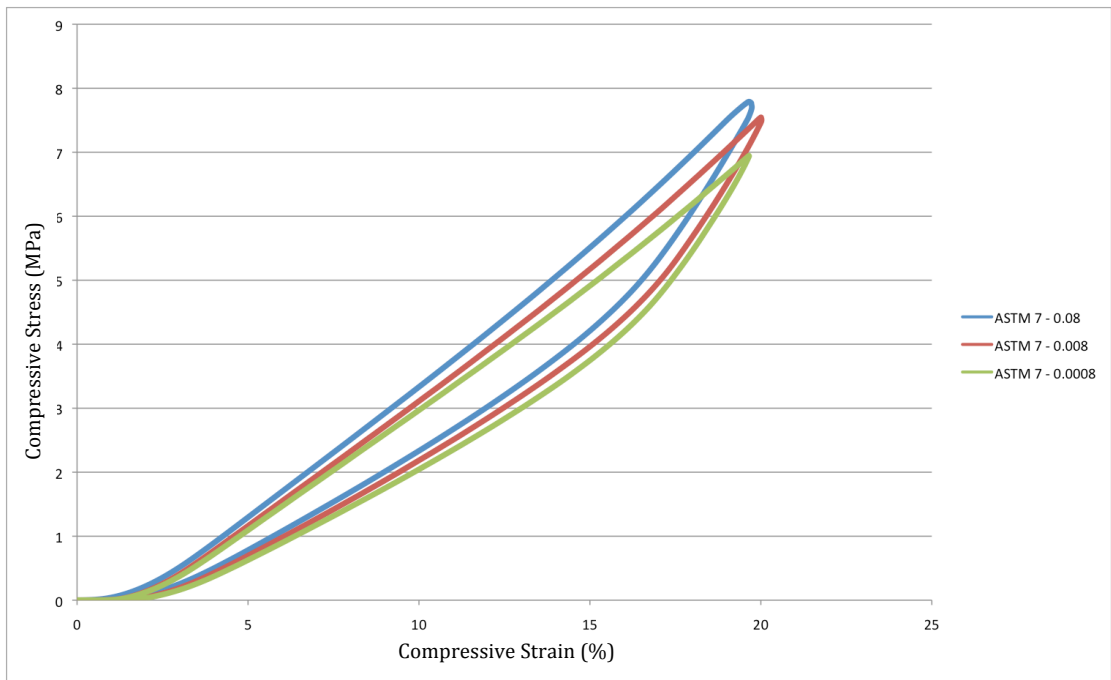
**Figure 6.1-9 - Rate dependence of ASTM Sample 7.**
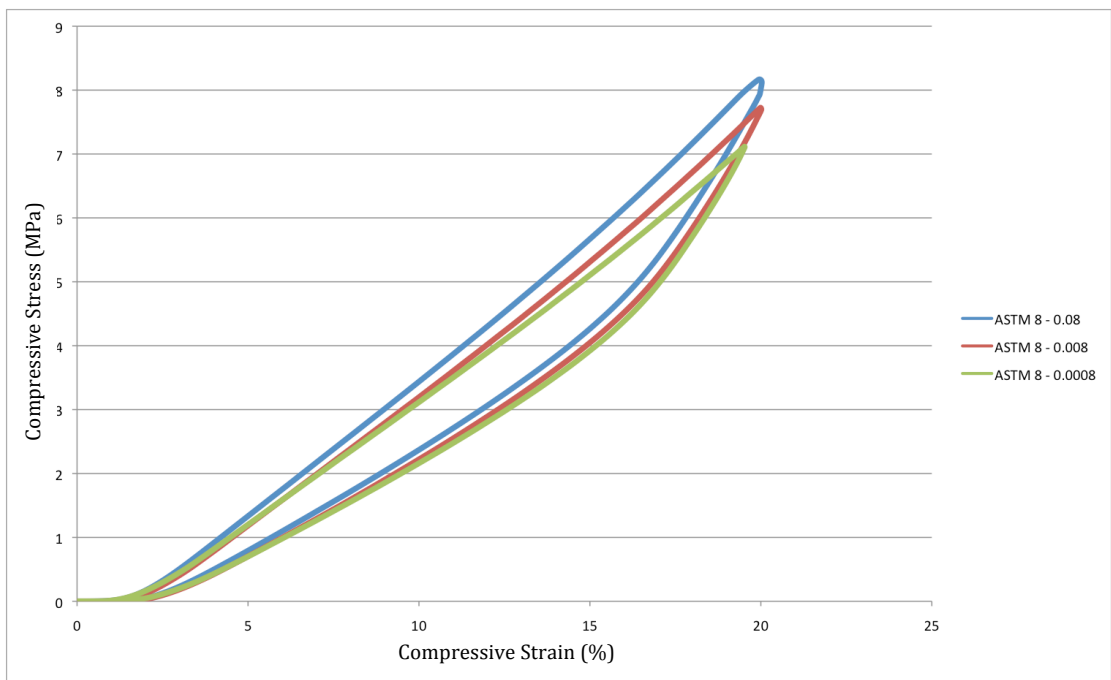


**Figure 6.1-10 - Rate Dependence of ASTM Sample 8.**

Figures 6.1-8 to 6.1-10 display of the rate dependence of the ASTM samples, this behaviour is consistent with previous tests and literature, with the highest strain rate yielding the stiffest response.

In comparison to the original small sample tests described in Chapter 4, it would be expected that the ASTM samples display fairly similar behaviour albeit with a slightly different modulus. Figure 6.1-11 is a plot of a typical response from the small inner, centre and outer samples against a typical response of the ASTM samples.
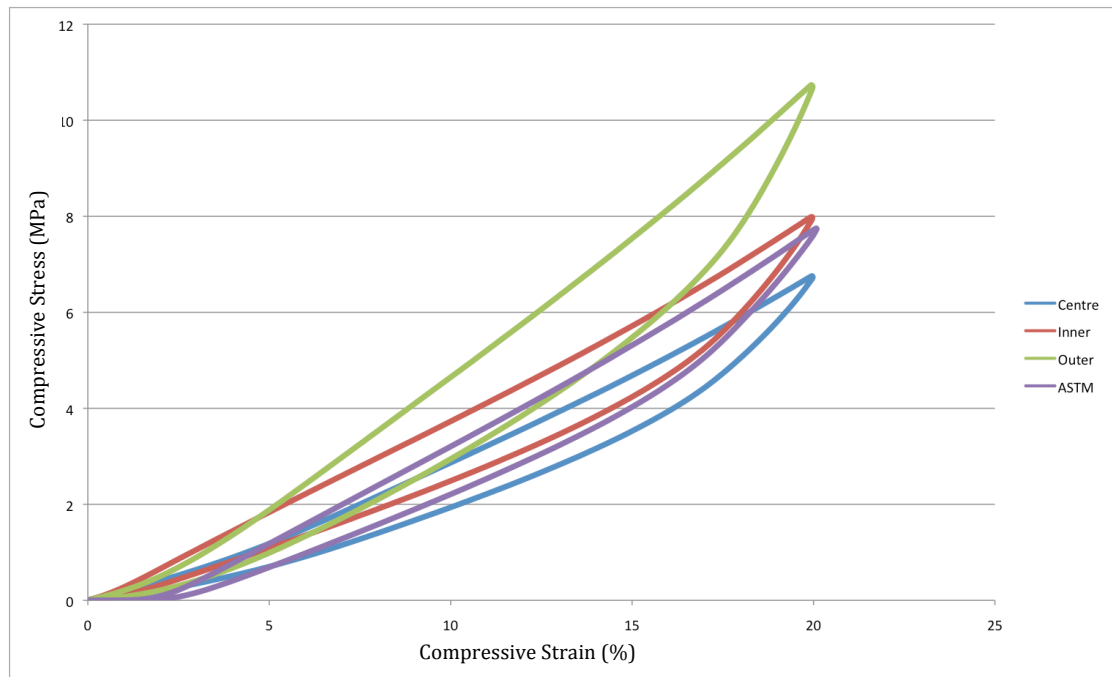


**Figure 6.1-11 - Small sample response versus ASTM sample response.**

Due to the increase in sample size, in the ASTM sample, the presence of "inner" material is increased. It therefore is reasonable to conclude that the ASTM sample response in slightly stiffer than that of the small centre sample, slightly softer than the small inner sample and noticeably softer than the small outer sample.

## 6.2 Large Cylindrical Samples

### 6.2.1 Sample Preparation

The aim for this phase of the testing was to maximise the material used for material model calibration yet maintain a testable geometry. The advantage of this over the ASTM geometry samples was that each large cylindrical specimen contains more material from the core resulting in a more accurate "average" of core properties. The ASTM samples primarily contain "centre" and very little "inner" material whereas the large cylindrical samples contain more "inner" and possibly some "outer" material. Material models will be calibrated using the data gathered from these samples and applied to homogeneous core FE models, to examine the accuracy of the "averaged" material parameters. The largest cylindrical sample that could be produced was removed from the core and had a depth of 24mm and a diameter of 29mm as shown in Figure 6.2-1.
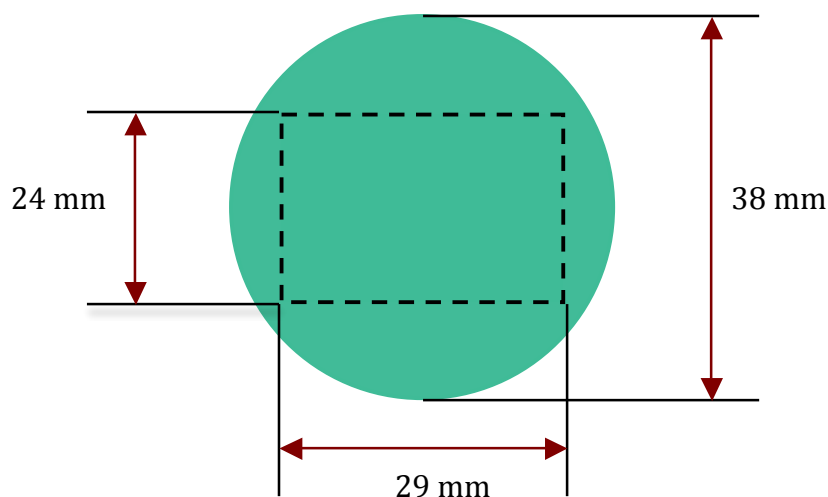


**Figure 6.2-1 - Location of large cylindrical sample in relation to core.**

For representation of the entire core, this specimen had the advantage of containing more "outer" material but did not maintain the ASTM standard compression sample geometry. The samples were produced using the same procedure as described previously (Section 6.1.1) for the ASTM samples, with the only alteration being the displacement values used to control the CNC milling machine.

### 6.2.2 Experimental Procedure

The method followed that described previously in Chapter 3, Section 3.3.1. Each sample was pre-loaded to ensure full contact between sample and compression platens. The samples were strained through a programme of 6 cycles to 20% at strain rates of 0.08 s$^{-1}$, 0.008 s$^{-1}$ and 0.0008 s$^{-1}$ as described in Section 3.3.1. In total four large cylindrical samples, L1, L2, L3 and L4 were examined each at three strain rates.

### 6.2.3 Results and Discussion

The data from large cylinder Sample 1 had to be disregarded due to a crack in the sample, which was discovered after the compression cycles test. Figures 6.2-2 to 6.2-4 show the repeatability of the large cylinder samples at 0.08 s$^{-1}$, 0.008 s$^{-1}$ and 0.0008 s$^{-1}$ respectively.
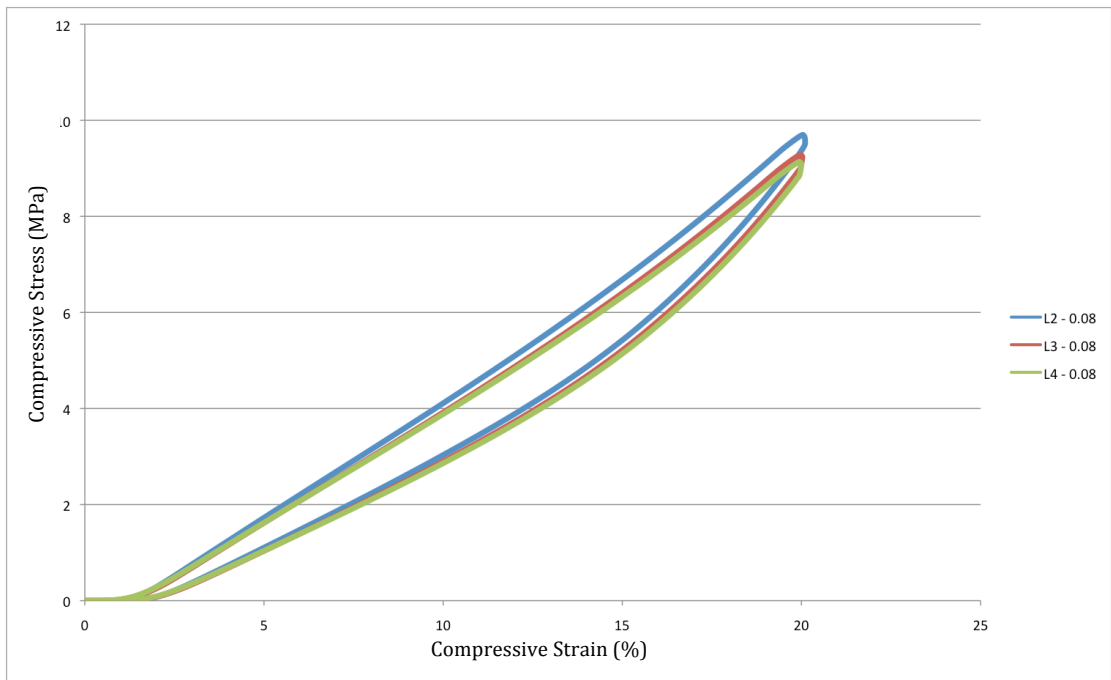
**Figure 6.2-2 - Repeatability of large cylinder samples at 0.08 s⁻¹.**
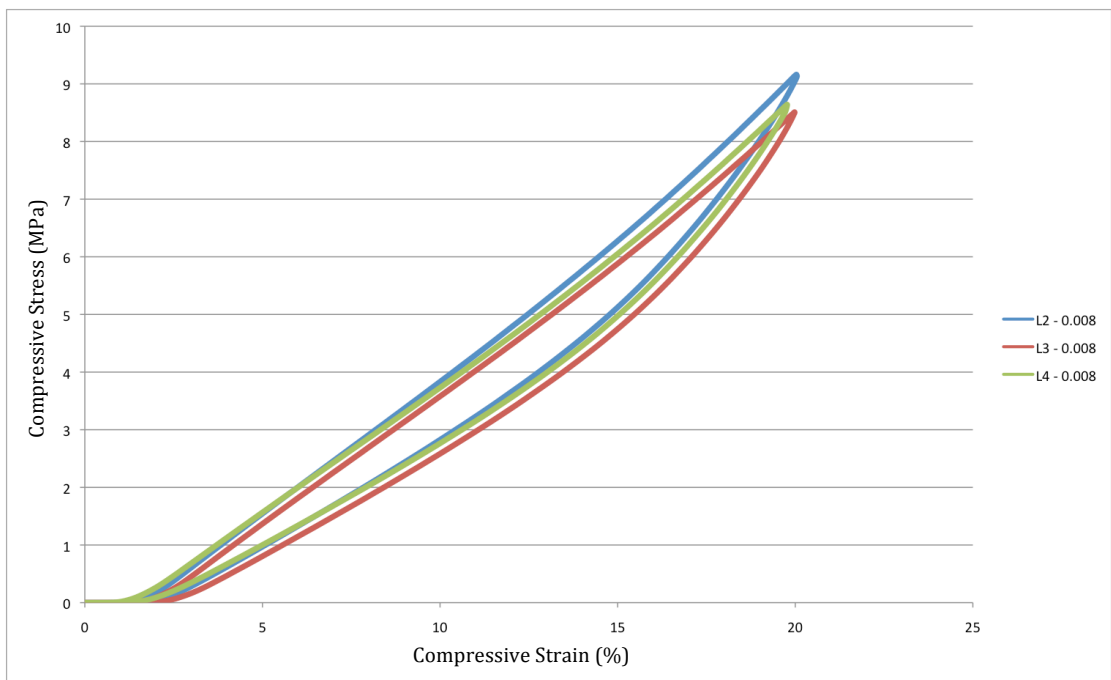


**Figure 6.2-3 - Repeatability of large cylinder samples at 0.008 s⁻¹.**

123
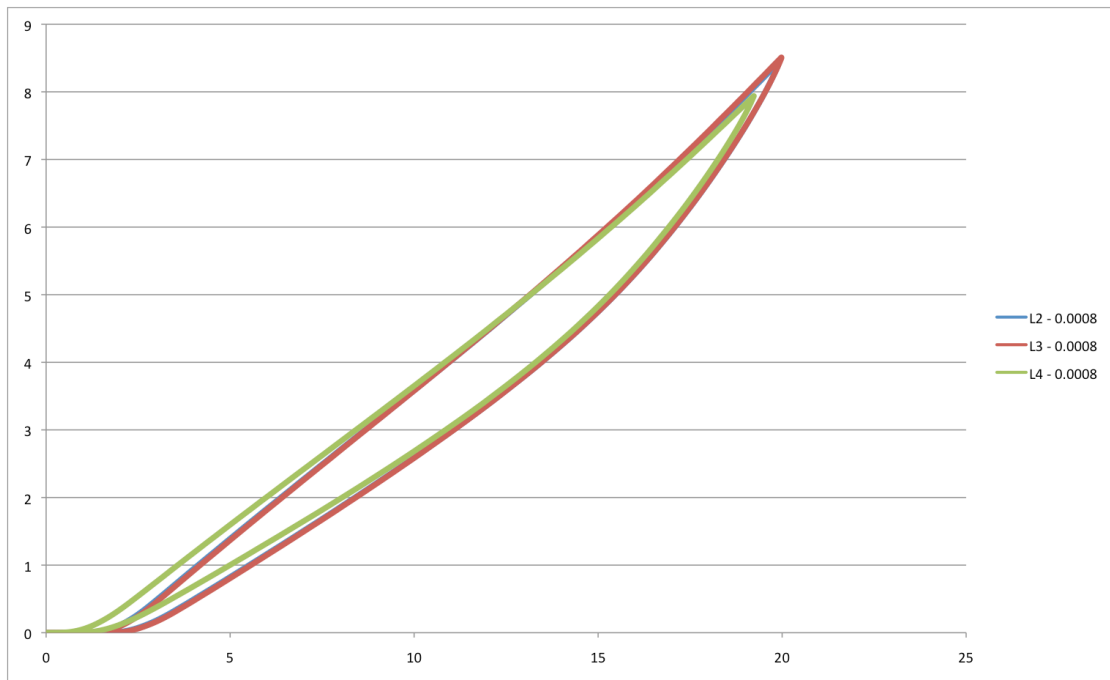
**Figure 6.2-4 - Repeatability of large cylinder samples at 0.0008 s⁻¹.**

As with all experiments undertaken in this study there is the presence of manufacture and experimental error but it is interesting that the large cylindrical samples visually show less repeatability than the small cylindrical samples. It is expected that this could be due to the large cylindrical sample not maintaining the correct height to diameter ratio as specified in the ASTM testing standards. Not adhering to these test standards could increase the chance of the material experiencing deformation modes, such as material shearing, which changes the material behaviour from the desired state of pure compression.
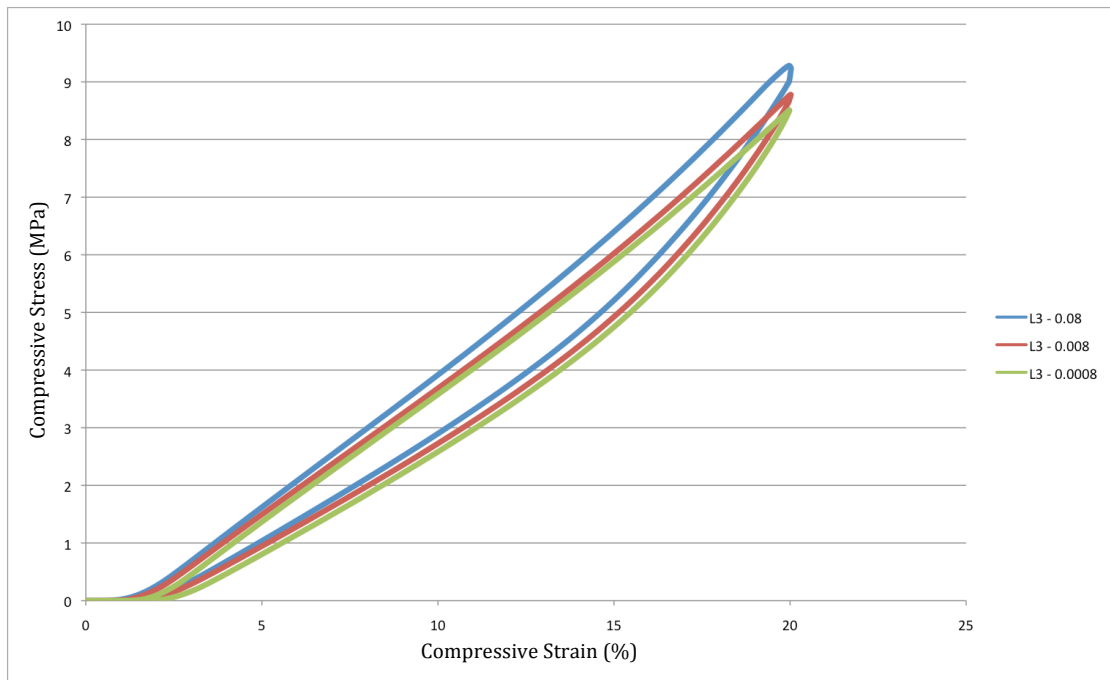
**Figure 6.2-5 - Typical rate dependence of large cylindrical samples.**

The rate dependence of the large cylindrical Sample, L3 is shown in Figure 6.2-5 and the trend agrees with the results from Samples L2 and L4, which are omitted for brevity. The results agree with the previous outcomes from the rate dependence studies of the other cylindrical samples.

As the volume of "inner" and "outer" material has increased it was expected that the overall response of the large cylinder sample would be stiffer than both centre and inner small samples but softer than the outer small samples. It is important to note that due to the increased size and height to width ratio, the issue of sample bulging becomes an area of concern. Sample bulging is the name given to the behaviour shown in Figure 6.2-6. It occurs when the sample expands laterally as a result of the Poisson's effect but the friction coefficient

between the compression platen and sample face is to high to allow free movement perpendicular to the compression direction. As the sample bulges under loading, the material experiences shearing which can lead to an artificially stiff result [24].
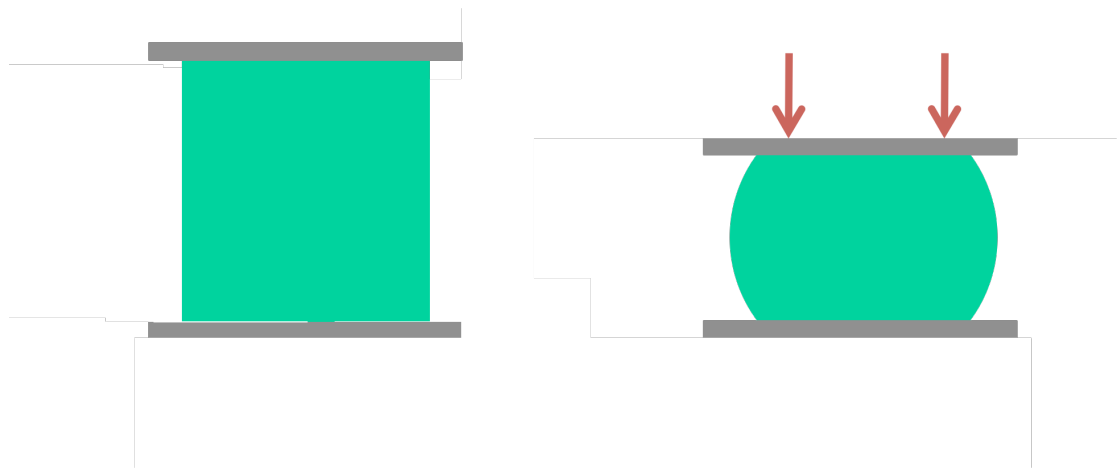


Figure 6.2-6 - Simple representation of sample bulging.

It is difficult to quantify sample bulging without the use of extensometers but through observation, bulging seemed to be more noticeable with the large cylindrical samples than previously observed with the ASTM and small samples. Through the use of PTFE tape every care was taken to reduce the magnitude of sample bulging and due to the softness of the material being investigated, contact extensometers were not used. The literature suggests [24] that non-contact devices may be used but these were not readily available for the test dates. Figure 6.2-7 shows the results that best represent each data set from the small samples (centre, inner and outer), the ASTM samples and the large cylinder samples plotted together.

126
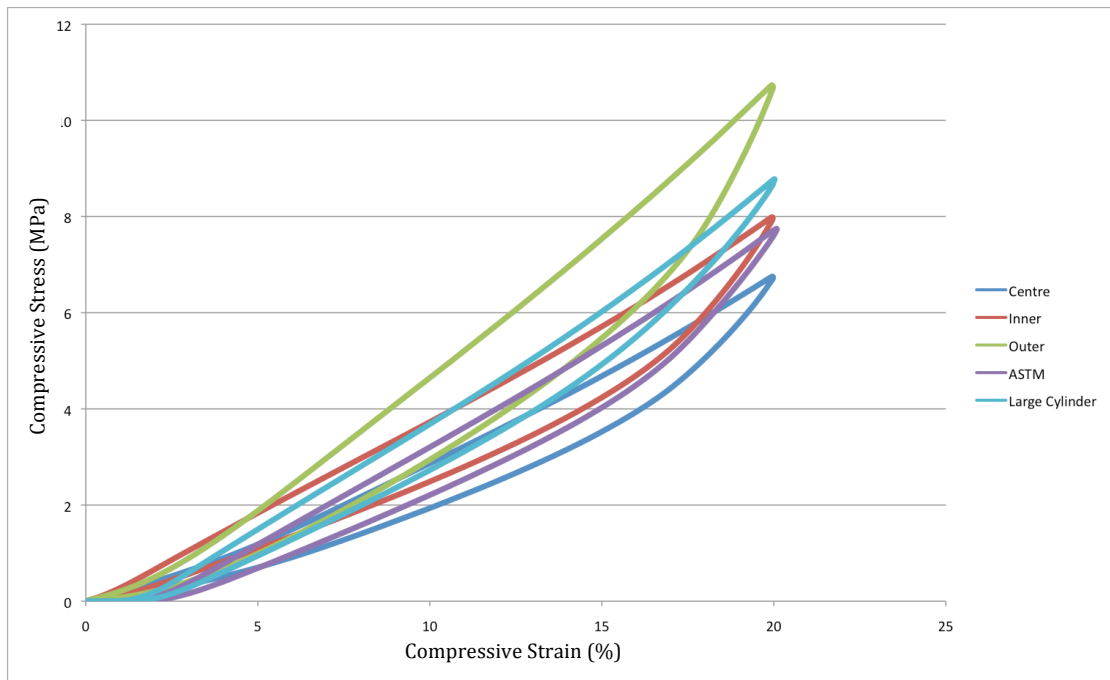
**Figure 6.2-7 – Response curves for small sample, ASTM sample and large cylindrical sample.**

As expected, the large cylinder sample response is stiffer than the inner small sample, stiffer than the ASTM sample and softer than the outer small sample.

## 6.3 Wide Cylindrical (Tree Trunk) Samples

The obvious disadvantage of the using the data described in the previous two sections (the ASTM and Large Cylinder sample data) to calibrate material models is that they do not capture any material heterogeneity. However the purpose of these investigations was to discover if an averaged set of homogeneous parameters were capable of capturing the core behaviour sufficiently. Ideally the final core model would include some degree of material heterogeneity.

In Chapter 5 the behaviour of the small cylindrical samples was successfully captured and modelled. The material models were then combined and applied to a spherical core geometry. There was a need for an intermediate step between the testing and analysis of the small cylindrical samples and production of the full heterogeneous core. The desired test would involve testing the initial machined column (consisting of the small cylindrical samples) in compression but due to the sample geometry this was not possible. Under uniaxial compressive loading the sample would inevitably buckle, rendering the data unusable. Figure 5.3-1 shows the ideal test and the problems associated.
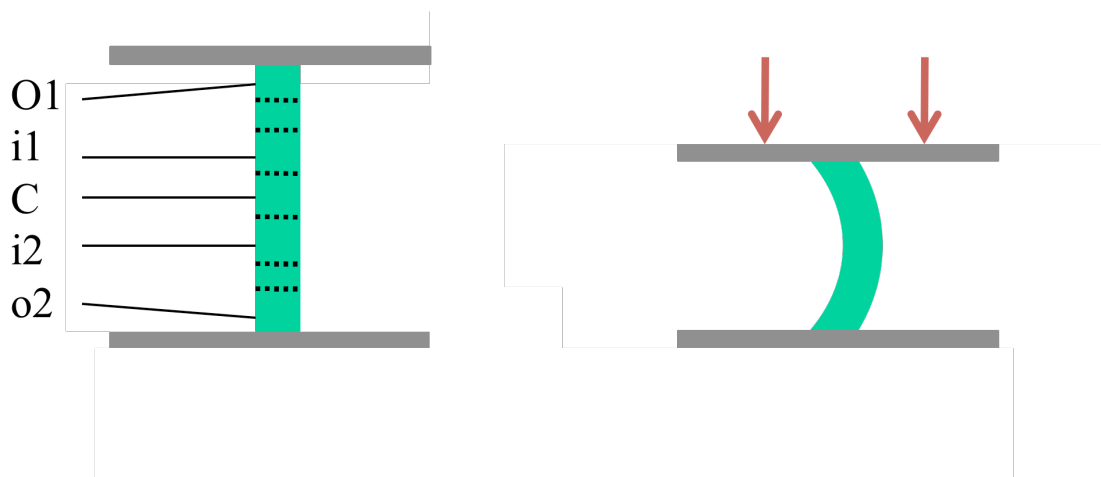


**Figure 6.3-1 – Simple representation of the buckling effect loading would have on original cylindrical sample.**

The objective in this stage was to test a heterogeneous model that maintained a standard geometry in order to alleviate the spherical geometric complications. The solution involved visualising the overall sample rotated 90 degrees so that it lay on it side. It was not possible to test the sample in this orientation as the surfaces in contact with the compression platens would be curved, however this

prompted discussion of further ideas. Instead of stacking the samples vertically, they could be arranged in a standard geometry horizontally through a series of concentric rings. Figure 6.3-2 shows the overall idea and the separate material regions. The advantage of this method was that the FE simulation maintained a constant, conforming (the same points on the contact surfaces were always in contact) contact area between sample and compression yet the model consisted of the various material models.
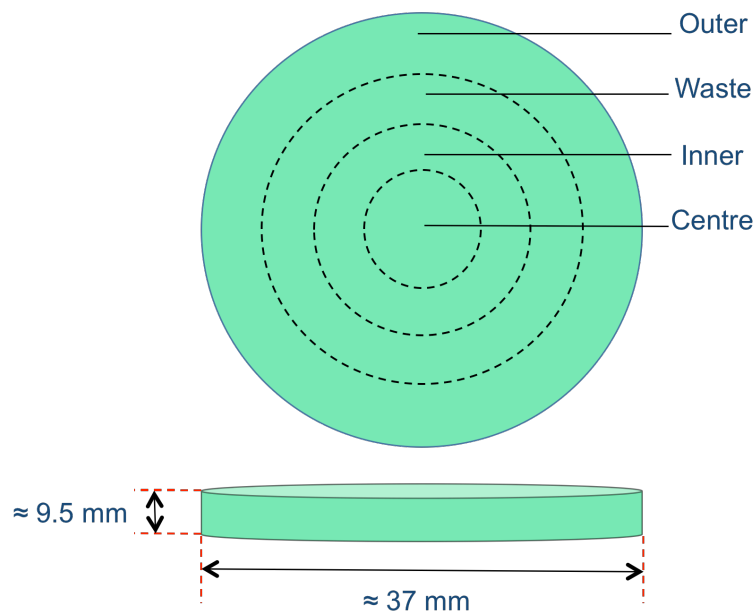


Figure 6.3-2 - Representation of the tree trunk sample.

### 6.3.1 Experimental Procedure

The experimental procedure used to test the samples in compression was the same as described previously in Section 3.3.1, however the three samples were only tested at one strain rate as they were not required for material model calibration, instead the data gathered from the tests was to be used for FE

model verification. The strain rate chosen for this was 0.008 s$^{-1}$ as it was the intermediate rate in the range investigated within the study.

### 6.3.2   Results and Discussion

Although the samples were not intended for material model calibration the repeatability still had to be investigated for validation purposes. Figure 6.3-3 highlights the repeatability of the tree trunk samples.
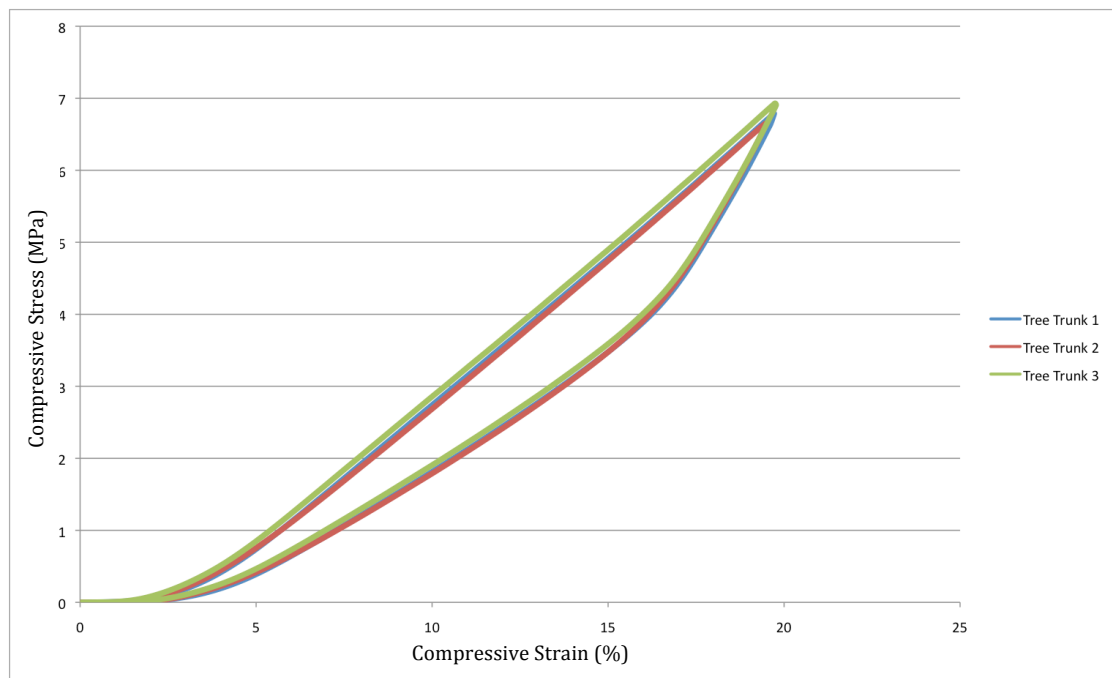


**Figure 6.3-3 - Repeatability of tree trunk samples at 0.008 s$^{-1}$.**

As previously explained the slight differences can be attributed to experimental and manufacturing differences. An FE model of the tree trunk sample is constructed in Chapter 7 and encompasses various material models (e.g. material heterogeneity) in a standard cylindrical geometry.

## 6.4 Full Core Compression

It was deemed necessary to obtain data from multiple core compression tests for comparative reasons. The repeatability of the selected cores was important to quantify along with the rate dependence. Another point of interest was the isotropicity of the core. If the exhibited behaviour differed depending on orientation then the validity of the material model would be further questioned as it was assumed that the core material is fully isotropic. Based on the manufacturing process that the core undergoes [12] it was expected that the core would display isotropic behaviour.

### 6.4.1 Core Isotropy

In order to examine the response in different orientations a compression direction line was marked on the core as shown in Figure 6.4-1.
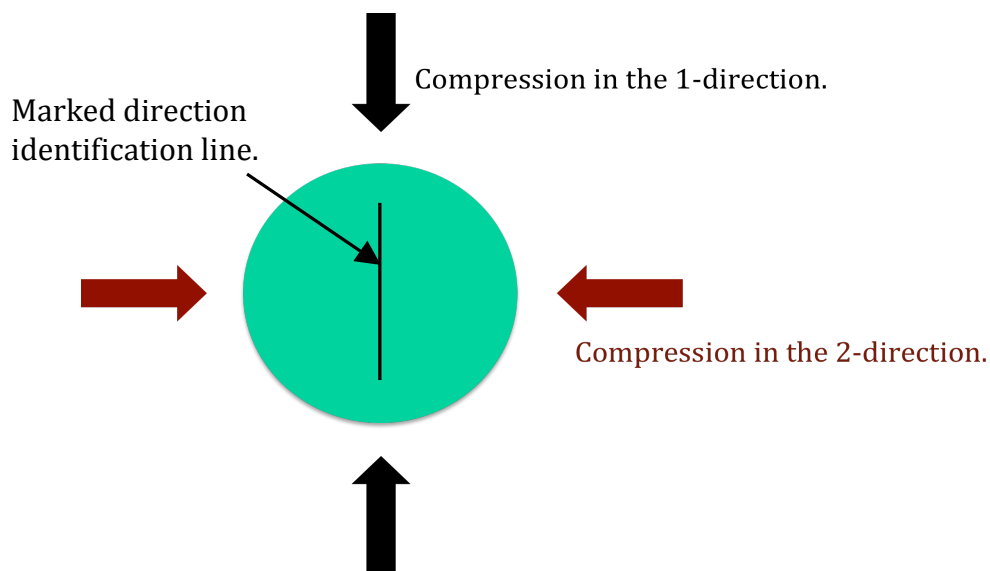


Figure 6.4-1 - Method for determining the isotropicity of the core.

The arrows in Figure 6.4-1 show the chosen compression directions. The marked line on the surface of the core was used as a reference for the compression direction. The core was compressed at a deformation rate of 11.664 mm/min. Deformation rate was favoured over strain rate for the spherical geometry due to the difficulty of the constantly changing contact area on strain rate calculations. A suitable deformation rate was calculated from the previously used strain rates. As described previously PTFE tape was placed between the ball and the compression platens to reduce the effect of friction. As this test was only meant as a comparison for the responses from various orientations, it was not strictly necessary to keep all variables consistent with the past tests carried out in this study. The emphasis was more directed to keeping the current test variables identical with the only change being the core orientation. The cores were compressed through a programme of 6 cycles and the data from the sixth load unload cycle was used for comparison. Figure 6.4-2 displays the results from the above investigation.
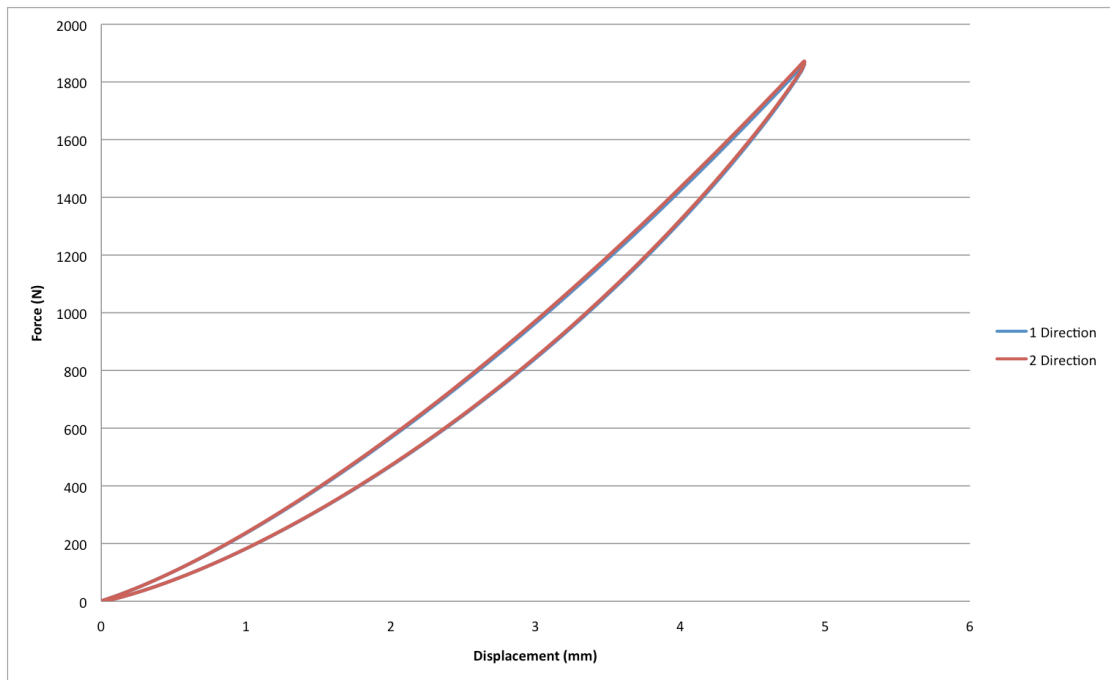
**Figure 6.4-2 - Comparison of compression of the core in multiple orientations.**

It is clearly shown by Figure 6.4-2 that the golf ball core behaves in an isotropic manner. The force displacement response is very repeatable from both directions. This is the overall structural behaviour, it is not known if the internal behaviour of discrete sections of the ball material are isotropic but the nature of the manufacturing process and the method of heat and pressure application would suggest that the properties will vary in the radial direction but there are no reasons to suspect that there is any orthotropic behaviour present in the core.

### 6.4.2   Core Repeatability

It was mentioned previously that the supplier of the test golf balls had changed the core material. This section aims to quantify the difference between these

materials. Three cores made from the new material and two cores made from the old material were tested in compression and the results compared. The three new cores were tested at three deformation rates that were calculated to roughly match the strain rates used in the cylindrical geometry tests. The rates used, in the load unload cycles, were 1.166 mm/min, 11.664 mm/min and 116.44 mm/min. Due to time restrictions the old cores were only tested at one deformation rate, 11.664 mm/min. The overall behaviour of the cores was discovered to be very repeatable. Figure 6.4-3 shows the response of the five cores plotted together.
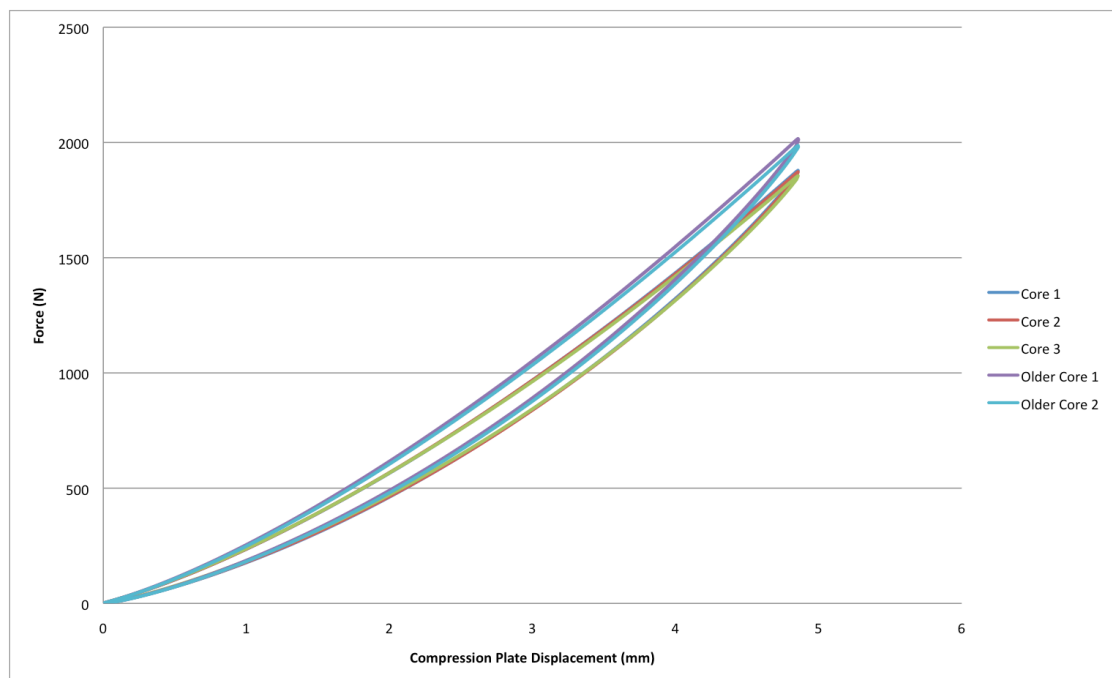


**Figure 6.4-3 - Repeatability of five full core samples at 11.664 mm/min deformation rate.**

It is shown here that the old core requires approximately 100N more compressive force to reach the same plate displacement. It is interesting to note that the overall response of the core is more repeatable than the individual

manufactured cylindrical samples. This suggests that the primary area of concern with sample repeatability is associated with the manufacturing process.

### 6.4.3   Core Rate Dependence

As previously reported for all experimental tests the core samples displayed the expected trend of published behaviour for polymers regarding strain rate dependence. The fastest strain rate producing the stiffest response and the slowest strain rate producing the softest response.

### 6.5   Summary

An experimental investigation has been undertaken with the aim of establishing whether "averaged" material parameters from larger samples are more, less or as capable of predicting the behaviour of a golf ball under compressive loading when compared to experimental results. The material data captured from the ASTM and large cylinder models will be used, in Chapter 7, to calibrate new material models. The material models will then be applied to the spherical core geometry to investigate whether they are more or less accurate than the current heterogeneous model presented in chapter five.

An FE model of the tree trunk samples will be constructed with the material models from the small samples assigned to the relevant concentric ring. The results of this FE analysis will be compared to experimental results from the tree trunk samples. This aim of this phase, described in Chapter 7, is to see if the model is capable of predicting the behaviour of multi-material systems that

maintain a simple geometry and conforming contact behaviour under deformation.

# 7 Finite Element Analysis of the Tree Trunk Samples, The ASTM Core Model, The Large Cylinder Core Model and Material Model Calibration - Phase 2

Chapter 5 introduced the techniques involved in the development and procedure for the finite element analysis and material model calibration. This Chapter employs the same techniques with different data sets. The aim here is to calibrate two new material models that that followed the same architecture as the PNM models in Section 5.3.2. The chosen model from the investigation reported in chapter five contained two distinct networks. Network A was represented by a Yeoh spring and defined the non-rate dependent elastic response, whereas Network B contained a Neo-Hookean (NH) spring and Bergström-Boyce (BB) flow dashpot defining the viscoelasticity of the material. This material model architecture was maintained and the data gathered from the large cylinder and ASTM geometries, in Chapter 6, was used to calibrate the material parameters that describe the material model. A finite element (FE) model of the tree trunk samples was also constructed to investigate how various material models interacted in a standard geometry with constant conforming contact area between specimen and compression platen.

### 7.1 Material Model Calibration

The MCalibration software [35] from Veryst Engineering was again used for the material model calibration.

### 7.1.1 ASTM Sample Data

The purpose of using the ASTM geometry samples was to investigate whether or not a homogeneous set of material parameters obtained from a larger core sample would be sufficient to describe the behaviour of the core. Although it is known to be highly heterogeneous it was hypothesised that a set of "averaged" parameters might obtain as accurate a result with less complications with regards to experimental analysis and FE modelling.

The experimental data from ASTM Sample 5 was selected as it best represented the overall response of all ASTM tests, this was decided by simply examining the responses and selecting the data set that fell within the upper and lower bounds of the data. A series of initial parameter guesses, based on the parameters obtained from the small sample material models, were entered into the MCalibration software and optimised to reduce the NMAD fitness error. After a series of iterations the NMAD error stabilised at 7.26, Figure 7.1-1 shows the predicted response and overall fitness of the material model to the experimental data.
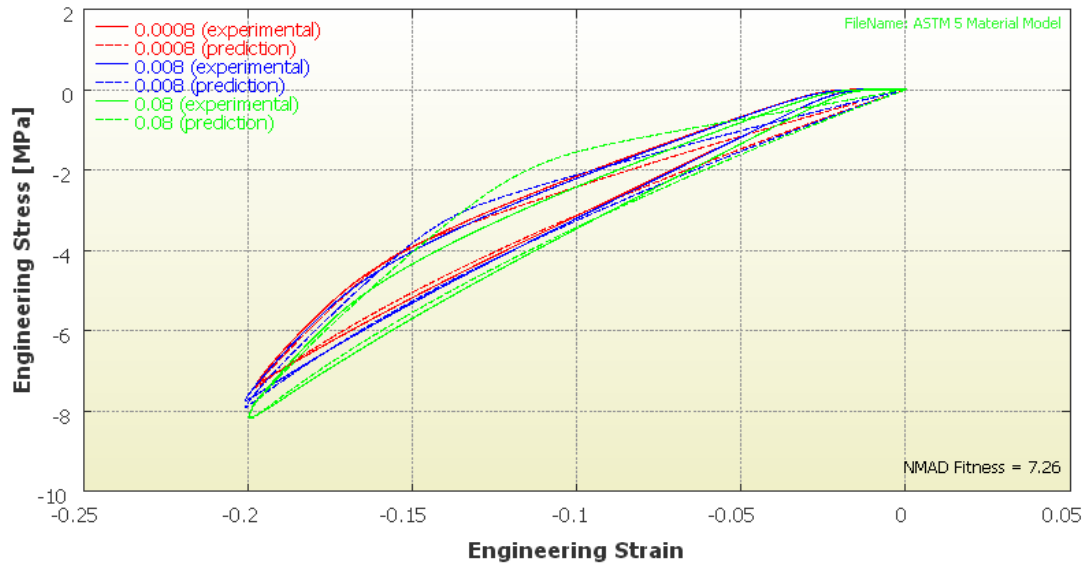
**Figure 7.1-1 – Results of material parameter optimisation for ASTM sample 5.**

Figure 7.1-1 shows the prediction of the material model at all strain rates. It is evident that the material model is having difficulty capturing the initial behaviour. It is considered that this is due to "experimental slack". Figures 7.1-2 to 7.1-4 show the predictions at the various strain rates in greater detail.
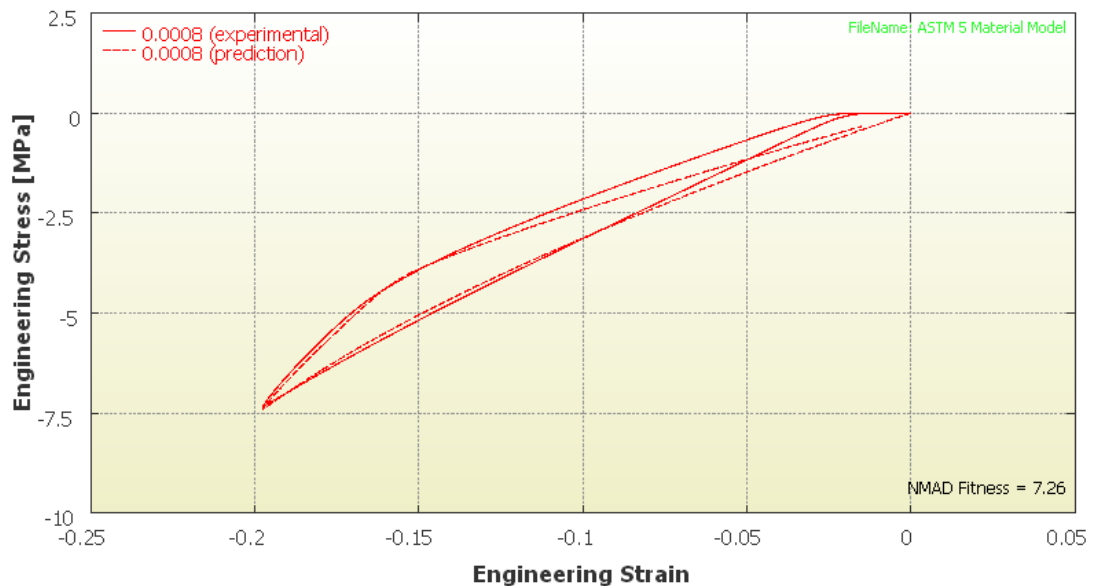


**Figure 7.1-2 - Prediction of PNM model at $0.0008s^{-1}$.**
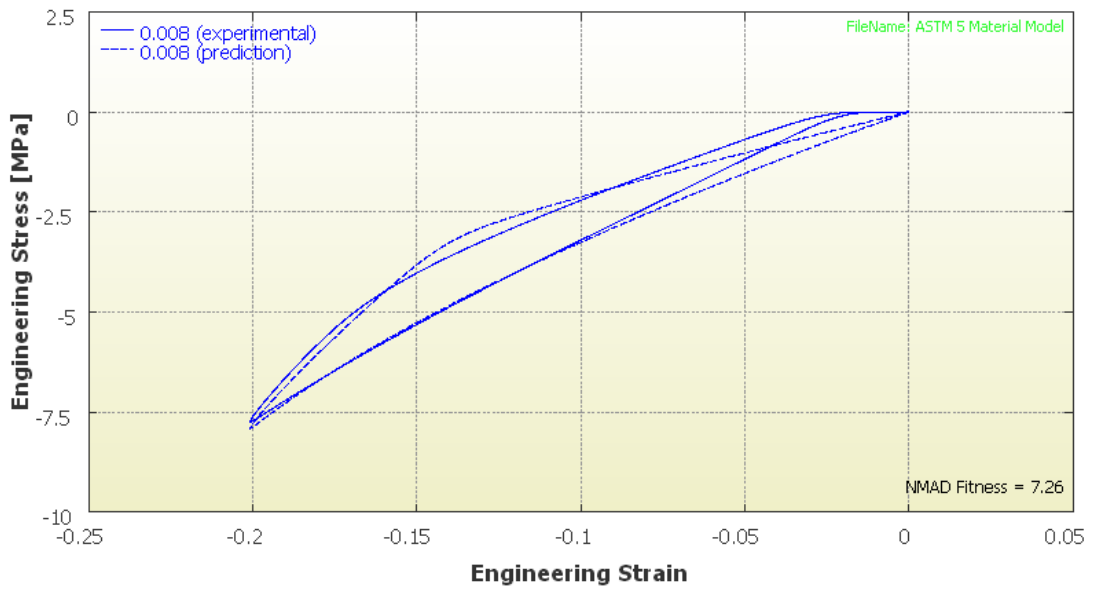
**Figure 7.1-3 - Prediction of PNM model at 0.008s⁻¹.**
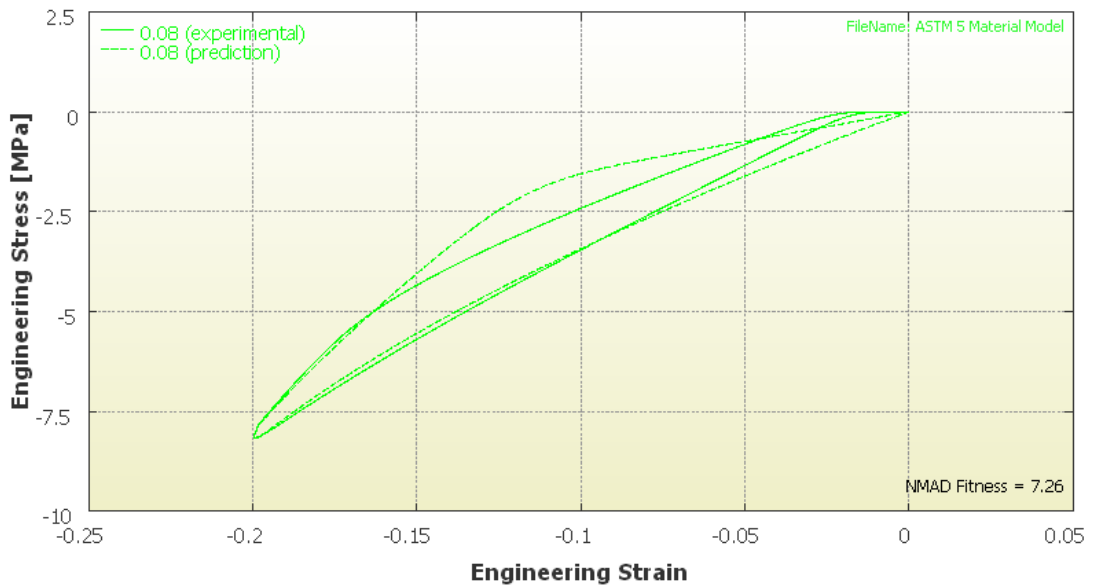


**Figure 7.1-4 - Prediction of PNM model at 0.08s⁻¹.**

In the figures presented the NMAD Fitness refers to the overall fitness. The NMAD fitness at $0.08s^{-1}$, $0.008s^{-1}$ and $0.0008s^{-1}$ was 6.97995, 6.5541 and 8.2648 respectively. As with the small samples from Chapter 5 the most accurate prediction of material behaviour is at the intermediate strain rate, however

with the ASTM geometry this is not as pronounced. The material model has difficulty predicting the slow tangent stiffness discussed previously but successfully captures the loading behaviour from approximately 7%-20% at all three strain rates. The initial unloading path is also accurately represented from approximately 20%-15%. The possible experimental slack was removed from the experimental data to investigate whether or not this would yield a smaller NMAD fitness error. However correcting the data to remove the initially low tangent stiffness artificially stiffens the sample. Figure 7.1-3 shows that at a strain rate of 0.008 $s^{-1}$, the engineering stress at engineering strain of 20% is approximately 7.5 MPa. If the initial slack is removed so that the loading response starts nearer to 0 engineering strain (effectively displacing the experimental data response to the left in Figure 7.1-4 so that the response at approximately 1.5% strain now lies at 0% engineering strain) as shown in Figure 7.1-5, the sample now experiences an engineering stress of 7.5 MPa at an engineering strain of 17.5%; hence it has a stiffer response as the strain associated with the same stress is lower.
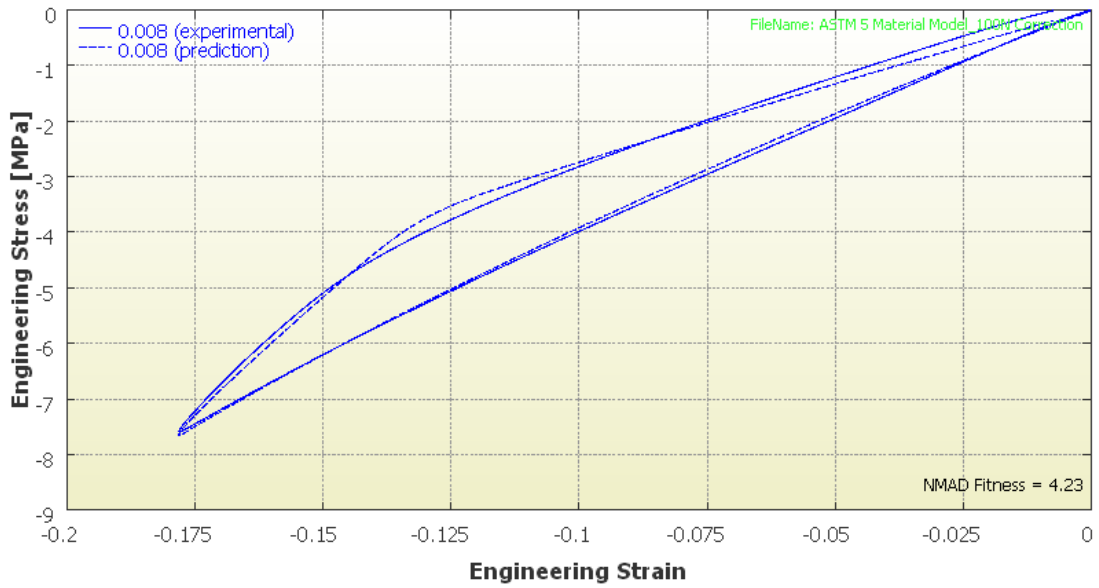
**Figure 7.1-5 - Prediction of material model to "corrected" data.**

It is shown in figure 7.1-5 that the material model now has an accurate fit with an NMAD error of 2.56 at the intermediate strain rate and an overall NMAD fitness for all strain rates of 4.22. Using this method to correct the data was deemed unsuitable due to the uncertainty associated with the artificial stiffening of the sample. The experimental slack therefore remains an area of concern with regards to material model calibration and FE analysis. Table 7.1-1 highlights the final parameters used to define the ASTM material model used in the FE simulations and quantifies the NMAD fitness at each strain rate along with the overall fitness across all strain rates.

| Name | Description | ASTM Material Model | |
|---|---|---|---|
| EType | Elastic component type | 5 | Network A |
| C10 | Linear term in $I_1$ | 4.26828 | |
| C20 | Quadratic term in $I_1$ | -0.807169 | |
| C30 | 3$^{rd}$ order term in $I_1$ | 7.68992 | |
| kappa | Bulk modulus | 500 | |
| EType | Elastic component type | 2 | |
| mu | Shear modulus | 7.56942 | |
| kappa | Bulk modulus | 500 | Network B |
| FType | Flow model type | 503 | |
| xi | Strain adjustment factor | 6.71931e$^{-6}$ | |
| C | Strain exponent | -2.72812 | |
| tauHat | Shear flow resistance | 14.0209 | |
| m | Shear flow exponent | 5.25608 | |
| NMAD - 1 | Fitness of load case 1 – 0.08s$^{-1}$ | 8.25 | |
| NMAD – 2 | Fitness of load case 2 – 0.008s$^{-1}$ | 6.55 | |
| NMAD – 3 | Fitness of load case 3 – 0.0008s$^{-1}$ | 6.97 | |
| NMAD – Overall | Overall fitness of three strain rates | 7.26 | |

**Table 7.1-1 – Parameters and NMAD fitness of ASTM material model.**

### 7.1.2    Large Cylinder Sample Data

The above process was repeated with the data from the large cylinder experimental investigation. The large cylinder was produced with the purpose of maximising the material whilst maintaining a standard geometry. It is worth noting that the large cylinder did not maintain the standard height to width ratio (as set out by the ASTM test standards [25]) therefore the potential sources of error have been increased, especially the possibility of the sample bulging. As with previous samples, time, stress and strain data from the large cylinder experimental investigation was read into the MCalibration software along with an initial guess of material parameters which were taken from the ASTM material data. The software then adjusted the material parameter guesses to reduce the overall NMAD fitness. Figures 7.1-6 to 7.1-8 show the predictions of the large cylinder parameters at the three strain rates.
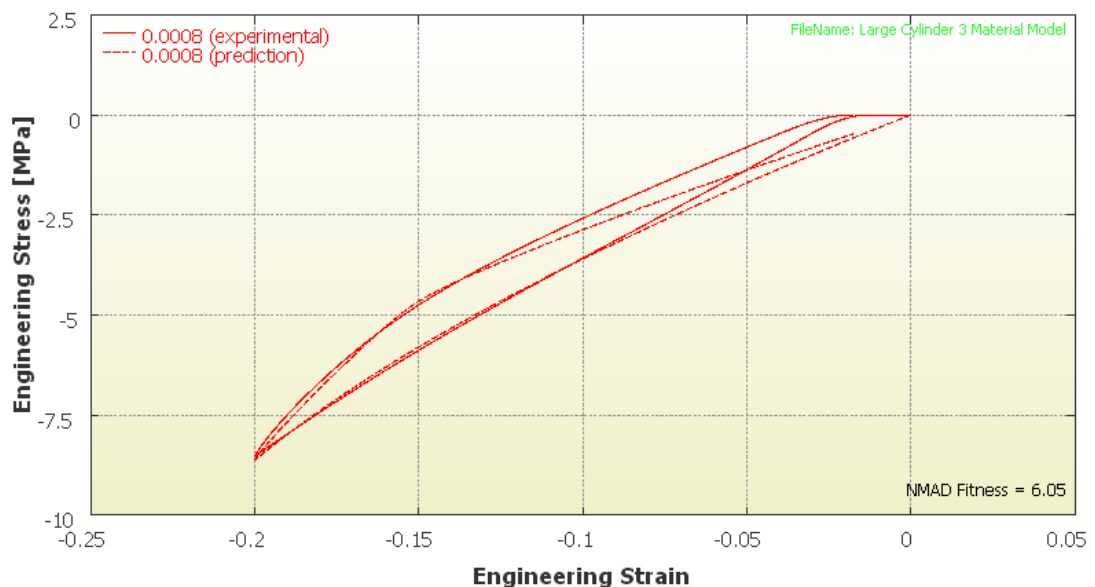


**Figure 7.1-6 – Prediction of PNM model at 0.0008s$^{-1}$.**
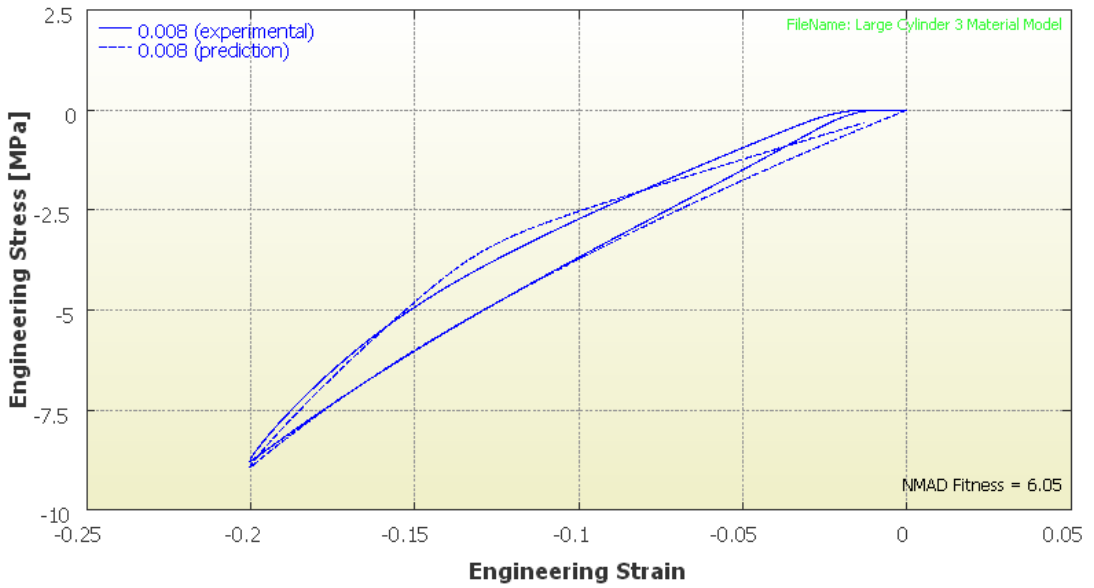
**Figure 7.1-7 – Prediction of PNM model at 0.008s⁻¹.**
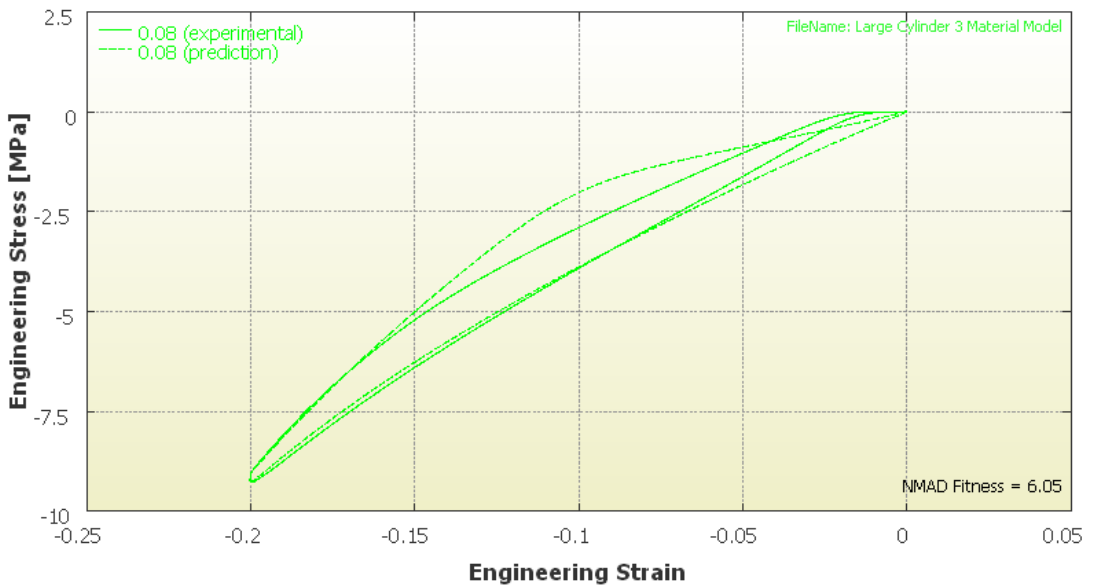


**Figure 7.1-8 - Prediction of PNM model at 0.08s⁻¹.**

As with the ASTM samples the material model is capable of predicting the loading path between 7% and 20% strain. The unloading path is correctly predicted in all three cases from 20% to roughly 15% strain. The issue with experimental slack, as described for the ASTM samples, is also present with this

data set. It was decided to progress with this material model as removing the experimental slack artificially stiffened the material, as with the ASTM geometry. Table 7.1-2 highlights the final parameters used by the Large Cylinder material model and the NMAD fitness achieved.

| Name | Description | ASTM Material Model | |
|---|---|---|---|
| EType | Elastic component type | 5 | Network A |
| C10 | Linear term in $I_1$ | 4.99579 | |
| C20 | Quadratic term in $I_1$ | -1.00188 | |
| C30 | $3^{rd}$ order term in $I_1$ | 8.16284 | |
| kappa | Bulk modulus | 500 | |
| EType | Elastic component type | 2 | Network B |
| mu | Shear modulus | 6.52552 | |
| kappa | Bulk modulus | 500 | |
| FType | Flow model type | 503 | |
| xi | Strain adjustment factor | $7.01302e^{-6}$ | |
| C | Strain exponent | -2.81933 | |
| tauHat | Shear flow resistance | 15.2571 | |
| m | Shear flow exponent | 5.29236 | |
| NMAD - 1 | Fitness of load case 1 – $0.08s^{-1}$ | 6.58 | |
| NMAD – 2 | Fitness of load case 2 – $0.008s^{-1}$ | 5.02 | |
| NMAD – 3 | Fitness of load case 3 – $0.0008s^{-1}$ | 6.53 | |
| NMAD – Overall | Overall fitness of three strain rates | 6.05 | |

**Table 7.1-2 - Parameters and NMAD fitness of Large Cylinder material model.**

It is interesting to note that the overall fitness of the Large Cylinder material model is better than that of the ASTM model. The Large Cylinder sample data

achieved a fitness value of 6.05 whereas the ASTM sample data achieved a fitness value of 7.26. It is thought that the degree of experimental slack is less prominent in the large cylinder data compared with the ASTM sample data. The overall shape of the response has an effect on the fitness of the material model as each spring damper combination has certain shape characteristics. It would, potentially, be beneficial to use different spring models for each application but the aim of the study was to present a new model that was capable of predicting the behaviour of multiple golf balls. It was therefore decided to keep that variable constant and use only one material model for all applications.

## 7.2    Finite Element Analysis

Using the material data gathered in the second experimental investigatory phase various FE simulations were analysed. The aim of these various simulations was to investigate how effective the modelling techniques employed were on the tree trunk model, which relates to the tree trunk model discussed in Chapter 6. The ASTM calibrated material model and the large cylinder calibrated material model were applied to a homogeneous spherical core geometry to examine the accuracy of reproducing the stress strain behaviour of the golf ball core using an "averaged" set of homogeneous material parameters.

### 7.2.1  Tree Trunk Model

The objective of the tree trunk model was to model a multi-material system using FE but not have the complication of spherical geometry. Previously, a jump had been made from homogeneous cylindrical samples to heterogeneous spherical samples, meaning that both material systems and sample geometry had been altered. By creating a sample consisting of concentric rings, of differing material properties, it was possible to control geometry whilst altering the number of material models present. FE geometry, as shown in Figure 7.2-1, was created and the material models described in chapter five (centre, inner and outer) were applied to the relevant sections using the property module inside ABAQUS.
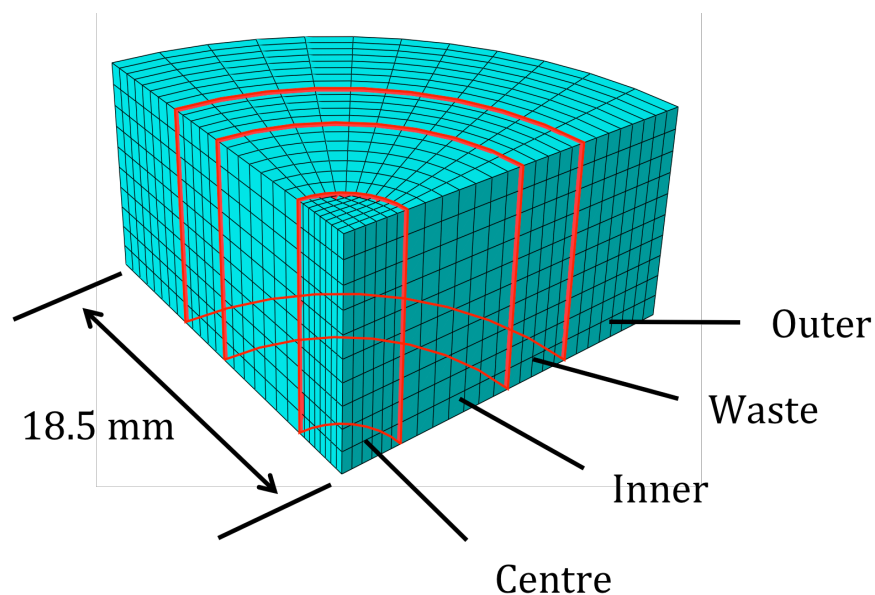


**Figure 7.2-1 - Elemental plot of tree trunk sample geometry.**

The tree trunk model consisted of 2870 ABAQUS elements of type C3D8. Symmetry boundary conditions were applied to the rectangular faces so that

the cylindrical disc geometry could be modelled as quarter cylinder. The FE assembly was similar to that described previously in Chapter 5. As previously discussed, an analytically rigid plate was used to compress the sample to a pre-defined strain of magnitude 20%. The modelling techniques employed were identical to those used for the small sample compression simulations with the only difference being sample geometry and compression platen displacement. The reaction force experienced by the compression plate was taken as the output from the FE simulation and plotted against the experimental results in order to verify the model. Figure 7.2-2 shows a plot of stress versus strain for the experimental and FE results of the tree trunk simulations.
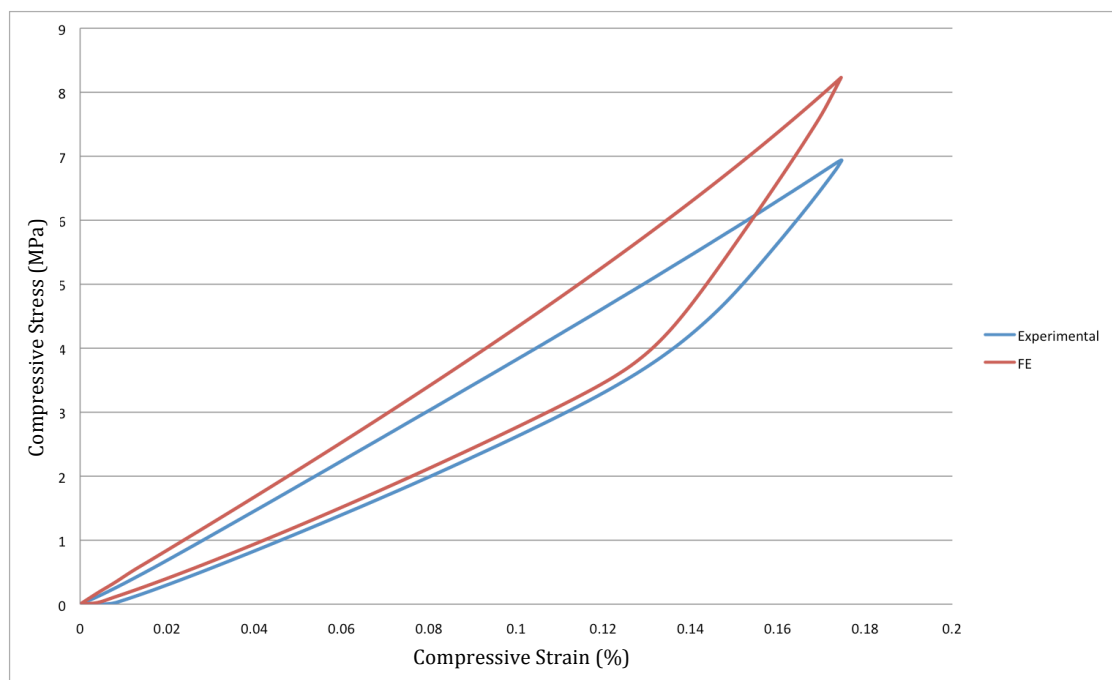


**Figure 7.2-2 - Experimental and FE stress strain plots for tree trunk samples.**

It is clear that the FE simulation is predicting a behaviour that is stiffer than observed experimentally. To quantify the error present, percentage errors of peak stress and hysteresis were calculated. The FE model over predicts the peak stress by 18.6% and over predicts the hysteresis by 25.7%. Hysteresis was calculated using the following trapezium rule, $z_n = z_{n-1} + (x_n - x_{n-1}) \times (y_n + y_{n-1})/2$ Each data point has an x and y value, if they are used to calculate $z_n$ the area contained by the hysteresis loop is the final value in z column. The source of this error cannot be singled to one source but there are various physical differences between the FE model and actual specimen. The most notable difference concerns an earlier point regarding the heterogeneous core model. In reality the material properties vary continuously whereas in the FE model there are areas containing a step change in properties. A difference of this severity is likely to produce some degree of error but there are other sources that may contribute to the overall error. The region labelled "waste" relates to the waste section of the initial small samples. In this model it was divided into two sections with the outer and inner material models assigned to the relative halves of the divided waste section. This is therefore a potential source of error as there is no guarantee that the properties vary in this manner radially through the specimen.

Alongside the physical differences there are a number of typical reasons that result in finite element models producing a response that is too stiff. The mesh density was increased to examine the possibility of volumetric locking within the model however no change in response was observed. Figure 7.2-3 shows the

increased mesh density, consisting of 13594 elements as opposed to 2870 elements in Figure 7.2-1.
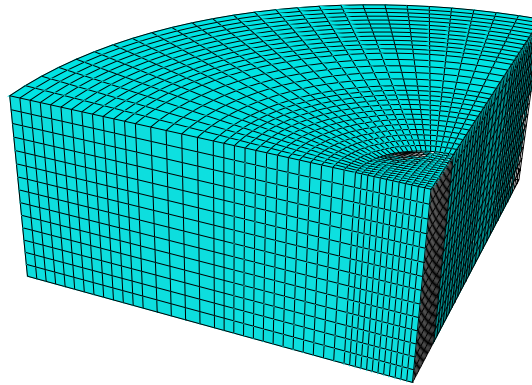


**Figure 7.2-3 - Elemental plot of tree trunk geometry with increased mesh density.**

It is noted [38] that if volumetric locking is present, rapid changes in hydrostatic pressure stresses should be observed. The hydrostatic pressure stresses were examined with no rapid changes observed. Figure 7.2-4 shows the pressure stresses as a contour plot at one frame of the tree trunk sample deformation. It can be observed that there are no rapid changes present.
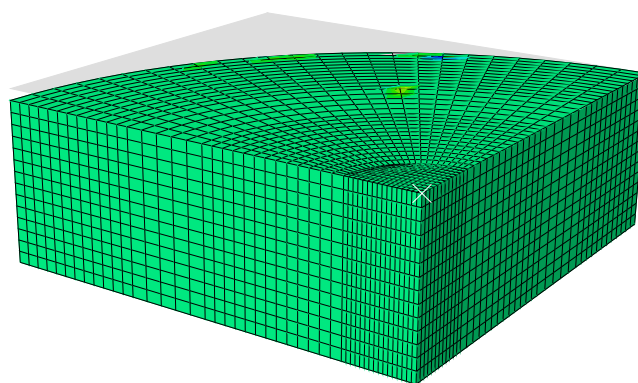


**Figure 7.2-4 - Typical contour plot of the pressure stresses present during deformation of the tree trunk sample.**

The analytically rigid plate used to compress the sample was replaced with a pressure force on the top surface of the sample to rule out any possible problems associated with the contact algorithm. The analytically rigid plate was also replaced, in a separate simulation, with a large block given standard steel properties, again no significant change was observed. The FE investigation carried out indicated that the error is associated with the material models. It is expected that the small errors associated with the individual materials models accumulate a bigger overall error and the step changes in properties contribute further to the observed error. It is, however, encouraging looking at the overall shapes of the responses, shown in Figure 7.2-2. The FE analysis successfully predicts the shape of the load-unload curve with the loading path displaying fairly linear behaviour and the unloading path almost having two defined linear sections with different gradients.

### 7.2.2   ASTM Core Model

The material parameters obtained from the ASTM specimens were applied to an FE model of a golf ball core. This model was assumed to be homogeneous and the ASTM material parameters, presented earlier, were used to define the material model applied to the full core. Figure 7.2-5 shows an elemental plot of the homogeneous core model. The modelling techniques applied were identical to those described in Chapter 5 for the heterogeneous core model, only the material model differed.
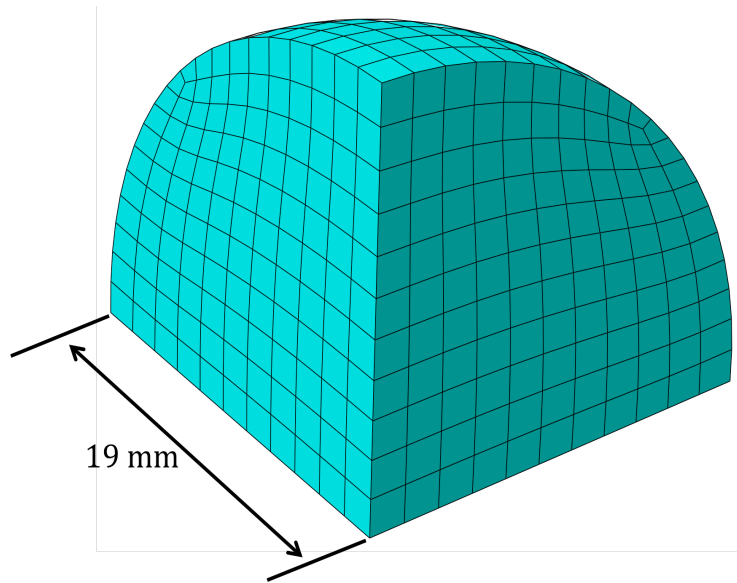
**Figure 7.2-5 - Elemental plot of homogeneous core model.**

The above model consisted of 1300 ABAQUS elements of type C3D8. Compression to 20% was simulated using the same procedure as described in Chapter 5. A typical stress contour plot from the FE compression simulation is shown in Figure 7.2-6.
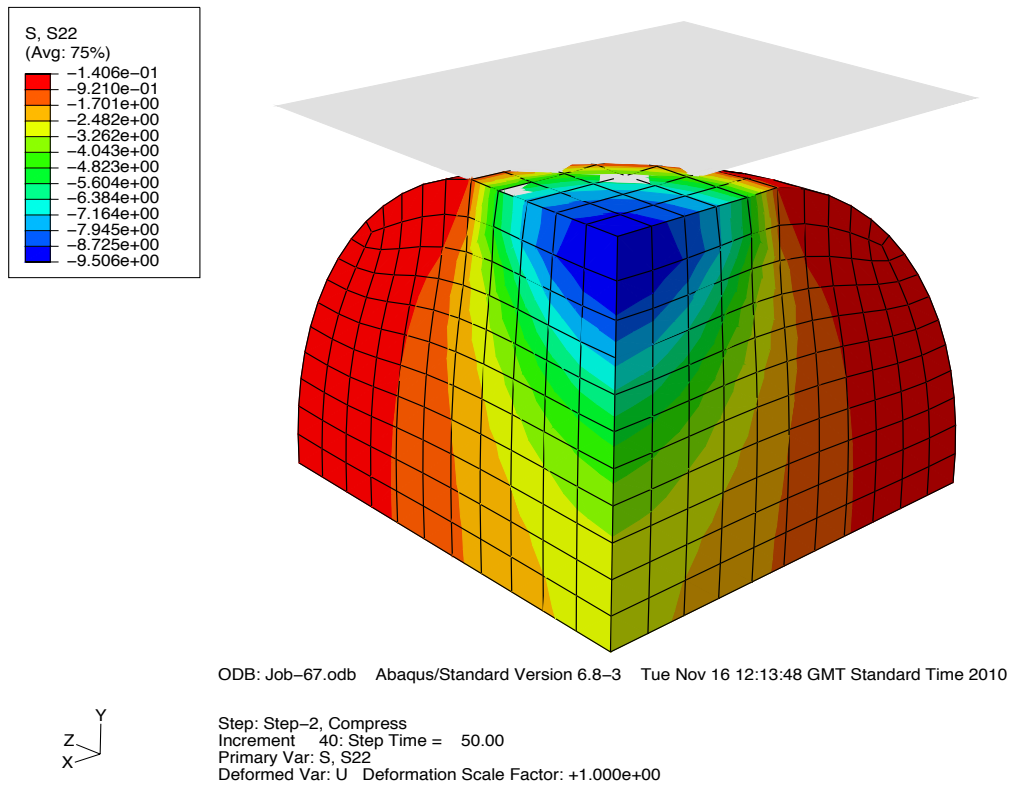
**Figure 7.2-6 - Plot of stress component, S22 (y-direction), in core compression simulation.**

Figure 7.2-6 highlights the stress response S22 (y-direction), which is the stress in the compression direction. As expected, the peak stress is observed at the contact point and is symmetrical around the central axis. The reaction force experienced by the compression plate was a requested output from the FE model and plotted against the reaction force obtained experimentally. It is worth noting that for the spherical models the results are presented in terms of force-displacement and not stress-strain. This is due to the constantly changing, non-conforming, contact area between the sample and the compression platens. Figure 7.2-7 presents a comparison of the force versus displacement plots of the FE and experimental results.
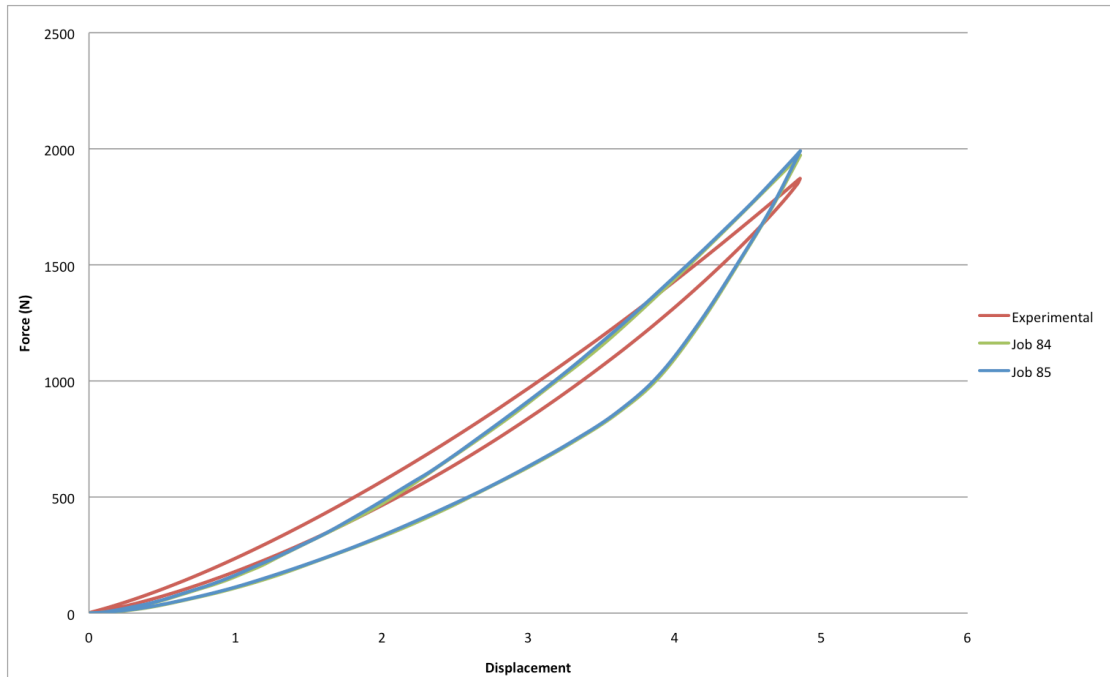
**Figure 7.2-7 - Comparison of FE and experimental force displacement results for the ASTM geometry samples.**

The above graph includes two FE results. "Job 84" refers to a simulation consisting of 1300 elements and "Job 85" refers to a simulation employing a more refined mesh with 6750 elements. The results of "Job 84" and "Job 85" are shown in Figure 7.2-7 with negligible differences shown, therefore it can be concluded that the mesh density is not affecting the result.

It is clear that the FE analysis is predicting behaviour that does not completely match with the experimental data. The loading path of the experimental results displays a more linear behaviour than the FE result, the peak stress is over predicted by 5.4% and the hysteresis is over predicted by 94%. As with previous simulations there are various factors that can affect the accuracy of the FE simulation. The material model that describes the system is essentially a

model for a different material than the core itself. The ASTM geometry removed from the core does not take into consideration the "outer" material region; it focuses on the "inner" and "centre" regions. The behaviour observed is therefore the response of an essentially different material. It is interesting to note that the ASTM material model produces a response that is too stiff when the material data used to calibrate the model was removed from the centre of the core where the material is reported as being softer. The issue of volumetric locking was also investigated in this model. The number of elements was increased from 1300 to 6750 with no noticeable change in results, Figure 7.2-7. The hydrostatic pressure stresses were also examined for rapid changed and unusually high values (stress peaks). Figure 7.2-8 shows the hydrostatic pressure stresses at maximum deformation.

S, Pressure
(Avg: 75%)
+7.486e+00
+6.856e+00
+6.225e+00
+5.594e+00
+4.963e+00
+4.332e+00
+3.701e+00
+3.070e+00
+2.439e+00
+1.809e+00
+1.178e+00
+5.467e−01
−8.415e−02

ODB: Job−74.odb    Abaqus/Standard Version 6.8−3    Mon Jan 10 13:49:26 GMT Standard Time 2011

Step: Compress, Plate compresses ball
Increment    20: Step Time =    25.50
Primary Var: S, Pressure
Deformed Var: U   Deformation Scale Factor: +1.000e+00
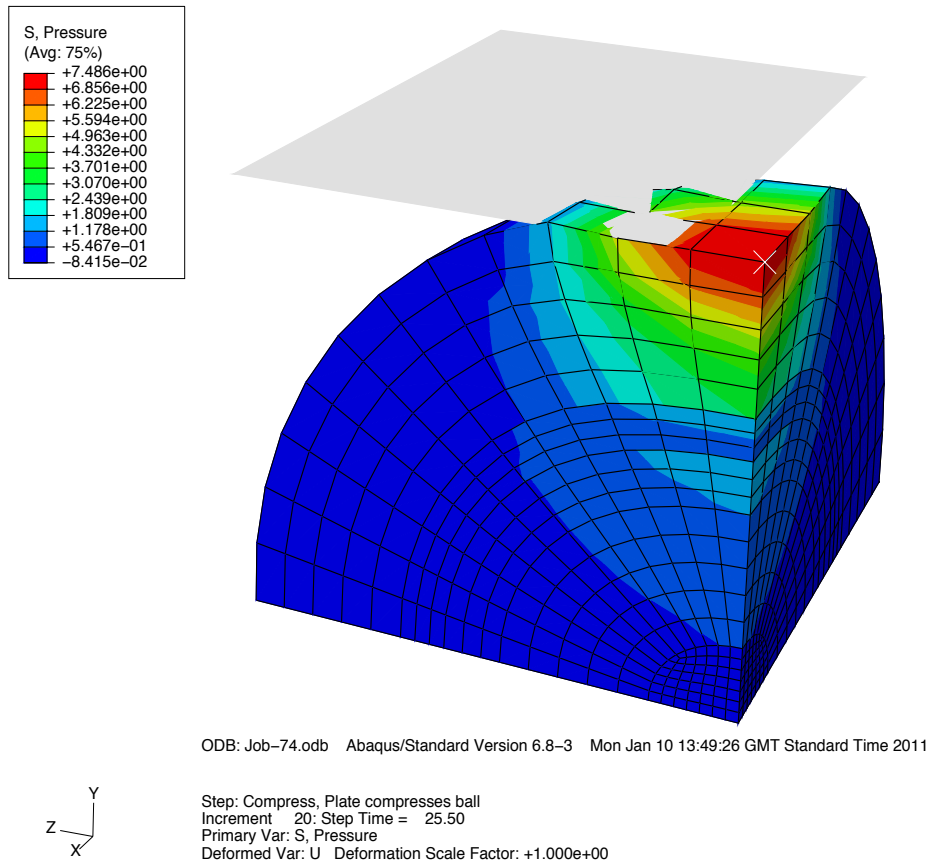
**Figure 7.2-8 – Typical contour plot of hydrostatic pressure stresses at maximum deformation.**

Although the overall strain rate was known, there were concerns about the strain rate at discrete internal sections of the core. For example, if the overall strain rate was 0.008 s$^{-1}$, there is the possibility that internal sections are experiencing strain rates higher than the collected data covers. In ABAQUS it was possible to get the strain rates at various points throughout the model which all fell within the experimental range thus ruling out the possibility of overly stiff internal regions as a results of the strain rate experienced.

ER, Max. Principal
(Avg: 75%)
+1.797e−02
+1.654e−02
+1.511e−02
+1.368e−02
+1.224e−02
+1.081e−02
+9.377e−03
+7.944e−03
+6.511e−03
+5.078e−03
+3.645e−03
+2.212e−03
+7.793e−04

ODB: Job−74.odb    Abaqus/Standard Version 6.8−3    Mon Jan 10 13:49:26 GMT Standard Time 2011

Step: Unload, Compressive force is released
Increment    1: Step Time =    1.000
Primary Var: ER, Max. Principal
Deformed Var: U   Deformation Scale Factor: +1.000e+00

**Figure 7.2-9 – Typical ABAQUS plot of maximum principal strain rates.**

Figure 7.2-9 shows that the strain rates experienced at that specific step but the strain rates experienced at all analysis steps never exceeded the experimental strain rates gathered.

Due to the inherent differences present, this method of modelling the ball was not suitable as an overall prediction. If peak force was the primary variable of comparison the model reports results that are satisfactory (error of 5.4%) but overall the model is of limited use.

### 7.2.3 Large Cylinder Core Model

The above process was repeated with the parameters obtained from the large cylinder calibration. The FE model used and the modelling techniques employed were identical to the model used in Section 7.2.2. Figure 7.2-6 presents the results from the FE model calibrated with large cylinder material data and compared with experimental data.
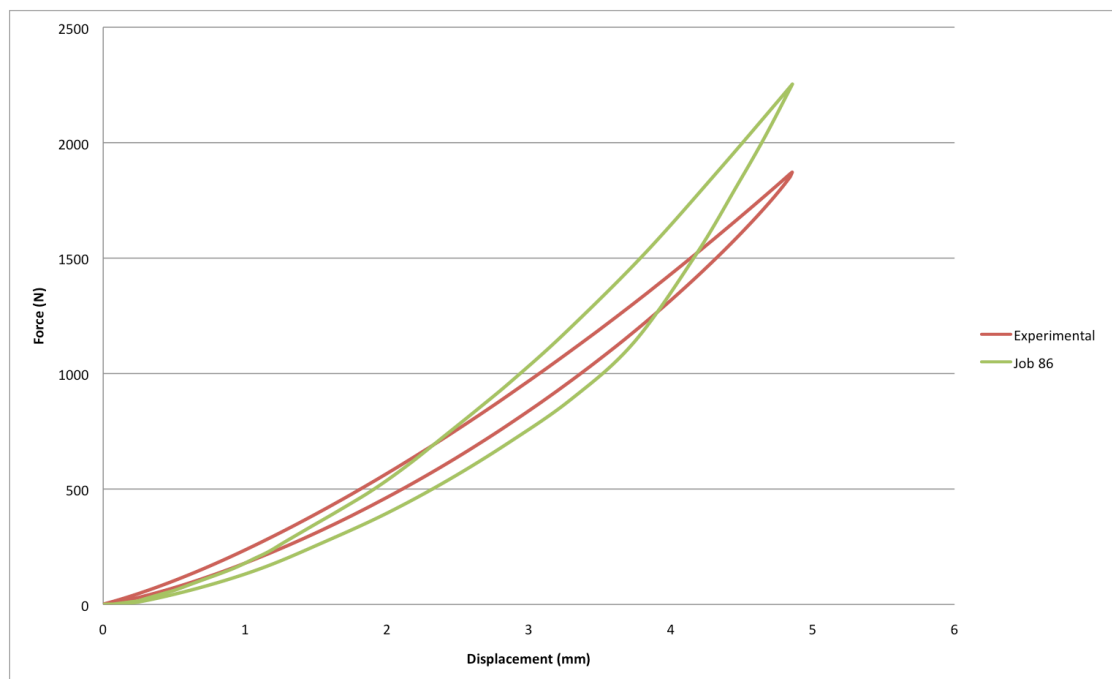


**Figure 7.2-10 – Comparison of FE and experimental results for large cylinder sample data.**

As with previous FE simulations the result obtained through FE analysis is overly stiff and over predicts the peak force and hysteresis by 20.4% and 83.5% respectfully. The same issues are present as with the ASTM homogeneous core. Each possible source of uncertainty (volumetric locking etc.) was investigated, as described previously for the ASTM core, however the source of the error

could not be traced. In relation to the ASTM sample result, the result presented seems logical. The presence of the stiffer "outer" material is more apparent in the large cylinder samples therefore the FE result should be stiffer, which it is. The issue of sample bulging in the experimental phase was also thought to have been increased with the larger sample geometry; therefore the data used to calibrate the relevant material models is potentially artificially stiffened. As with the ASTM sample results it was concluded that the differences present in the two materials were too great for this to be regarded as a suitable modelling methodology. However it is encouraging to note that the ASTM material data produced an FE response that is softer than the large cylinder data but in terms of a possible future modelling methodology, it was deemed that the above was unsuitable due to the homogeneous assumption and geometry of the test samples used to gather the material data.

## 7.3    Summary

Chapter 7 has presented further material model calibration and finite element analysis. An intermediate experimental investigation between the original small cylindrical samples and the spherical heterogeneous core model was presented, the tree trunk model. This model over predicted peak stress and hysteresis but captured the overall shape of the response successfully. Two homogeneous core models were presented, one calibrated with data from the ASTM samples and one calibrated with data from the large cylindrical samples. Both models over predicted peak stress and hysteresis.

# 8 Conclusions and Future Work

The overall aim of the study was defined by R&A Rules Ltd. and involved the development of a fully validated FE model of a golf ball. Following a review of relevant publications, there were five resulting areas that were then investigated in detail:

- Experimental protocol for the production of test samples from commercially available golf balls.

- A material model that can accurately predict material behaviour over a full range of strain rates.

- A finite element (FE) model that represents the previously reported material heterogeneity present in golf ball cores.

- An FE model that does not require tuning based on impact data, as described in Chapter 1.

- The production of a fully validated FE model of a golf ball that can predict hysteresis on cyclic loading and coefficient of restitution (CoR) on impact.

Each area was investigated thoroughly with varying success. This Chapter presents the final outcomes of the study, suggests possible improvements to the current work, presented in this thesis, and proposes direction for future work.

## 8.1 Final Outcomes

### 8.1.1 Experimental Investigations

The thesis introduces and develops a suitable testing technique for establishing material data from various sample geometries of golf ball core material. The results obtained experimentally agreed with published behaviour for polymers in terms of strain rate, Mullins effect and hysteresis. The stress-strain responses all displayed stress softening over the first few cycles and the response suitably stabilised after approximately 5 cycles. Each sample displayed rate dependence with the fastest strain rate producing the stiffest response. Having machined cylindrical samples from the core and tested them in compression it was concluded that the core exhibits highly heterogeneous behaviour with the modulus at the centre of the core and the modulus at the outer edge of the core varying by approximately 63%. In general the samples were found to be repeatable, with the outer small samples displaying the greatest repeatability. This was thought to be a result of the proximity to the heat source during the manufacture of the golf ball samples and the fact that there was less material to affect the heat energy dissipation. The uncertainties with regard to the experimental data associated with repeat tests were suspected to be a result of imperfections in the manufacturing process. Although limited testing was carried out on the cover, the results obtained show that hysteresis is clearly present and it was thought that using a purely hyperelastic material model was not sufficient for accurate prediction of the material behaviour of this component of the ball. It was thought that a viscoelastic material model would

be more suited. The results obtained from the relaxation tests highlighted that non-linear viscoelastic material models might be better suited to the specific application.

### 8.1.2 Material Model Calibration

Using the data obtained through experimentation, various non-linear viscoelastic material models were calibrated. It was discovered that a parallel network model (PNM) with two networks provided the most accurate fit with experimental data. Using a Yeoh spring to define Network A and a Neo-Hookean (NH) spring coupled with the Bergström-Boyce (BB) flow model to define Network B resulted in a good compromise of simplicity and accuracy. Although every care was taken to reduce the likelihood of sample bulging, this remained a concern throughout the experimental investigations. If the data used for material model calibration was obtained from samples that experienced bulging it would represent a stiffer material due to the shear stresses associated with bulging. The samples were prepared as carefully as possible and the application of a pre-load in the compression tests, ideally ensured that the contact area was consistent throughout the compression tests, however the observed material slack suggests that there might be some degree of inaccuracy associated with this area of work. Based on the response of the small samples it is unlikely that the behaviour observed in the ASTM and large cylinder samples is a true representation of the actual material.

### 8.1.3 Finite Element Analysis Studies

 The results from the FE simulations had varied success. All FE simulations displayed a behaviour that was too stiff and the predicted hysteresis was too large. All the probable finite element behaviour reasons for this were investigated. Mesh density did not have an affect on the response and no rapid changes in hydrostatic pressure were observed, reducing the likelihood of volumetric locking. The contact algorithm within ABAQUS was ruled out as a source of error by replacing the compression platen with a pressure force which resulting in the same overly stiff response. The above suggests that the error present is likely due to material model calibration and possibly the accumulation of smaller manufacturing errors and uncertainties associated with the experimental testing mentioned previously. Referring back to Figure 5.4-6, in Chapter 5, it is shown that the FE model behaves as expected which leads to the conclusion that the source of the uncertainty is present in all simulations and of a consistent magnitude. The results from the second phase of FE analysis point to the same conclusion as the simulation of the core calibrated with the large cylinder data producing a stiffer response to the model calibrated with the ASTM material data. In terms of numerical results, it can be concluded that the homogeneous models calibrated with the averaged parameters perform better but in real terms the errors are still too large and the models do not include the material heterogeneity. Table 8.1-1 summarises the results from the three core models.

| Model | Percentage Error Peak Stress (Peak Force for core models) | Percentage Error Hysteresis |
|---|---|---|
| Homogeneous Core– ASTM | 5.4% | 94% |
| Homogeneous Core – Large Cylinder | 20.4% | 83.5% |
| Heterogeneous Core | 24.1% | 163.1% |
| Tree Trunk | 18.6% | 25.7% |

**Table 8.1-1 - Results of simulations of the various finite element models.**

The tree trunk models proved to be the most successful of the finite element simulations accurately capturing the shape observed experimentally. A stiffer response was achieved through FE compared with experimental.

## 8.2   Contribution of Knowledge to The Field

The sample preparation technique developed allows fast, accurate production of any sample geometry with or without the golf ball cover present. The introduction of an aluminium support, in experimental phase two, negates the complication of the three-jaw chuck compressing the sample and resulting in non-parallel faces. The preparation technique does not require the samples to be cooled prior to machining and does not produce excess heat that could significantly alter the properties of the sample.

Chapter 5 presented an FE model of a golf ball core that captured material heterogeneity. All previous models presented in the literature did not include

this characteristic, which is clearly evident from the present and previous studies. The combination of the small sample experimental investigation and first phase of FE modelling allows the creation of heterogeneous systems calibrated with actual material data. Although this characteristic is clearly present, it cannot be definitively concluded if this heterogeneity is important when examining the overall behaviour of the ball.

The work confirmed that the materials used in golf ball construction exhibit non-linear viscoelastic behaviour. The Prony series in ABAQUS is a linear viscoelastic material model and, based on published literature, is suited to applications with a narrow range of strain rate. The aim of the presented work was to produce an FE model of the ball that was validated at a full range of strain rates, from quasi static to the strain rates experienced at golf impact and beyond. The Bergström-Boyce (BB) model has been used in the past but this study reported that the material model fit could be improved by changing the spring and damper models. Although the current results presented here do not accurately capture the experimental response, it is still concluded that the inclusion of more complex material models is important.

The final contribution to knowledge worthy of note is with regards the cover material of the ball. Upon cyclic loading the cover exhibited viscoelastic behaviour disagreeing with the published model presented by Tanaka et al [13]. The inclusion of viscoelasticity is important as without it the material is

assumed to have no rate dependence or energy loss, which could lead to potentially significant inaccuracies.

The experimental work carried out has also confirmed the behaviour of polymers as reported in many published sources. It is important to further validate these other results through future experimental investigation to confirm their accuracy.

## 8.3   Future Work and Suggested Improvements

It is important in any research to realise the limitations of a study and report them clearly. The uncertainties associated with the sample bulging issue could have been quantified with the use of extensometers. This would have allowed measurement of the lateral expansion and a more accurate calculation of strain. However, because of the nature of the typical golf ball polymer it would be necessary to use non-contact devices to avoid interference with the sample.

Due to the characteristics of the unloading path found throughout the study (almost two separate linear sections of differing gradients) it was hypothesised that introducing a second dashpot to the PNM model would yield a more accurate fit. A three-network PNM model was constructed as shown in Figure 8.3-1.
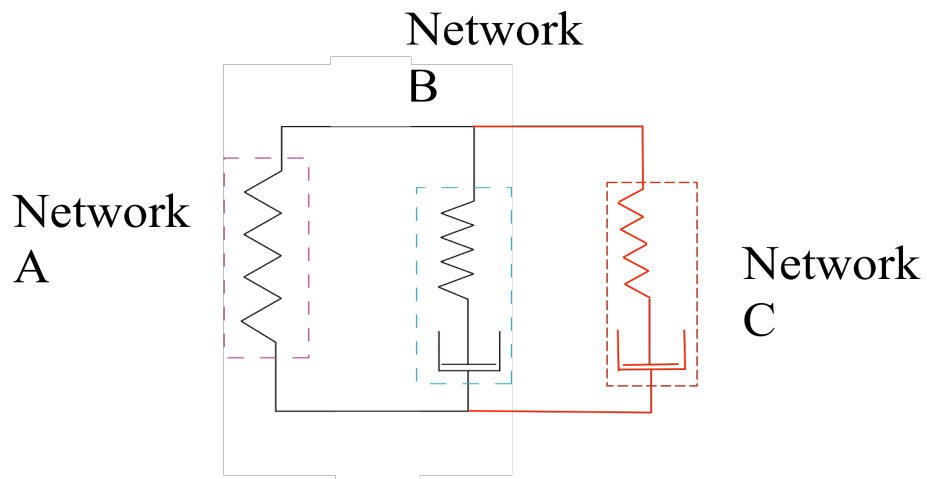
**Figure 8.3-1 - Schematic representation of three network PNM model.**

The above model is identical to the previous two-network PNM model with the addition of a network (signified by red). Network A and B are as before and Network C is the same as Network B. It was thought that the addition of the second dashpot and spring would improve the fitness of the model to the experimental data. The data from one of the small cylindrical samples, removed from the centre of the golf ball core, was used. Figure 8.3-2 summarises the result.
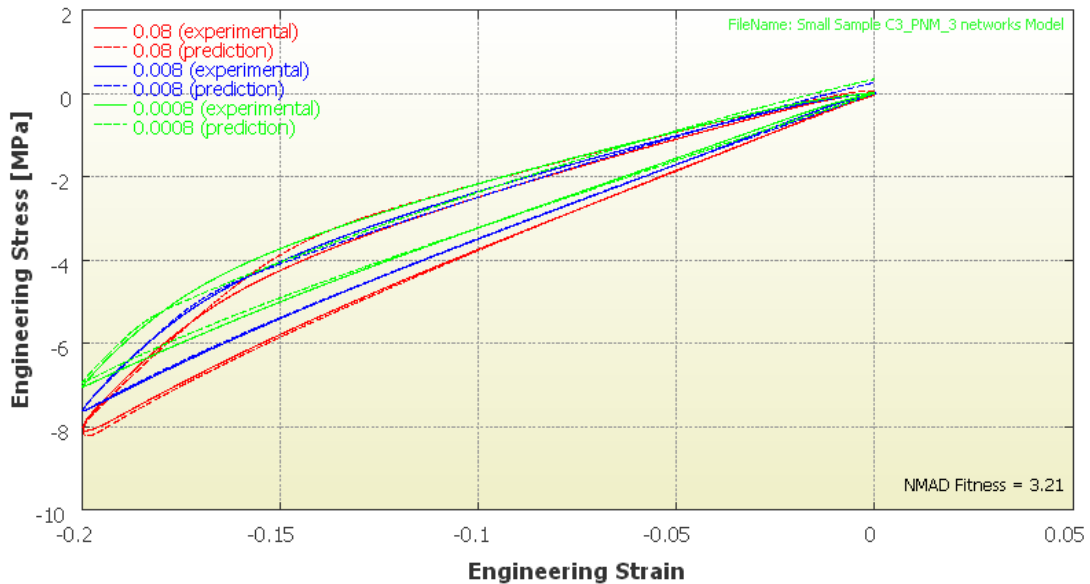
**Figure 8.3-2 - Three-network PNM model fitness for small centre sample.**

The overall NMAD fitness for the three-network model was reduced to 3.21 from a previous value of 5.27. The individual NMAD fitness values were: at 0.08 s$^{-1}$ the value was 3.79369, at 0.008 s$^{-1}$ the value was 1.71775 and at 0.0008 s$^{-1}$ the value was 4.10454. Hence increasing the complexity of the material model improved the overall fit of the material model and reduced the individual NMAD fitness values at the various strain rates. In general, increasing the complexity of a model by adding more parameters will always improve the fitness as there are more parameters to adjust but the consideration for a researcher is whether or not the increased complexity improves the fitness to such a degree that it is worth the extra computational cost.

During the sample preparation it was noticed that the rubbers used caused the machine tools to blunt extremely quickly. Tools that could handle years of aluminium and steel machining were blunt within a couple of passes during the

170

sample preparation. This was thought to be a result of the impurities in the rubber and the fillers added in the manufacture if the balls. This tool bluntening has a detrimental affect on the quality of the samples produced. Instead of cutting through the material the blunt tool tended to "chip" sections off leading to slight pitting on the machined face. To address this problem the mill tool had to be regularly changed, resulting in further cost.

Having reported the various limitations of the study it also suggests the future work that would be beneficial in the field. Non-linear viscoelastic models have to be further investigated to conclude whether the wide strain rate characteristics can be used to produce a fully validated FE model of the golf ball. It would be interesting to investigate further the idea of increased the number of networks in each model (as suggested previously in this section), with the aim of concluding whether or not the increased complexity improves accuracy enough to merit the increased computational cost. Cutting tool materials could be examined to determine if there is a better material for use with rubbers that will not blunt as quickly. An investigation of the current models ability to perform at higher strain rates would also be interesting, however due to the uncertainties at low strain rate the results would have limited validity. A major difference between the FE and physical ball is the manner in which the material properties vary. In the FE model there were step changes between layers of homogeneous material. These areas were made as small as possible however it would be interesting to investigate a gradient change of properties through the cores radius instead of step changes. A fully validated model of a two-piece ball

is required before progressing to the more complex three, four and even five piece balls. One advantage of the balls with a higher number of pieces though, is that the layers are thinner and therefore exhibit less material heterogeneity.

# 9   References

1. McGimpsey, K.W. (2003) *The Story of the Golf Ball*. Philip Wilson, London

2. http://www.quotegarden.com/golf.html

3. http://www.abc-of-golf.com/golf-basics/golf-history.asp

4. http://www.golfeurope.com/almanac/history/golf_ball.htm

5. Lewis, P. (1994) *The History of the Golf Ball in Britain*, in Golf the Scientific Way, ed. Cochran, A. pp165-170. Aston Publishing Group, Hemel Hempstead.

6. http://www.golfballmuseum.co.uk/shopscr3.html

7. http://www.pgatour.com/r/stats/info/?317

8. Topflite (1994) Advertisement in Golf the Scientific Way, ed. Cochran, A. pp134-135. Aston Publishing Group, Hemel Hempstead.

9. Nesbitt, R.D., Sullivan, M.J. and Melvin, T. (1998) *History and Construction of Non-Wound Golf Balls*. in Science and Golf III, Proceedings of the World Scientific Congress of Golf. Ed Farrally, M.R. and Cochran, A.J. pp407-414, Human Kinetics, Leeds.

10. Proctor, S.K. (1994) *The golf equipment market 1984-1994*. in Science and Golf II, Proceedings of the World Scientific Congress of Golf. Ed Cochran, A.J. and Farrally, M.R. pp 369-375, E and F.N Spon, London.

11. Dalton, J.L. (1998) *The Curious Persistence of the Wound Ball*. in Science and Golf III, Proceedings of the World Scientific Congress of Golf. Ed Farrally, M.R. and Cochran, A.J. pp415-422, Human Kinetics, Leeds.

12. Johnson, A.D.G. (2005), *The Effect of Golf Ball Construction on Normal Impact Behaviour*, PhD Thesis, The University of Birmingham.

13. Tanaka, K., et al. (2006), *Construction of the finite element models of golf balls and simulations of their collisions*. Proceedings of the Institution of Mechanical Engineers, Part L. Journal of Materials Design and Applications, vol. 220 no.1 13-22.

14. Iwatsubo, T., Kawamura, S., Furuichi, K. and Yamaguchi, T. (2002), *Influence of characteristics of golf club head on release velocity and spin velocity of golf ball after impact*. in Science and Golf IV, Proceedings of the World Scientific Congress of Golf. Ed Thain, E. pp 410-425, Routeledge, London.

15. Lucas, T.D., (1999), *Computational modeling of the golf stroke*, PhD Thesis, The University of Glasgow.

16. Mase, T., Kersten, A.M., (2004) *Experimental evaluation of a 3-D hyperelastic, rate-dependent golf ball constitutive model*. The Engineering of Sport 5, International Sports Engineering Association, California, pp 238–244

17. Dupont, (2004), web site http://www.dupont.com/industrial-polymers/surlyn/H-37063-2/H-37063-2.html

18. ABAQUS Version 6.5, (2004), *Analysis User's Manual Volume 3: Materials.*

19. Bergström, J., (2009), *Finite Element Modelling of Polymers Course Notes*, Veryst Engineering, LLC. Needham, MA. USA

20. Quintavalla, S.J., (2004) *Characterization of the High and Low Strain Rate Behaviour of a Filled, Crosslinked Elastomer*, PhD Thesis, Lehigh University.

21. Ward, I.M., Sweeney, J., (2004) *The Mechanical Properties of Solid Polymers*, pp 53-78, John Wiley & Sons, Ltd, ISBN 0471 49625 1

22. Bergström, J., (2005) *Calculation of Prony Series Parameters From Dynamic Frequency Data*, http://PolymerFEM.com

23. Bergström, J., (2009) *PolyUMod: A Library of User Materials for ABAQUS, User's Manual*, Veryst Engineering, LLC. Needham, MA. USA

24. Miller, K., (2004) *Testing Elastomers for Hyperelastic Material Models in Finite Element Analysis*, Axel Products, Inc., Ann Arbor, MI

25. ASTM, (1997) ASTM-D6147-97 *Test Method for Vulcanized Rubber and Thermoplastic Elastomer - Determination of Force Decay (Stress Relaxation) in Compression*, West Conshohocken, American Society for Testing and Materials.

26. Mullins, L., Tobin, N.R., (1965) *Stress Softening in Rubber Vulcanizates Part I. Use of a Strain Amplification Factor to Describe the Elastic Behavior of Filler-Reinforced Vulcanized Rubber*, J. Appl. Polymer Sci. **9**: 2993-3009.

27. Mullins, L., (1969) *Softening of Rubber by Deformation*, Rubber Chemistry and Technology, Vol. 42.

28. Gent, A.N., (1992) *Engineering with Rubber*, Oxford University Press, New York.

29. DuPont, (2011) *Fluoropolymer Comparison - Typical Properties, Mechanical Properties*.
http://www2.dupont.com/Teflon_Industrial/en_US/tech_info/techinfo_compare.html

30. Oyaddiji, S.O., (2004) *How To Analyse the Static and Dynamic Response of Viscoelastic Components*, NAFEMS Ltd., ISBN 1 874376 50 6

31. Monk, S., (2005), *The Role of Friction Coefficient on Launch Conditions in High-Loft Angle Golf Clubs*, PhD Thesis, The University of Birmingham.

32. ABAQUS v6.7

33. ABAQUS Version 6.7, (2008), *17.5.1 Hyperelastic behaviour of rubberlike materials*, Analysis User's Manual.

34. Bergström, J., (2002) *Determination of Material Parameters for the 8-chain model for use in ABAQUS, LS-Dyna and ANSYS,* Version 1.

35. Veryst Engineering, (2009) *MCalibration*, Veryst Engineering, LLC.

36. Veryst Engineering, (2009) *PolyUMod: A Library of User Materials for ABAQUS*, Veryst Engineering, LLC.

37. Bergström, J., (2010) Personal communication.

38. ABAQUS Version 6.8, (2008), *22 Elements*, Analysis User's Manual.